CHALMERS
UNIVERSITY OF TECHNOLOGY

Quantifying the greenhouse gas reduction potential of battery electric cars with integrated photovoltaics

Master's thesis in Sustainable Energy Systems

FRANCIS JESSY SIMANGAN LIGGAYU
SAHAR ABEDI

DEPARTMENT OF SPACE, EARTH AND ENVIRONMENT
CHALMERS UNIVERSITY OF TECHNOLOGY

Gothenburg, Sweden 2024
www.chalmers.se

MASTER'S THESIS IN SUSTAINABLE ENERGY SYSTEMS

Quantifying the greenhouse gas reduction potential of battery electric cars with integrated photovoltaics

FRANCIS JESSY SIMANGAN LIGGAYU
SAHAR ABEDI

Department of Space, Eartth, and Environment
Division of Physical Resource Theory
CHALMERS UNIVERSITY OF TECHNOLOGY
Göteborg, Sweden 2024

Quantifying the greenhouse gas reduction potential of battery electric cars with integrated photovoltaics

FRANCIS JESSY SIMANGAN LIGGAYU
SAHAR ABEDI

Supervisors:
Johannes Morfeldt, Researcher at Division of Physical Resource Theory
Johan Lindquist Holmberg, Technical Expert at Volvo Cars

Examiner:
Daniel Johansson, Associate Professor at Division of Physical Resource Theory

Department of Space, Earth and Environment
Division of Physical Resource Theory
Chalmers University of Technology
SE-412 96 Gothenburg
Sweden
Phone: + 46 (0)31-772 1000

Cover:
An illustration of battery electric cars with photovoltaics, generated using Microsoft Designer's Image Creator

Quantifying the greenhouse gas reduction potential of battery electric cars with integrated photovoltaics

Master's thesis in Master's programme is Sustainable Energy Systems

FRANCIS JESSY SIMANGAN LIGGAYU
SAHAR ABEDI
Department of Space, Earth and Environment
Division of Physical Resource Theory
Chalmers University of Technology

Abstract

This study quantified the potential for reducing greenhouse gas emissions of battery electric vehicles with integrated photovoltaic systems, compared to pure battery electric vehicles. The research employed a simulation model that integrates aggregated hourly onboard solar energy generation, vehicle electricity consumption for driving, vehicle electricity demand for charging with lifecycle greenhouse gas estimates for both vehicle types. The model analyzes solar energy charging potential, curtailment and the resulting reduction in vehicle electricity demand for charging across four geographically diverse regions: Gothenburg, Los Angeles, Taipei, and Madrid.

The results indicate that integrating photovoltaics can reduce electricity demand for charging on grid by 7-12% across the studied locations. Greenhouse gas emission reductions varied significantly, with Taipei showing the highest potential at 2.9%, followed by Los Angeles (1.3%) and Madrid (0.4%). Gothenburg, despite its clean electricity grid, saw a slight increase in emissions (2.3%) attributed to the GHG emissions from the manufacturing of the VIPV system. The results also show that long-distance drivers generally benefit more from integrated photovoltaic systems in terms of emission reduction during the car's usage phase compared to short-distance drivers.

A sensitivity analysis inspired by a 2030 case scenario suggests further improvements in the performance of battery electric vehicles with integrated photovoltaic systems. Taipei still shows the highest greenhouse gas emission reduction at 5.4%, followed by Los Angeles (2.0%) and Madrid (0.5%). Similarly, Gothenburg has seen a slight increase in emissions (1.7%) still attributed to the GHG emissions from the manufacturing of the VIPV system. The results highlight the importance of considering geographical factors, driving patterns, and future technological developments when assessing the greenhouse gas emission reduction of battery electric vehicles with integrated photovoltaic systems. In conclusion, this technology shows a potential for reducing transportation-related emissions, but its effectiveness varies significantly based on location and usage patterns.

Keywords: Vehicle-integrated photovoltaics; battery electric vehicles; Solar-powered electric vehicles; greenhouse gas reduction potential; solar charging potential

Contents

Preface

This thesis represents the culmination of an enriching journey at Chalmers University of Technology. This is part of the Master's programme Sustainable Energy Systems, carried out from January to June 2024. The thesis was both performed at the Department of Space, Earth and Environment at Chalmers University of Technology and at Volvo Cars AB, Torslanda.

The thesis was supervised by Johannes Morfeldt, Researcher at Chalmers University of Technology, and Johan Lindquist Holmberg, Technical Expert at Volvo Cars AB. This was examined by Daniel Johansson, Associate Professor at Chalmers University of Technology. Thank you for all the help and advice!

We would also like to express our gratitude to Roy Ogink for the help and pieces of advice. Thanks to Pepe Tan and Orujova Narmin for their help with modelling through Visual Studio Code and Python. We would also like to thank all other personnel at Volvo Cars AB and Chalmers University of Technology who have been involved in this thesis for their support.

Göteborg June 2024

FRANCIS JESSY SIMANGAN LIGGAYU
SAHAR ABEDI

Acknowledgement

Completing this thesis would not have been possible without the collaboration and support of many wonderful people. This journey has been a profound experience of growth and learning, for which I am deeply grateful.

We have been fortunate to have two exceptional supervisors. Johan, you took us on as master's thesis students when we are new in the vehicle energy discipline. I am deeply grateful for everything you have contributed—your knowledge, time and expertise. Johannes, thank you for always making time for us and sharing your expertise in academic writing, you consistently improved our output. It has been a true pleasure to work with both of you! Special thanks to Roy Ogink for the pieces of advice and encouragement you had given to us and to Daniel Johannson for giving us opportunity and support throughout the process.

I gratefully acknowledge the Swedish Institute for fully funding my master's programme. This publication has been produced during my scholarship period at Chalmers University of Technology. A special mention goes to Ralph Edrean Omadto and Sir Dennis Pagud for their support throughout my scholarship application process. To my dear Gothenburgers, your presence has made this experience in Gothenburg truly special.

To my family, your love and support have been my anchor. Mom, Pa, Dad, Mama, Nanay, Tatay, Ate Ja, Ate Jen, and Cenij—your presence gives me strength. To my nephews and niece, Kurt, Kirk, Kyrie and Jenu thank you for always believing in your tito. To Merle, your ability to bring a smile to my face even during the most challenging moments of writing has been my secret weapon on continuing in pushing forward. To Juno your presence has been a constant source of joy and comfort. Someday, you'll understand the significance of this journey we've shared.

To all my family and friends, both mentioned and unmentioned, this achievement belongs to all of us. Thank you for the support and being part of this incredible journey.

Francis Jessy Liggayu

I would like to extend my heartfelt thanks to my supervisors, Johannes Morfeldt at Chalmers and Johan Lindquist Holmberg at Volvo Cars, for their continuous support throughout this project. Their regular meetings, knowledge sharing, discussions, and guidance on thesis revisions greatly enriched my learning and ensuring the success of this work.

Special thanks to Roy Ogink at Volvo Cars for his insights, follow-ups, and support, which had a big impact on the project. I'm also grateful to my colleagues at Volvo Cars for their knowledge sharing, thoughtful discussions, and encouragement along the way. I also want to thank our examiner, Daniel Johansson at Chalmers, for giving us the opportunity to work on this thesis and for his trust in our work.

Lastly, I'm deeply grateful to my family and friends for their constant support and encouragement throughout this process.

Sahar Abedi

Abbreviations

A2Z	Accelerating to Zero
BEV	Battery Electric Vehicle
CO_2	Carbon dioxide
EV	Electric Vehicle
GHG	Greenhouse gas
ICE	Internal Combustion Engine
IEA	International Energy Agency
IPCC	Intergovernmental Panel on Climate Change
HV	High Voltage
LCA	Life Cycle Assessment
LCI	Life Cycle Inventory
NEV	New Energy Vehicles
MERRA-2	Modern-Era Retrospective Analysis for Research and Applications, Version 2
PHEV	Plug-in Hybrid Electric Vehicle
PV	Photovoltaic
SOC	State of Charge
TTW	Tank-to-Wheels
VIPV	Vehicle Integrated Photovoltaic
VIPV-BEV	Battery Electric Vehicle with Vehicle Integrated Photovoltaic
WTT	Well-to-Tank
WTW	Well-to-Wheels
ZEV	Zero Emission Vehicles

Nomenclature

A	Ambient temperature correction factor
C	Electricity demand for charging [kWh]
D	Electricity consumption for driving [kWh]
E	Solar energy charging potential [kWh]
F	Future carbon emission intensity [gCO_2/kWh]
H	Solar power generation potential [kW]
I	Carbon emission intensity [gCO_2/kWh]
P	Present carbon emission intensity [gCO_2/kWh]
S	Solar panel capacity [kW]
t	time [hr]
Wp	Watt-peak [W]

1 Introduction

Based on statistics presented by the IPCC (2023), the transportation sector is a major contributor to global greenhouse gas (GHG) emissions, accounting for around 23% of global energy-related GHG emissions in 2019. Direct GHG emissions from the transport sector were 8.7 billion tonnes of carbon dioxide equivalent ($GtCO_2$-eq) in 2019, a notable increase from 5.0 $GtCO_2$-eq in 1990. Most of these emissions, 70%, come from road vehicles, while 1%, 11%, and 12% come from rail, shipping, and aviation, respectively. Since 2010, this sector has experienced the fastest annual growth rate of 1.8% compared to all other end-use sectors. Notably, transportation represents the primary energy-consuming sector in 40% of the countries all over the world. This sector is typically the second-largest energy consumer in the remaining nations, reflecting the differences between countries in the interplay of urbanization patterns, land-use practices, demographic shifts, and socioeconomic development.

The electrification of transportation is a critical measure for reducing GHG emissions in the road sector by 2030 as discussed by the IEA (2023). This shift is being driven by the growing adoption of electric vehicles (EVs), including pure battery electric vehicles (BEVs) and plug-in hybrid electric vehicles (PHEVs). Numerous countries and organizations worldwide have set and implemented targets for EV adoption and usage in the coming years to support this shift. For instance, China's electric car market experienced growth in 2022, with electric vehicles capturing a 29% share of total domestic car sales. This surge has propelled China ahead of schedule in achieving its 2025 national target of a 20% sales share for new energy vehicles (NEVs), which includes BEVs, PHEVs, and fuel-cell electric vehicles. In another example, the primary objective established by Accelerating to Zero (A2Z), which was launched by a leadership group of more than 100 countries, businesses, and organizations in the Conference of the Parties (COP 27), is to achieve global sales exclusivity for zero-emission vehicles (ZEVs) for new cars and vans by the year 2040. This target date is accelerated to 2035 within leading markets. However, to maximize the emissions reduction potential of EVs, powering them with electricity generated from renewable energy sources is essential. As described by Araki et al. (2021), integrating more renewable energy sources like solar PV systems into transport infrastructure, such as on-board PV systems in vehicles or PV installations on the roofs of charging stations and parking garages, presents a decentralized approach to vehicle charging. This approach creates unique possibilities for recharging electric vehicles with lower dependency on grid electricity, enhancing convenience and autonomy.

Beyond established stationary PV applications, novel methods for utilizing PV within the transportation sector hold promise for contributing to reduced GHG emissions (Hoth et al., 2024). One of the most decentralized approaches for utilizing PV technology to charge EVs is through Vehicle Integrated Photovoltaics (VIPVs). VIPV refers to the integration of PV modules into the vehicle design to generate electricity from sunlight that will directly charge the battery. It involves the mechanical, electrical, and design-technical integration of PV modules into vehicles in a way that blends with

the vehicle exterior. The PV modules are connected to electric loads or the traction battery in electric vehicles and can replace other vehicle components like the roof or bonnet (Vehicle-Integrated Photovoltaics - Fraunhofer ISE, 2024). As described by Samadi et al., (2023), due to their frequent exposure to direct sunlight, the bodies of vehicles present themselves as viable locations for the installation of photovoltaic cells, and advancements in the manufacturing and development processes of photovoltaic cells have enabled their integration into the body of vehicles.

Battery Electric Vehicles with VIPV (VIPV-BEVs) offer several advantages by reducing reliance on the electricity grid and potentially minimizing necessary battery capacity, leading to decreased greenhouse gas emissions and resource strain. They provide a decentralized source of renewable energy to charge the vehicle's battery, reducing the need for frequent charging from the grid. By harnessing clean solar energy through integrated photovoltaic modules, VIPV-BEVs extend the operational range between charging occasions (Needell et al., 2023). However, it is important to consider broader environmental and social implications. A more holistic viewpoint is essential to fully understand the overall impact of VIPVs beyond their immediate benefits in reducing grid dependence and resource use. Manufacturing of solar PV systems, including solar panels and their components, can introduce its own emissions and increase demand for limited raw materials (Chandrasekharam & Ranjith Pathegama, 2020). The GHG footprint of solar PV systems varies depending on the region's energy sources used during manufacturing. Energy-intensive stages like silicon production for solar cells are especially impacted by reliance on fossil fuels, potentially negating some of the environmental benefits. The solar PV industry also faces significant human rights challenges, particularly concerning the use of forced labor in the production of polysilicon, a critical raw material for solar cells used in solar panels. This forced labor within the polysilicon supply chain has become a major human rights issue for the solar industry, as it is embedded throughout the manufacturing process of solar PV systems (Mulvaney & Bazilian, 2023). Therefore, to maximize the environmental benefits of the electric mobility transition, a more comprehensive assessment of the net environmental impact of VIPV-BEVs is crucial. This assessment should include an examination of the factors influencing VIPV-BEV effectiveness, particularly those related to real-world operation.

Thiel et al. (2022) discuss several factors that influence the performance of VIPV systems. One of the primary influences on VIPV effectiveness is vehicle's geographical location, particularly regarding variations in solar irradiation and ambient temperature. These variations impact the electricity generation of the PV cells, which in turn directly affects the achievable driving range that VIPVs can provide for the vehicle. Consumer behavior, such as car use patterns, also affects the electricity that can be generated by the PV cells and the vehicle’s energy consumption. Frequent short trips limit the opportunity for substantial solar charging. Conversely, longer commutes allow for more time under sunlight, potentially replenishing a larger portion of the battery. Additionally, parking location plays a role – cars left in shaded areas receive less sunlight, hindering electricity generation. Furthermore, charging habits can impact

utilization. Consumers who frequently top off the battery at charging stations might not give the solar panels enough time to contribute to battery charging. According to Samadi et al. (2023), another crucial factor impacting performance is the interplay between the solar PV panels and their placement on the vehicle. Maximizing a vehicle's solar energy capture requires strategically integrating the most efficient solar cells possible into the largest, most sun-facing surface areas. This might involve using flexible or transparent cells on a curved hood or trunk lid while prioritizing high-efficiency, durable cells for the expansive roof. The key is to find the optimal balance between capturing sunlight and seamlessly integrating the VIPV system into the vehicle's design. Understanding how these factors impact the VIPV system is crucial for assessing the emission reduction potential of VIPV-BEVs. This knowledge allows for the identification of user –profiles, and locations, where the emission reduction potential of VIPV-BEVs is the largest.

1.1 Contribution to research

This study explores the implications of integrating solar PV systems into BEVs, with focus on quantifying the GHG emissions reduction potential through a simplified energy model. The model assesses solar energy charging potential and vehicle energy consumption, focusing on regions with distinct geographical features and electricity generation mixes. This study also examines the conditions under which VIPV-BEV systems offer a more attractive alternative to pure BEV systems regarding GHG emissions. A sensitivity analysis is conducted to explore the possibilities of VIPV-BEV technology in 2030 and observe the impact of changing factors such as advancements in solar PV capacity, system losses, energy consumption, charging demand, and carbon emission intensity. This research also uses Volvo Cars as a case study, utilizing detailed data to examine VIPV-BEV potential in diverse regions and driving conditions. Volvo’s mission to achieve climate neutrality by 2040 and its commitment to sell only fully electric cars by 2030 provide a pertinent context, while the findings contribute broadly to the automotive industry's shift towards renewable energy.

1.2 Aim and research questions

This study aims to estimate the GHG emission reduction potential of VIPV-BEVs. The study presents results for a diverse range of locations, Gothenburg in Sweden, Los Angeles in the USA, Taipei in Taiwan, and Madrid in Spain, considering their distinct geographical features and variations in the electricity generation mix.

The research questions to be answered in this thesis are as follows:

1. *How does the geographical location influence the potential for reducing electricity usage from the grid and lifecycle carbon dioxide emissions by using VIPV systems in BEVs?*
2. *Which types of users would benefit the most from VIPV-BEVs in terms of driving pattern and geographical location?*
3. *How could future advancements in solar PV capacity, system losses, energy consumption, charging demand, and carbon emission intensity affect the GHG emissions reduction potential of VIPV-BEVs?*

1.3 Scope and delimitations

The findings of this study are specific to Volvo Cars and the regions studied, namely Sweden (Gothenburg), USA (Los Angeles), Taiwan (Taipei), and Spain (Madrid). Consequently, the findings may not be directly applicable to other car manufacturers or to regions that have not been studied. The environmental analysis covers GHG emissions, presented in CO_2-equivalent emissions. The time horizon of the study is framed to the most recent available data for the year 2023, which serves as the baseline for most analyses. However, for certain parameters, such as temperature and solar irradiation, average data from 2019 to 2023 is utilized to account for variability. To explore potential future developments, this study employs sensitivity analyses to examine scenarios for the year 2030. These analyses consider various factors that may change by then. No attempts to predict costs are made in the report.

There are also limitations due to confidentiality. This thesis utilizes internal data and materials from Volvo Cars, such as vehicle energy consumption and charging patterns. These include proprietary information regarding the VIPV technology, car use patterns, and other relevant factors necessary for the analysis. Consumer-related data, like car use patterns, will be aggregated to ensure privacy and comply with Volvo Cars' confidentiality agreements, safeguarding individual privacy, concepts, and facts.

2 Background

This chapter introduces the foundational concepts for analysing VIPV-BEVs. It begins with exploring the concepts of solar irradiation, including its definition, influencing factors, and implications for generating electricity in VIPV-BEVs. Next, it discusses VIPV systems, covering the types of photovoltaic cells currently used and their strategic placement on the vehicle to optimize energy production. The effect of weather conditions on these systems is also explained. Moving forward, the chapter introduces the Life Cycle Assessment (LCA) framework as a tool for understanding the environmental impact of VIPV-BEVs. Finally, the chapter explores the approach for estimating the potential reduction in carbon footprint achievable through the adoption of VIPV-BEVs.

2.1 Solar-powered cars

A VIPV-BEV, also known as solar-powered car, is a type of electric vehicle that utilizes solar energy to help power various energy consumers within the vehicle thereby reducing the load on the main battery. These vehicles are equipped with PV panels, which capture sunlight and convert it into electrical energy. Solar-powered cars aim to minimize environmental impact by reducing reliance on fossil fuels and decreasing greenhouse gas emissions (Reddy et al., 2024). Figure 2.1 shows the Lightyear solar-powered car, which exemplifies the integration of photovoltaic panels into the vehicle's design for on-board solar charging.

As stated by Reddy et al. (2024) conversion efficiency is a critical parameter in the performance of solar-powered vehicles. It refers to the ratio of the electrical power output from the PV panels to the solar power input. High-efficiency PV cells are crucial for maximizing the energy harvested from sunlight, especially given the limited surface area available on a car. Modern PV technologies typically achieve efficiencies between 15% and 22%. Advanced technologies like monocrystalline silicon cells can reach efficiencies over 22%, while thin-film cells offer efficiencies between 10% and 12% but are more flexible and lighter. The efficiency of a solar-powered car is influenced not only by the efficiency of the PV panels but also by the efficiency of the battery, the electric drivetrain, and the auxiliary systems. Effective energy management and minimizing energy losses are key to improving the overall efficiency of the system.

Figure 2.1 Illustration of the Lightyear 0 solar-powered car with VIPV panels for on-board solar charging (Source: Lightyear).

2.1.1 Solar irradiation

Solar irradiation has long been utilized as a source of energy. Solar irradiation consists of two components (1) direct irradiation, which is the sunlight that travels in a straight line from the sun to the Earth's surface without being scattered or absorbed by atmospheric particles and molecules (i.e., the discrete "beam" from the sun), and (2) diffuse irradiation, which results from sunlight scattered by atmospheric particles and molecules (i.e., through clouds, aerosols, etc, spreading the light in various directions before it reaches the Earth's surface (Leftheriotis & Yianoulis, 2012; Pfenninger & Staffell, 2016). Figure 2.2 shows an illustration of the difference between direct irradiation and diffuse irradiation.

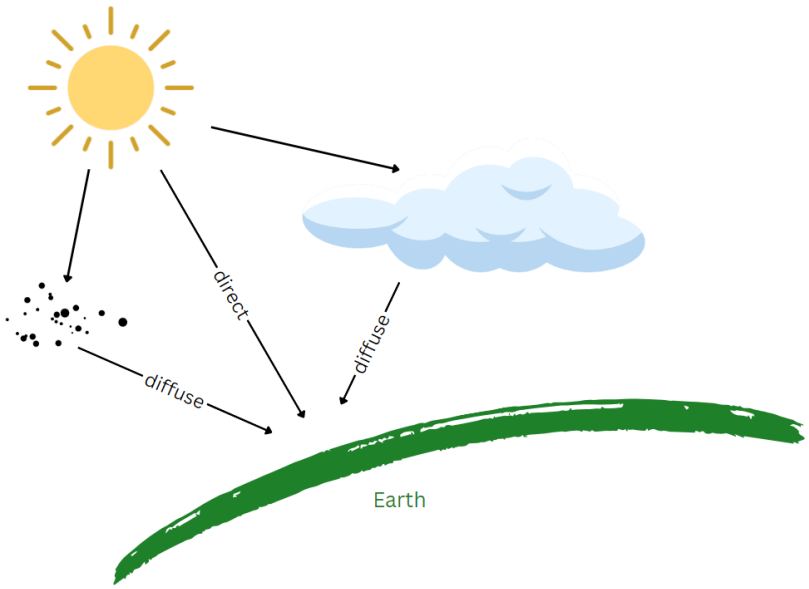

Figure 2.2. This figure shows a simple visualization on how sunlight reaches the Earth's surface through direct and diffuse irradiation.

Aside from the amount of solar irradiation, the azimuth and tilt angles affect the potential energy that could be absorbed from the incoming solar irradiation (Desai et al., 2021). The azimuth angle represents the angle between the sun's rays and the due south direction in the Northern Hemisphere, or the due north direction in the Southern Hemisphere. The tilt angle is the angular orientation of an object with respect to the ground surface. As a rule-of-thumb for optimal orientation of PV modules, the azimuth angle should be directed towards the south for the northern hemisphere and toward the north for the southern hemisphere (Al Garni et al., 2018, as cited in Mahmoudi et al., 2023).

Accurate retrieval of solar irradiance reaching the earth's surface from satellite measurements is key to a large number of atmospheric observations and modeling studies, including climate monitoring (Posselt et al., 2012; Vuilleumier et al., 2020).

The Modern-Era Retrospective Analysis for Research and Applications, Version 2 (MERRA-2) product is an atmospheric reanalysis project from the National Aeronautics and Space Administration (NASA) that provides several variables, including global horizontal irradiance. An atmospheric reanalysis is a systematic approach to produce datasets describing the recent climate by combining observational data from various sources (e.g. satellites, weather stations) with a numerical weather prediction model using data assimilation techniques. The temporal resolution of MERRA-2 for the 2D diagnostics dataset is hourly, and its spatial resolution is 0.5° latitude × 0.625° longitude, which is roughly 55 km x 70 km (Rienecker et al., 2011 Tahir et al., 2018). This dataset is used for solar energy studies with the advantage of high temporal resolution, which is more frequently used compared to other datasets with 3 or 6-hourly intervals. It incorporates space-based aerosol observations, potentially improving the accuracy of solar irradiance modeling (Pfenninger & Staffell, 2016).

2.1.2 Vehicle integrated photovoltaic systems

The electrical output of VIPV systems can, depending on vehicle type, contribute to powering auxiliary functions (e.g., ventilation, air conditioning, audio systems), thereby indirectly extending the driving range by reducing the load on the main battery, or even directly extending the range and supporting battery charging in both stationary (parked) and mobile scenarios (Samadi et al., 2023). Vehicle integration of PV technology necessitates the development of novel PV modules with distinct characteristics compared to those employed in traditional utility applications. These in-vehicle modules must prioritize aesthetics, lightweight design, and the ability to conform to curved surfaces. Additionally, unlike stationary PV systems, they require durability to withstand mechanical stresses and vibrations encountered during vehicle operation. However, established performance metrics, such as watt-peak per square meter (Wp/m^2), reliability, and safety, remain equally important considerations. Material selection and technological advancements should also prioritize cost-effectiveness to facilitate mass production (Commault et al., 2021).

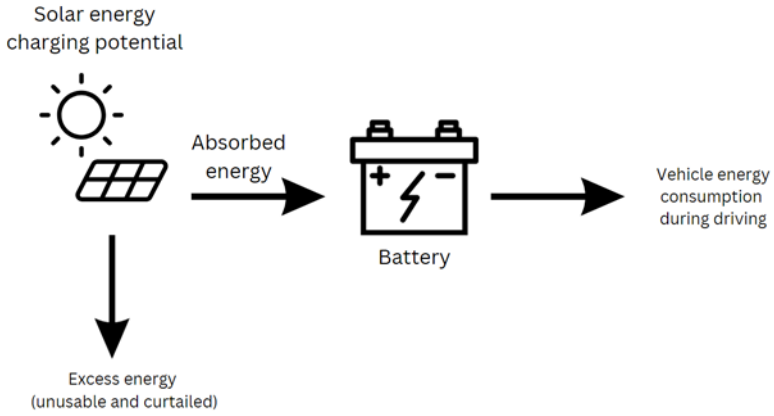

Figure 2.3. This figure illustrates the generated electricity from solar energy, reduced electricity usage from the grid, and excess energy.

Highlighting the potential benefits, Heinrich et al. (2020) investigated integrating PV panels on a sedan roof in Freiburg, Germany. Their findings suggest that a moderately sized PV system (1.7-2 m², 20% efficiency) installed on a car roof could provide an additional driving range of 1,900-3,400 km annually. This translates to roughly 13-23% of the average yearly driving distance for cars in Germany (15,000 km). The study further suggests potential benefits for everyday driving, including a reduction in charging frequency by approximately one instance per month during summer and an extended range on sunny days. However, it is important to consider these findings do not account for energy losses due to shading, which could potentially impact the real-world effectiveness of the PV system. This complexity highlights the influence of numerous factors on the performance of VIPVs. Some of these factors, including the specific photovoltaic cell technology employed and the location chosen for cell installation as discussed by Heinrich et al. (2020) as well as the atmospheric and climatic conditions as discussed by Pavlovic et al. (2020) are explored below.

2.1.3 Photovoltaic modules

A crucial aspect of VIPV design is the selection of PV modules. Various solar cell technologies, including silicon crystal, thin film, and multi-junction cells, have been developed for integration into vehicle bodies (Samadi et al., 2023). Based on research by Commault et al. (2021), Gallium Arsenide (GaAs) single-junction cells and multijunction cells achieve the highest efficiencies but also come with the highest costs. Single-junction cells consist of a single semiconductor material with a single p-n junction, while multijunction cells are composed of multiple subcells made of different semiconductor materials stacked on top of each other, with each subcell designed to absorb a specific range of the solar spectrum. Commault et al. (2021) also highlight that Crystalline Silicon-based cells are currently the dominant technology due to their well-balanced performance, cost-effectiveness, and reliability. However, their inherent rigidity restricts their design options. Thin-film technologies deliver lower efficiencies but make up for it with better flexibility and lighter weight. Finally, Commault et al. (2021) note that promising new PV technologies, such as perovskite solar cells, hold the potential to achieve high efficiency, low cost, ultralight weight, and flexibility all at once. These solar cells utilize a perovskite-structured compound, typically a hybrid organic-inorganic lead or tin halide-based material (Afre & Pugliese, 2024). However, compared to established crystalline silicon cell modules, perovskite technology currently faces limitations in terms of reliability, longevity, and production yield. According to a study by Yamaguchi et al. (2023), the utilization of high-performance PV modules, achieving a conversion efficiency above 35%, can facilitate a daily solar-powered driving range surpassing 30 kilometers. This is achievable under average irradiation conditions of 4 kWh/m²/day, reducing the need for external charging.

Commault et al. (2021) state that choosing the most suitable PV module necessitates a careful trade-off among various material properties:

- **Weight:** Similar to traditional PV panels, curved photovoltaic modules use a glass back sheet or a glass-glass structure with a thick front glass cover (typically 2.0 to 3.2 mm). This design incorporates three-dimensional curved glass, and commercially available options already exist. However, while offering established reliability and production methods, curved PV modules are significantly heavier (> 11 kg/m²) compared to alternatives. This additional weight can negatively impact vehicle performance and range. Figure 2.4 illustrates the relationship between power density and module weight for various PV technologies.

- **Flexibility and aesthetics:** Flexible PV modules utilize a diverse range of technologies. These include established crystalline silicon-based cells and more recent thin-film technologies such as Copper Indium Gallium Selenide (CIGS) solar cells and organic films. These modules offer a lighter-weight solution (0.7 to 6.7 kg/m²) and the ability to conform to vehicle curves, enhancing aesthetics. As stated by Wijewardane & Kazmerski (2023), their flexible nature also provides better resistance to mechanical stresses and vibrations encountered during vehicle operation compared to rigid modules. This durability is achieved through the use of materials and structures designed to absorb and distribute mechanical loads more effectively. However, their power density may be lower compared to their rigid counterparts, see Figure 2.4.

- **Integration potential:** Light, rigid PV modules, currently under development, hold the potential to become integral vehicle body components. This complete integration could minimize weight compared to add-on panels and enable a more streamlined design. Commercially available these PV modules typically weigh between 5.6 and 8.9 kg/m², with some options even lighter at under 4 kg/m², see Figure 2.4.

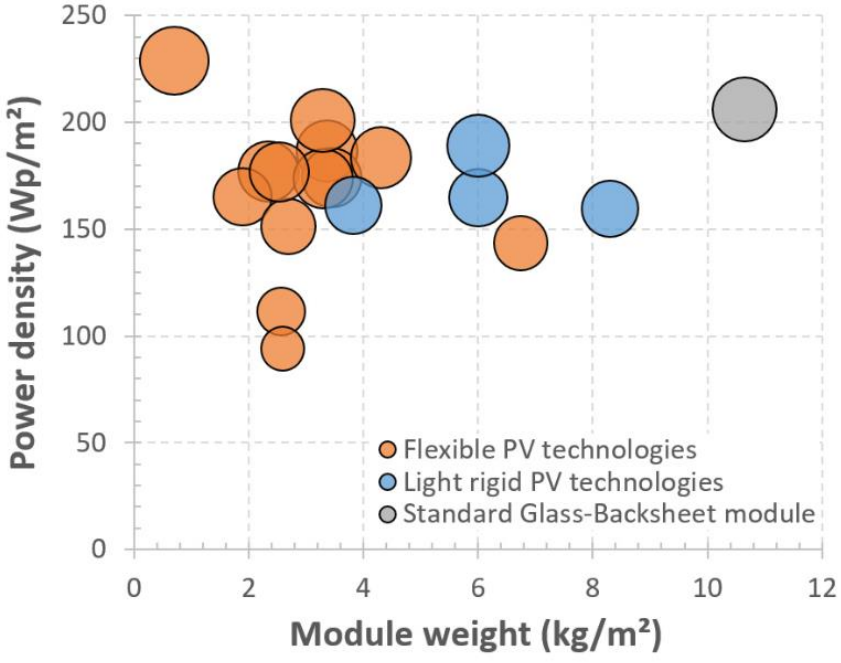

Figure 2.4 Power density as a function of module weight for different PV technologies (Source: Commault et al., 2021)

Commault et al. (2021) conclude that the optimal PV module selection for a VIPV application depends on the specific priorities of the design. In the context of passenger cars, scenarios where maximizing power generation is crucial typically involve vehicles where the primary goal is to maximize the energy harvested from sunlight to supplement the vehicle's energy needs. In such cases, traditional glass-based modules, despite their weight, are often considered due to their typically higher efficiency and reliability over time. Conversely, applications prioritizing aesthetics and minimal weight gain tend to favor flexible PV options. Ultimately, the future of VIPVs lies in advancements of light, rigid PV modules, allowing for seamless integration and weight reduction through material innovation.

2.1.4 Photovoltaic placement and environmental conditions

A significant portion of a vehicle's exterior is directly exposed to sunlight, making it a prime candidate for integrating PV cells. The versatility of these cells in terms of color, shape, and size allows for their incorporation into the vehicle body itself. However, most VIPV projects prioritize the roof for solar panel installation. This preference stems from encountering fewer technical limitations and installation challenges compared to other vehicle sections (Samadi et al., 2023). Additionally, car roofs typically receive more solar radiation compared to other body sections, although this difference can fluctuate based on external factors like weather, temperature, and seasonal changes. For instance, a study conducted in Hanover, Germany found that the roof of a van received up to around 4 times more radiation than its sides, depending on the specific conditions, including shading patterns throughout the day (Wetzel et al., 2022). The study further reveals that the roof received most of the sunlight (54.3%) compared to the sides (45.7%) on average across a year, with winter's lower sun angle favoring the sides and summer's higher angle favoring the roof. This effect of lower sun angles during winter months is more pronounced at higher latitudes. Closer to the equator, where the sun is more directly overhead year-round, this seasonal variation in sunlight distribution between roof and sides would be less significant. Therefore, locations closer to the equator tend to favor roof installations of photovoltaic systems.

Despite the advantages of the roof, technological progress in PV cell production has spurred efforts to maximize solar energy capture on other parts of the vehicle. Researchers and engineers are exploring the integration of PV cells on various vehicle surfaces, including the sides, hood, trunk, and even windows (Peibst et al., 2022). A study by Tiano et al. (2020) assessed the potential net energy output of hybrid and battery electric vehicles (HEVs and BEVs) equipped with PV cells. The study analyzed data from 28 countries and reported a maximum annual net energy output of approximately 4,200 Wh/day, assuming a roof surface area of 2 m². However daily averages ranged from 1,000 to 2,750 Wh/day, varying based on geographic location. This variability reflects the impact of solar irradiance levels influenced by latitude, climate, and local weather conditions on PV-equipped vehicles across different regions.

Furthermore, the investigation by Tiano et al., (2020) extended to the inclusion of lateral (vertical) surfaces on the vehicle. This consideration resulted in a higher estimated maximum annual net energy output of 6,500 Wh/day. Similarly, the average net energy output for lateral surfaces ranged from 1,800 to 4,200 Wh/day. These findings highlight the potential for increased power generation by incorporating both horizontal (roof, bonnet, and hood) and lateral (doors and windows) surfaces for PV cell installation on solar vehicles (Tiano et al., 2020).

On the other hand, while efforts to maximize solar energy capture on vehicles through PV cell integration have shown promise, the performance of VIPV systems is highly dependent on geographical location and solar irradiation levels. The amount of electricity generated depends on the available solar irradiation, which varies strongly based on the geographical location. Locations with high solar irradiation, such as high-elevation areas and subtropical regions, tend to have the highest solar electricity charging benefits from VIPV systems (Thiel et al., 2022). In contrast, regions with lower solar irradiation, like Sweden may see a notable decrease in their overall potential for solar energy generation throughout the year. This reduction, however, is not limited to such regions; it can also be influenced by factors like shading from surrounding structures, which can affect even sunnier areas (Hoth et al., 2024).

This variation in solar irradiation due to geographical location is further influenced by weather conditions. Based on the study by Golubev and Lunt (2021), solar irradiation is generally higher in sunny weather compared to cloudy conditions. Additionally, seasonal variations play a role in cloudy weather, with minimal difference between cloudy and sunny conditions in winter, while sunny weather in summer receives about eight times more radiation than cloudy weather.

Despite these insights, accurately assessing the real-world impact of shading on PV potential remains a complex challenge. Many studies focus primarily on vehicle parameters, including the PV systems themselves, vehicle geometry, and battery and charging management systems. However, evaluating shading dynamics is inherently difficult due to its variability and dependence on numerous environmental factors. Consequently, these studies often rely on generalized reduction factors to approximate shading effects, which may not capture the full extent of its influence on actual energy generation (Hoth et al., 2024).

For instance, the study by Lodi et al. (2018) evaluated how shading affects the solar radiation received by a vehicle's PV roof during real-world driving. It calculated the average solar irradiance received by an unshaded PV module (143 W/m^2) and compared it with actual received radiation during a typical day, factoring in shading from obstacles and parking events. Results show a significant reduction in radiation due to shading, resulting in an average yearly irradiance of 83.5 W/m^2 on a PV panel installed on a car roof, with 58% usage of available solar radiation. These findings align with Araki et al.'s (2023) research that emphasizes the need for specialized models and methodologies to assess the real-world performance of VIPVs under dynamic and non-

uniform shading environments encountered during driving conditions. It is important to clarify that while acknowledging the need for detailed shading models, this study utilizes a generalized reduction factor for shading in its calculations, rather than addressing the full complexity of shading effects across different regions.

2.2 Life cycle assessment framework

Life Cycle Assessment (LCA) is a pivotal tool for comprehensively assessing the environmental footprint of a product throughout its lifespan, taking into account resource usage and emissions to provide a holistic perspective. LCA emerged from the necessity to examine the complete life cycle of a product rather than isolated segments. Concentrating solely on individual phases risks sub-optimization, where environmental burdens are simply transferred from one stage to another. To mitigate this, LCA encompasses all stages from cradle to grave within a defined system boundary. However, as mentioned by Rödger et al. (2021) it's essential to acknowledge that obtaining a comprehensive overview of all environmental impacts may not always be feasible. This limitation arises from several factors. First, traditional LCA models often use static data, which can fail to capture the dynamic and variable nature of environmental impacts in real-world scenarios. Rödger et al. (2021) further explain that the static nature of traditional LCA models can lead to inaccuracies in representing the actual environmental performance of products during different phases of their life cycle. Additionally, there are challenges related to data availability and quality, as comprehensive and precise data for all life cycle stages can be difficult to obtain. The authors also highlight the integration of LCA with manufacturing system simulations as a way to address these gaps by allowing for a more dynamic and accurate assessment of environmental impacts. Despite these advancements, the inherent complexity and variability in product lifecycles mean that achieving a truly complete and accurate environmental overview remains challenging.

Figure 2.5 outlines the phases of a LCA as defined by the DIN 14044 and ISO 14040:2006 standards (Kanz et al., 2020). According to Kanz et al. (2020), the first step in the LCA process is establishing the goal and scope, which is crucial because the definition of system boundaries directly affects the outcomes. The second step, inventory analysis, involves collecting data on all processes within these boundaries, referred to as Life Cycle Inventory (LCI) data. In the third step, the impact assessment phase evaluates the LCI data by categorizing emissions based on their environmental impacts, such as climate change or acidification. The fourth and final step is interpretation, where the results are analyzed to refine the goal, scope, inventory, or impact assessment. This iterative approach ensures that the LCA effectively addresses the original objectives.

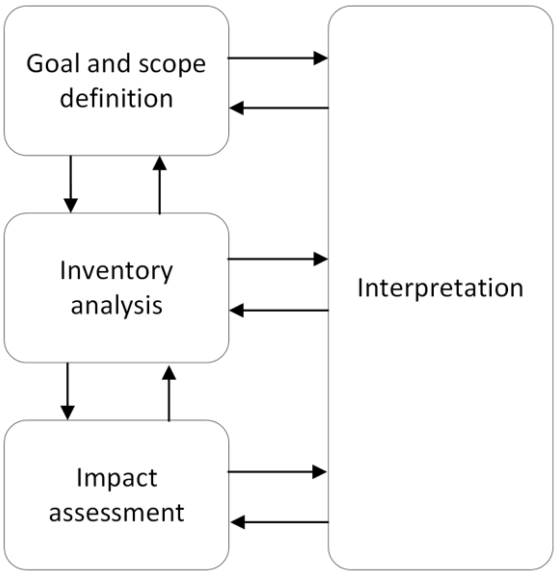

Figure 2.5. LCA framework (ISO 14044:2006)

Within LCA studies, established products are typically assessed by comparing a new generation to its current version. However, for emerging technologies in early developmental stages, a distinct methodology is required, known as prospective LCA. Prospective LCA is an approach suited for technologies that are still in early developmental stages, where there is flexibility to make substantial design modifications that can influence environmental impacts. Unlike traditional LCA studies, which analyze products at a specific point in time, prospective LCA projects the modeled system into a future timeframe to anticipate potential environmental impacts. Consequently, the timeframe considered in prospective LCA closely aligns with the projected future, moving away from the present-day focus of traditional LCA methodologies (Arvidsson et al., 2018).

In the context of environmental assessments within the BEVs and PV sectors, prospective LCA holds particular relevance. This methodology allows for anticipatory evaluations of emerging vehicle technologies as well as the evolving landscape of photovoltaic modules and VIPV systems. By extending our foresight beyond present-day assessments, prospective LCA facilitates in-depth analyses essential for steering sustainable progress in these pivotal sectors.

2.2.1 Life cycle assessment of vehicles

According to Que et al. (2015), in the past years, the analysis of life cycle energy and environmental impacts for conventional transportation fuels and their alternatives has gained significant research interest. The life cycle is typically divided into two parts: the vehicle cycle and the fuel cycle, primarily focusing on energy consumption and GHG emissions. The vehicle life cycle encompasses vehicle material production and refining, manufacturing and assembly, distribution, and disposal. In contrast, the fuel cycle includes feedstock production, feedstock transportation, fuel production, fuel

distribution, and fuel consumption. The fuel cycle, often referred to as the well-to-wheels (WTW) model, consists of two primary stages: Well-to-Tank (WTT) and Tank-to-Wheels (TTW). The Well-to-Tank stage encompasses feedstock production and transportation, as well as fuel production and distribution, while the Tank-to-Wheels stage involves fuel consumption and related direct emissions (Que et al., 2015). In the case of EVs, as stated by Idris & Koestoer (2023), the WTT emissions pertain to electricity production and distribution, which can vary significantly depending on the electricity generation mix and efficiency of the power grid in each region. For the Tank-to-Wheels (TTW) stage, EVs do not produce tailpipe emissions, thus eliminating direct GHG emissions during operation. On the other hand, for vehicles with internal combustion engines (ICE), emissions are produced both during the WTT stage, which involves the production, refining, and distribution of fuel, and the TTW stage, where tailpipe emissions occur. The environmental impact of these emissions depends on various factors including the type of fuel used, engine efficiency, and driving conditions (Idris & Koestoer, 2023).

A Volvo Cars report analyzing the carbon footprint of their XC40 ICE and C40 Recharge (pure BEV) models reveals that the electric C40, excluding the battery, initially generates around 30% more GHG emission during the material production and manufacturing phase compared to the XC40 ICE, primarily due to its greater reliance on aluminum and other materials. Including battery production increases the C40's manufacturing emissions by up to nearly 70%. However, over its entire life cycle, the C40 achieves a lower overall carbon footprint thanks to its cleaner use phase when different electricity mixes are considered. The "break-even" point, where the C40's reduced use phase emissions offsets higher manufacturing emissions, varies depending on the difference in manufacturing emissions between the vehicles and the carbon intensity of the electricity used to charge the C40 during its operation. Notably, Volvo's manufacturing processes and end-of-life treatment contribute minimally to the total carbon footprint (Evrard et al., 2021).

2.2.2 Life cycle assessment of photovoltaic systems and vehicle integrated photovoltaics

In the context of VIPV-BEVs, LCA can serve as a methodology for evaluating their potential environmental advantages over traditional grid charging methods. When comparing pure BEVs with VIPV-BEVs, it's important to consider various factors, including GHG emissions from the production of the PV panel, as well as energy efficiency, resource use, and overall environmental impact, as these considerations could yield divergent outcomes.

As demonstrated by Frischknecht et al., (2015), conducting a comprehensive LCA for PV systems involves analysing the potential environmental impacts across all stages - from raw material extraction and manufacturing, to installation, operation, maintenance, and ultimately end-of-life decommissioning and disposal or recycling. The manufacturing phase is particularly noteworthy, as it accounts for the energy-

intensive production of PV cells and modules. Depending on the technology, it may involve the use of materials like cadmium or lead, which are toxic. While toxicity is an important consideration in assessing environmental impacts, it is not included within the scope of this study.

Frischknecht et al. (2015) further highlight that the emissions from energy use, chemical processes, and processing of raw materials like silicon, metals, and glass are quantified during this stage. Additionally, they note that the production of balance-of-system components like inverters and mounting structures contributes to the environmental footprint. According to Frischknecht et al. (2015), the specific environmental impacts can vary depending on the PV technology. For crystalline silicon PV (mono-c-Si and multi-c-Si), the most carbon-intensive processes are the energy-intensive Czochralski crystal growth method used to produce silicon ingots, followed by wafering of the ingots into thin slices. They emphasize that emissions are primarily from the high electricity consumption and heat required for these processes. Frischknecht et al. (2015) also discuss how thin-film PV technologies like cadmium telluride (CdTe) and copper indium gallium diselenide (CIGS) generally have lower carbon footprints and emissions during manufacturing compared to crystalline silicon, as their deposition processes are less energy-intensive. However, there are concerns around the toxicity of some materials used. Emerging technologies like perovskite silicon tandem cells show promising lower environmental impacts, but data is still limited (Frischknecht et al., 2015).

According to Frischknecht et al. (2015), during operation, PV systems have relatively low emissions and energy requirements, primarily due to their renewable energy generation. However, maintenance activities such as cleaning, minor repairs, and the electricity used for these tasks can involve using the local electricity grid. Additionally, while inverter replacements are required, the manufacturing of replacement inverters typically involves processes similar to those of the original inverter production and can have broader supply chain impacts. The end-of-life stage evaluates the impacts of decommissioning, removal, and recycling or disposal of the system components. Based on Frischknecht et al. (2015) key impact indicators in life cycle assessments of PV systems include:

- Energy payback time: the time required for the system to generate the amount of energy used in its production, typically 0.7-3 years for current PV technologies.
- GHG emissions: the total CO_2 equivalent emissions over the system's lifetime, usually around 40-80 g CO_2-eq/kWh.
- Other emissions: including particulates, sulfur oxides, and nitrogen oxides.

Frischknecht et al., (2015) highlight that while manufacturing contributes significantly to environmental burdens, LCA studies consistently demonstrate that PV technologies have relatively low emissions and environmental impacts compared to conventional

fossil fuel-based electricity sources over their long operational lifetime (Frischknecht et al., 2015).

As demonstrated by Kanz et al. (2020), LCA methodology for assessing the environmental impact of VIPV systems during the manufacturing phase largely mirrors that of conventional PV modules. However, integrating PV cells directly into the vehicle body introduces an additional step in the manufacturing chain. This extra step is estimated to contribute around 20% of the total emissions associated with VIPV production, with the remaining 80% stemming from the production of the PV modules themselves.

In their study, Kanz et al. (2020) employed the LCA methodology to evaluate the environmental impact of a VIPV system integrated into a light electric utility vehicle (StreetScooter Work L) in Germany. The research compared on-board electricity generation from solar panels to grid charging. To enable a more precise comparison of the environmental impact between VIPV and grid charging, they selected "1 kWh of electricity delivered by the VIPV system" as the functional unit. This approach eliminates the variability associated with driving distance and allows for a direct comparison of the environmental impact per unit of electricity generated by the VIPV system versus the environmental impact per unit of electricity obtained from grid charging. The study's findings suggest that a 930 Wp PV system operating for 8 years with an average shading of 30% could potentially achieve around 18% lower emissions compared to grid charging. By increasing the shading factor to 40%, this advantage is diminished, as the emissions from the VIPV system become higher than those associated with grid charging. However, extending the operation duration to 12 years allows the breakeven point for installing VIPV to accommodate a shading factor of up to 55%, resulting in emissions comparable to those from grid charging. This study further highlights that the environmental benefits of VIPVs, as measured by LCA studies, depend heavily on three key factors: the location where the vehicle is used, the annual solar irradiation received in that location, and the carbon footprint of the electricity generation mix powering the local grid.

2.2.3 How to estimate carbon footprint reduction potentials

Estimating the carbon footprint reduction potentials involves assessing the current emissions and evaluating the impact of various reduction measures. This process, as illustrated in Kanz et al., (2020) study, begins with establishing a baseline by measuring the emissions associated with conventional energy sources. In this case, the study calculates the emissions from grid electricity. The potential reduction is estimated by comparing this baseline with the emissions from alternative solutions, such as using PV systems to power EVs. The LCA method used in the study considers the entire lifespan of the PV system, from production through use to disposal, taking into account factors like energy efficiency, system losses, and operational lifetime. By integrating PV-generated electricity, which has a lower environmental impact compared to grid electricity, the study demonstrates that significant reductions in carbon emissions can

be achieved, particularly when optimizing for factors such as minimizing shading and maximizing operational efficiencyof the carbon footprint reduction potentials achievable by VIPV across its entire lifecycle.

3 Methodology

This chapter outlines the methodology utilized to evaluate the GHG emissions reduction potential of VIPV-BEVs. A framework has been established to quantify the potential benefits of VIPV-BEVs. The framework includes an empirically based energy use and charging model and a method to assess the life cycle GHG footprint of VIPV-BEVs based on GHG emissions generated during solar panel manufacturing and avoided GHG emissions from the grid due to the reduced reliance on grid charging. Lastly, a sensitivity analysis is employed inspired by how assumed parameters may shift by the year 2030.

A functional unit of passenger car travel in kilometers over the course of one year is employed in this study to analyze the energy consumption and GHG emissions associated with travel. This choice enables a comprehensive comparison between pure BEVs and VIPV-BEVs across diverse geographical locations and conditions. By breaking down this annual travel pattern into hourly data points, the energy consumption and emissions per unit of delivered energy can be evaluated. Additionally, the corresponding reduction in grid-based charging for VIPV-BEVs is assessed by enabling solar energy penetration to the battery, allowing for a thorough examination of the GHG emission reduction potential of these vehicles.

3.1 Framework for assessing GHG emission reduction potential

The analytical framework is established, which combines data on solar irradiation, vehicle usage patterns, and estimations of lifecycle GHG emissions. The approach involves calculating the harnessed solar energy, assessing vehicle energy consumption, quantifying the reduced electricity that would otherwise be sourced from the grid, and estimating the GHG emissions based on statistics on GHG intensity from other sources. A schematic of this model, illustrating the key steps involved is presented in Figure 3.1.

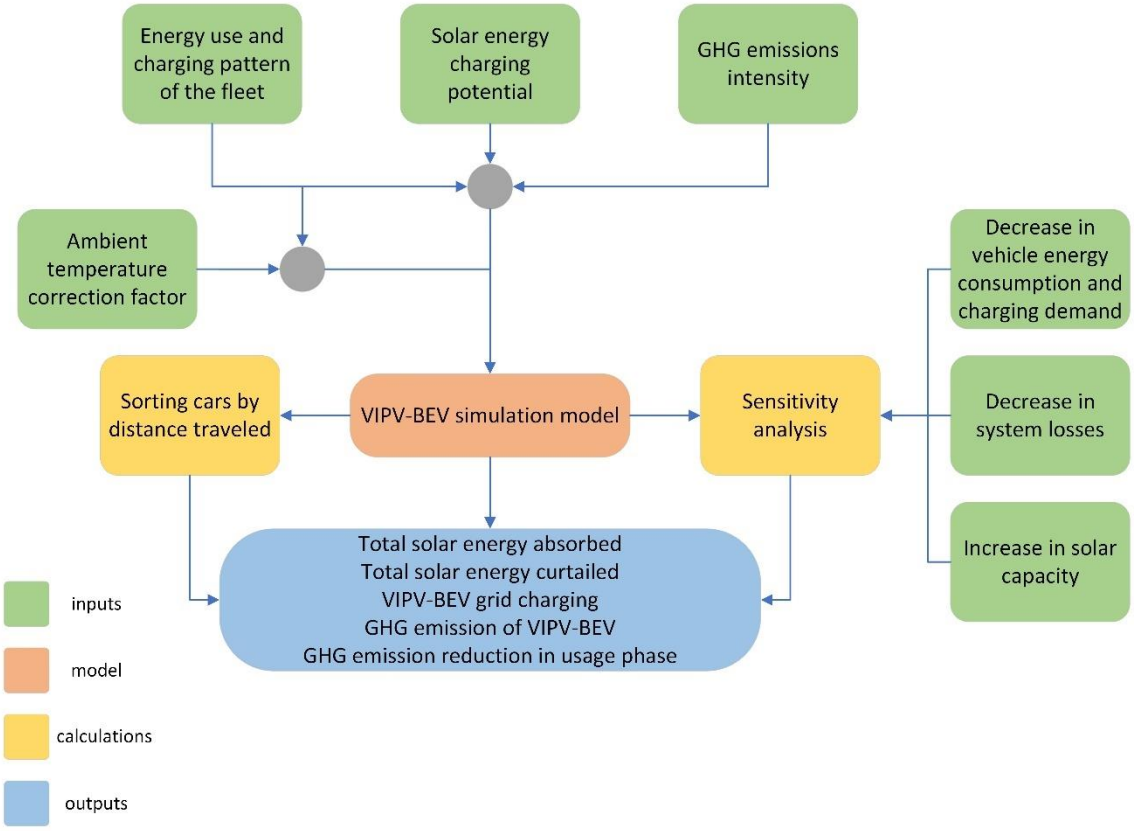

Figure 3.1 This figure depicts the constructed energy model for determining the generated electricity from solar energy, reduced electricity usage from the grid, and excess energy.

The complete utilization of onboard PV-generated electricity exhibits limitations due to the inherent variability in driver behavior and the finite capacity of the onboard battery. In other terms, the capability of absorbing solar energy is dependent upon both individual driving patterns and the storage capabilities of the car's battery. In cases where electricity is generated but cannot be stored due to capacity limitations, it will be curtailed (Komoto et al., 2021).

The GHG reduction potential is derived from the comparison between the GHG emissions of the pure BEV fleet and the VIPV-BEV fleet. When a pure BEV is charged using electricity from the grid, indirect GHG emissions are associated with it. Consequently, the anticipated decrease in energy demand from the grid due to the integration of photovoltaic systems in VIPV-BEVs is assumed to result in a reduction in GHG emissions, but this relationship is heavily influenced by the time of charging. As demonstrated by Arvesen et al. (2021) the emissions associated with electric vehicle charging can vary significantly depending on the charging profile and the corresponding electricity generation mix at different times of the day. Their study found that for Europe in the year 2050, day charging of electric vehicles showed the lowest emissions compared to other charging profiles. This highlights the importance of considering the temporal aspect of reduced energy demand from VIPV-BEVs, as the emission reduction potential may be maximized when the grid electricity being replaced has a high GHG intensity, which occurs during periods when the low-carbon generation sources have a lower proportion of the grid mix. To accurately quantify the GHG

emission reduction potential in this study, a comprehensive electricity system model that accounts for the temporal variations in the electricity grid's generation mix would be required. However, for simplicity, a generalized relationship between reduced energy demand and GHG emission reductions is assumed, acknowledging the potential variations based on the specific charging patterns and grid characteristics.

Given that both solar irradiation and the carbon emission intensity of the electricity grid are influenced by geographical location, different locations were chosen for this study. Gothenburg (Sweden), Los Angeles (USA), Taipei (Taiwan), and Madrid (Spain) were selected as focal points to explore the interplay between solar irradiation and the carbon emission intensity of the electricity grid. These locations were chosen for their diverse solar irradiation profiles throughout the year, coupled with the variations in temperature and their energy mix. It is important to note that Taipei, Taiwan, was chosen as a proxy for mainland China due to limitations in publicly available data on the hourly carbon emission intensity of the Chinese electricity grid.

Furthermore, considering that onboard PV generation fluctuates from time to time as influenced by seasonal and weather variations, an hourly time resolution has been employed for solar irradiation, carbon emission intensity, driving energy consumption, and charging energy demand for these locations. This level of granularity improves the precision of the assessment and provides valuable insights into capturing these fluctuations.

3.1.1 The VIPV-BEV simulation model

A VIPV-BEV simulation model is constructed to establish a reference for evaluating the GHG reduction potential of VIPV-BEV systems. This scenario utilizes average data on solar irradiation from the past five years, from 2019 to 2023, to mitigate the effects of any extreme weather conditions that may occur in a single year. Meanwhile, specific vehicle energy consumption, charging energy demand, and carbon emission intensity over the year 2023 are used.

An assumption is made that the GHG emissions from vehicle and battery manufacturing, and end-of-life of the pure BEV and VIPV-BEV are the same, which is at 26.9 ton CO_2-eq according to Evrard et al. (2021), and the GHG emission penalty is added to VIPV-BEV due to the manufacturing of onboard solar PV. Figure 3.2 below shows the illustration of which GHG emission reduction potential is seen in VIPV-BEV as compared with pure BEV.

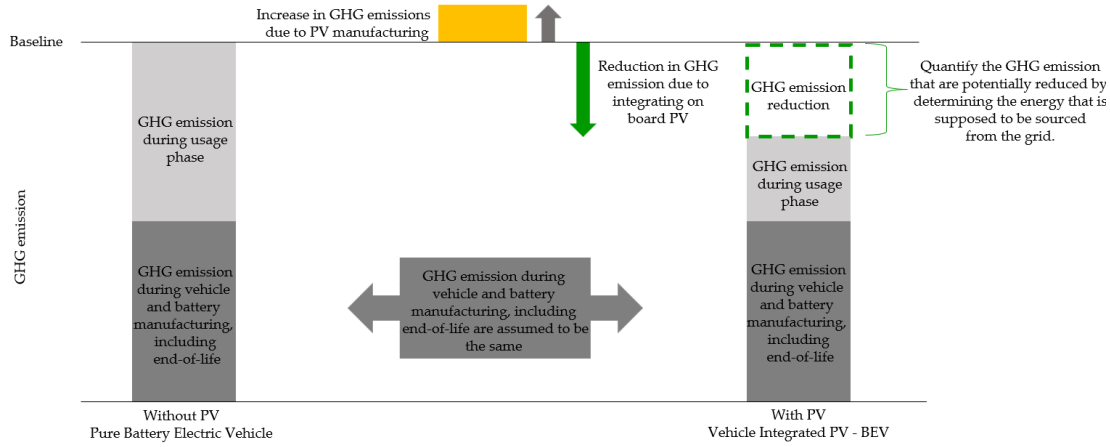

Figure 3.2. This figure shows how VIPV-BEV would potentially contribute to reducing GHG emissions.

To illustrate further, Figure 3.3 demonstrates the methodology employed to calculate the potential reduction in GHG emissions from VIPV-BEV during its operational phase only. This reduction is attributed solely to the decreased reliance on grid-supplied electricity. The approach considers two key factors which are (1) the diminished consumption of grid electricity and (2) the associated GHG emissions mitigated by integrating PV systems into the vehicle (Komoto et al., 2021).

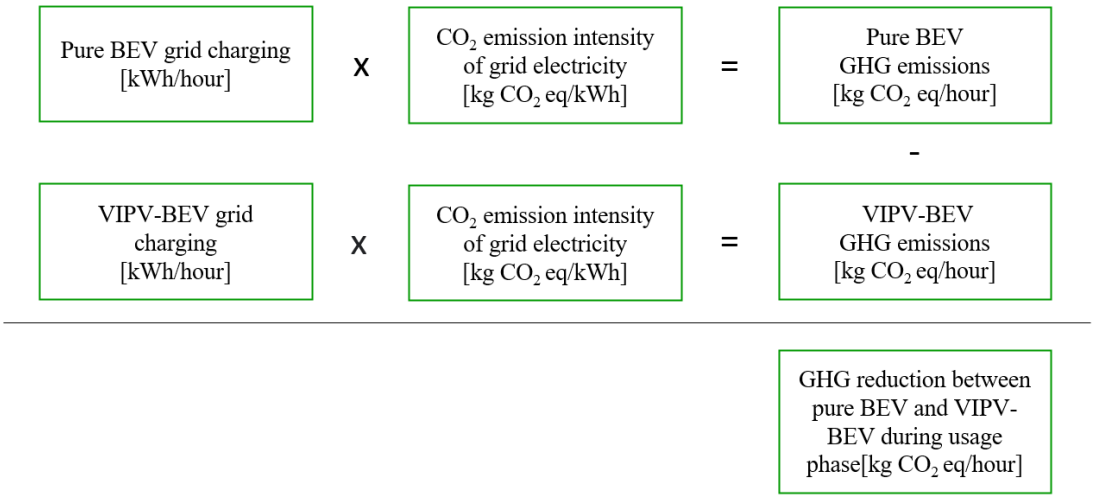

Figure 3.3. This figure shows the approach to computing the GHG emission reduction of VIPV-BEV during the usage phase.

The proposed framework employs a calculation flow to quantify the reduction in grid energy usage, as depicted in Figure 3.4. The energy sourced from the grid for pure BEV is denoted as "Electricity from the grid". On an hourly basis, this grid electricity is multiplied by the corresponding carbon emission intensity to determine the equivalent CO_2 emissions associated with a pure BEV operation.

After conducting the simulation and determining the pure BEV GHG emissions during the operation phase, the onboard PV electricity generation was incorporated. The model assessed whether the available solar energy would be absorbed or curtailed. To incorporate the potential benefits of solar energy, the framework models the integration of onboard PV electricity generation into the battery system. By introducing this

renewable energy source, the model computes the reduced grid energy demand as the solar energy penetrates the battery system. Furthermore, the model quantifies the absorbed solar energy and the curtailed solar energy when the state of charge (SOC) reaches its maximum limit.

The VIPV-BEV absorbs available solar energy in each hourly iteration starting from the first hour of the year, whether the vehicle is driving, charging, or in a parked position. Energy absorption stops when the battery's SOC is in full condition. The charging hour for the VIPV-BEV is synchronized with the charging hour of the pure BEV. This temporal alignment directly compares the two vehicle configurations, facilitating an assessment of the energy savings achieved through the VIPV system. Once the amount of energy needed for VIPV-BEV charging is determined, the "Charging losses" are added to determine the VIPV-BEV grid charging. Based on assessment by Volvo Cars, these "Charging losses" are assumed to be equivalent to 10% of energy from the grid compared to actual energy stored in the battery, primarily caused by losses in AC/DC conversion but also due to electrical consumers such as the battery management system (BMS) and other monitoring functions being active during the charging. Once the VIPV-BEV grid charging is determined, its corresponding carbon emission intensity is multiplied, and its GHG emission is calculated. Since both BEV and VIPV-BEV GHG emissions are quantified, obtaining their difference is the GHG reduction potential during the usage phase. By implementing this calculation flow and incorporating solar energy generation, the framework aims to quantify the potential electricity demand usage reduction and associated benefits of integrating PV systems into EVs.

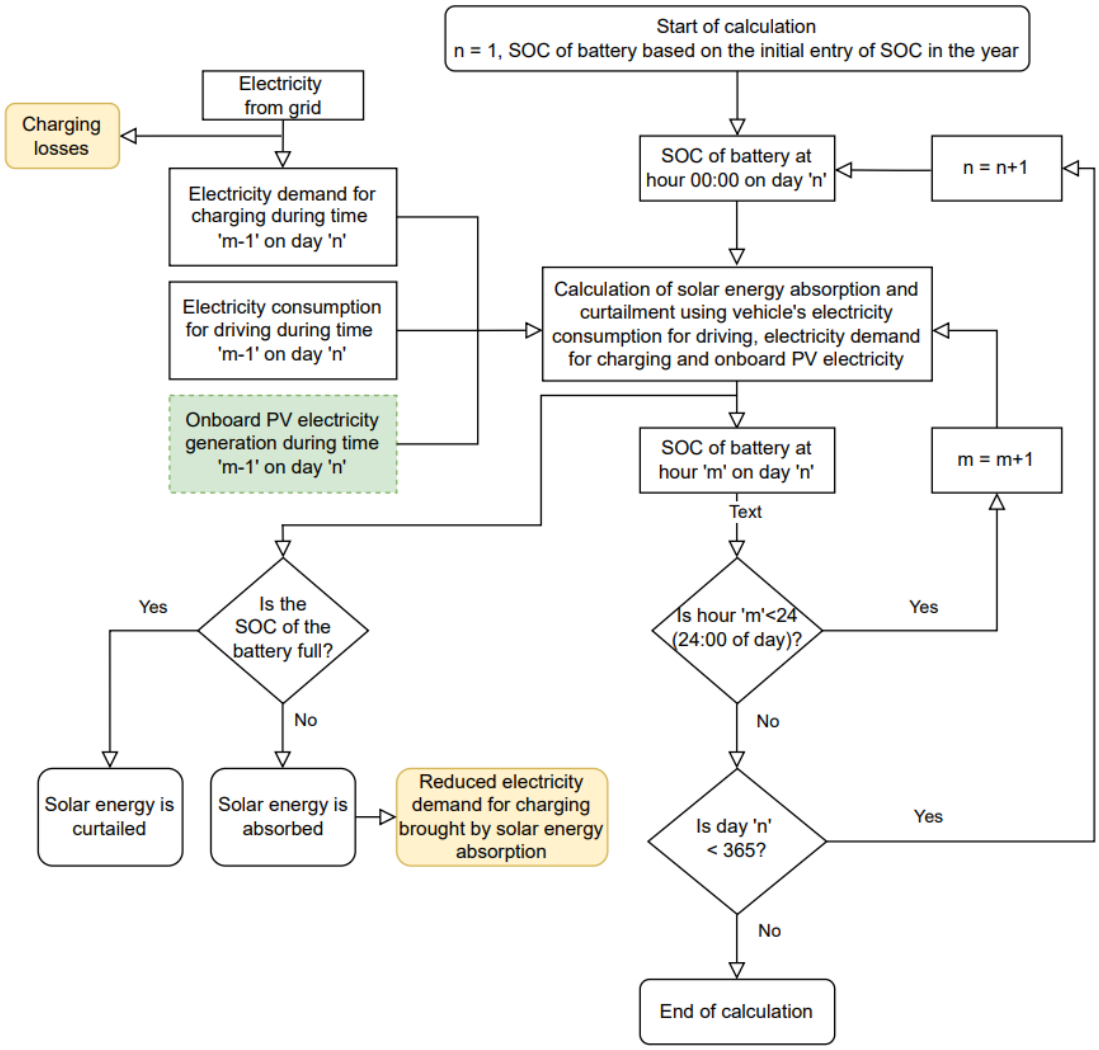

Figure 3.4. This figure shows the calculation flow on computing the absorbed solar energy, curtailed solar energy, and the VIPV-BEV electricity demand for charging.

As for GHG quantification, each car had the same life cycle GHG emissions for onboard solar PV. According to an LCA by Kanz et al. (2020), the manufacturing process of a 930-watt-peak (Wp) solar PV system emits 1143 kg of CO_2-eq. The solar PV systems are manufactured in China, using China's electricity grid mix, and then shipped to Germany for integration and assembly into the vehicles, using Germany's electricity grid mix. By specifying the manufacturing and integration locations, it shows that the electricity mixes of both China and Germany influence the manufacturing GHG emission of the solar PV system. In the VIPV-BEV simulation model, a 500 Wp solar PV system is used. Assuming that the manufacturing emission is proportional to the watt-peak of the VIPV system, a straightforward calculation was performed to determine the life cycle emissions of a 500 Wp system which is denoted as GHG emissions for VIPV. This was calculated by scaling the estimate from Kanz et al. (2020) for a 930 Wp system.

The average GHG reduction potential of the fleet was then calculated using equation (3-1) below wherein $GHG_{op,t}$ stands for GHG emission during operation at any time (t), VL represents for vehicle life and $VIPV_{GHG\ emission}$ denotes for the GHG emission of the VIPV during its manufacturing stage.

$$\frac{\sum_{car=1}^{fleet\ size}(\sum_{t=1}^{8760} BEV_{GHG\ op,t} - \sum_{t=1}^{8760} VIPV{-}BEV_{GHG\ op,t})}{fleet\ size} \cdot VL - VIPV_{GHG\ emisssion} \quad (3\text{-}1)$$

To ascertain the GHG reduction potential per vehicle, the calculated value was divided by the fleet size, totaling 352 cars which is then multiplied by the life of the vehicle which is assumed to be 15 years based on Evrard et al.'s (2021) estimation and to be reduced with the GHG emissions for VIPV. This normalization process ensured that the result represented the average GHG reduction potential attributable to each vehicle within the fleet.

3.1.2 Categorizing car users based on distance travelled

In the VIPV-BEV simulation model, each car's GHG emission reduction was assessed during its usage phase. In order to allow for an examination of the relationship between GHG emission reduction and annual distance travelled, the fleet was divided into four equal quartiles sorted from the shortest to the farthest distance travelled in a year. Each quartile has an equal number of populations which is 88 cars. Inspired by the methodology of Hiselius & Rosqvist (2018), this approach ensures an equal distribution of vehicles across quartiles. Table 3.1 below presents the grouping description below.

Table 3.1. Summary of car groupings with corresponding population and annual distance driven.

Group type	Number of cars	Distance range, km
Long-distance car users	88	18400 - 45321
Mid-distance car users	88	11238 - 18267
Moderate-distance car users	88	3605 - 11200
Short-distance car users	88	70 - 3591

3.1.3 Estimation of solar energy charging potential

To estimate the potential for solar energy charging (E, kWh) within the investigated VIPV-BEV fleet, this study employs a methodology for computing solar energy generated based on acquired solar irradiance data from the online source "Renewables.Ninja" (*Renewables.Ninja*, 2016). This data is then incorporated into an equation to calculate the solar energy generation of solar PV:

$$E = H \cdot t \quad (3\text{-}2)$$

where

- E is solar energy generated (kWh),
- H is simulated solar power generation from Renewables. ninja (kW), and
- t is the time interval (hour).

The solar panel capacity (S), signifies the maximum power output under optimal conditions. This capacity is compared against the calculated H from the simulation to ensure the solar panel capacity is sufficient to handle the expected power generation for each hour which is mathematically expressed below.

$$S \geq H \; \forall \, t \tag{3-3}$$

3.1.4 Renewables.ninja

Renewables.ninja (*Renewables.Ninja*, 2016) is a web-based tool that simulates the potential generation of wind and solar energy for single locations or countries around the globe (Pfenninger & Staffell, 2016). It includes the MERRA-2 climate dataset for the period 1980-2023. To model PV power, the tool combines irradiation based on MERRA-2 for a given solar PV capacity, tilt angle, azimuth angle, and system loss. To validate these simulations, data from over 1000 PV systems and national aggregate outputs, as reported by transmission network operators, were collected in a time series format, incorporating significant correction factors to ensure accuracy (Pfenninger & Staffell, 2016).

The following are the technical assumptions that were applied to retrieve the available solar energy output from the onboard PV system and ambient temperature in an hourly resolution.

- **Ambient temperature and solar irradiation:** Ambient temperature and solar irradiation data spanning from the year 2019 to 2023 are obtained from the MERRA-2 dataset. This dataset provides information on the sunlight intensity and duration at specific locations, facilitating an evaluation of solar energy availability for electric vehicle charging across different geographical regions. To accommodate broader weather variations, data from the five years were averaged hourly, yielding an annual dataset representative of typical hourly conditions.

- **Solar PV efficiency:** This temperature-dependent factor represents the percentage of sunlight converted into usable electrical energy by the solar panels on the car. The energy conversion efficiency of PV modules exhibits a non-linear relationship with both irradiance level and module temperature. This relationship typically manifests as a decline in efficiency at both low irradiance and high operating temperatures (Huld et al., 2010). To account for this, the panel temperature is derived from the surrounding ambient temperature, while also considering the impact of sunlight exposure on efficiency (Pfenninger & Staffell, 2016).

  In the context of utilizing Renewables.ninja for this study, explicit specification of solar panel efficiency is not a prerequisite. The tool's settings account for efficiency factors such as solar irradiance and any user-provided panel specifications. The required solar PV capacity of 0.5 kW is directly inputted into the web tool for simulation. However, to provide additional context regarding the practical implications of achieving the specified 0.5 kW solar PV capacity, a crystalline

silicon (c-Si) solar PV system with a module efficiency of 24.4% (Green et al., 2021) can be used as an example. This would necessitate an active area of approximately 1.64 m^2 on the roof of a car for panel installation.

- **System losses:** A conservative estimate of 25% system loss is employed on top of the solar PV efficiency, encompassing factors such as partial shading, curvature of the PV module, mismatches in electrical connections, or transformation losses during power conversion (Centeno Brito et al., 2021).

- **Tilt angle:** The PV panels are integrated into the car's roof with a tilt angle assumed to be zero degrees (0°). While changing the azimuth could impact solar irradiation results in other scenarios, for VIPV, where the solar panels are fixed on the roof of the car with a tilt angle of zero degrees, the azimuth is not considered to have an impact.

- **Hourly resolution:** A high-resolution approach is adopted by investigating the solar energy potential with an hourly resolution (t, hr). This granular analysis allows for a more accurate assessment of the charging potential and the calculation of the grid carbon intensity effect across different seasons and diverse weather patterns.

Figure 3.5 below shows a screenshot of the user interface for the Renewables.ninja online tool.

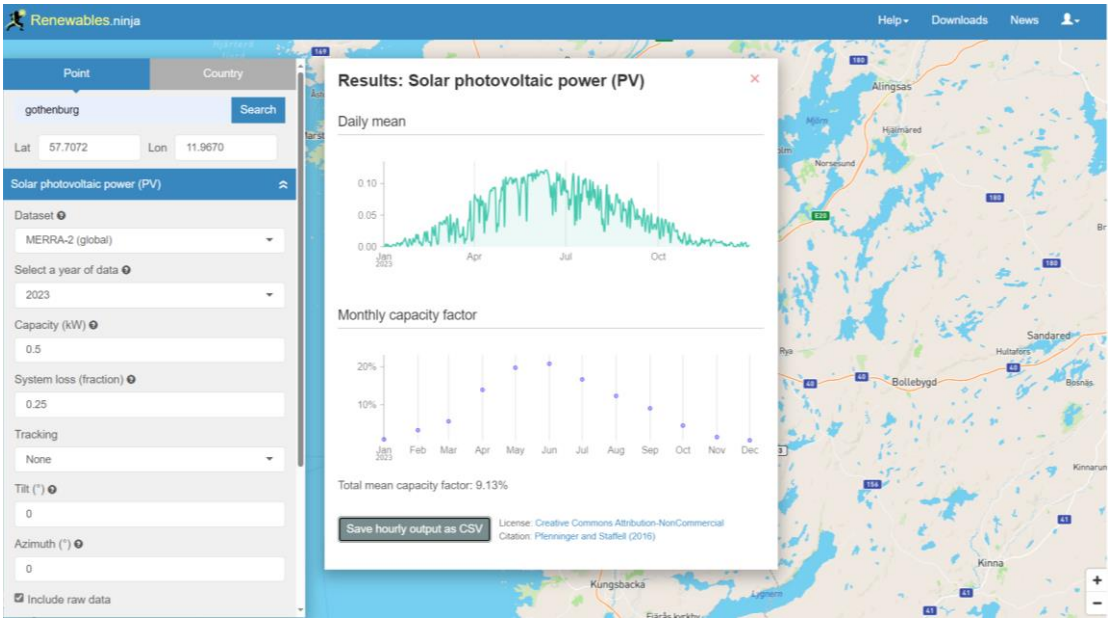

Figure 3.5. Screenshot of the Renewables.ninja web application.

3.2 Assessment of specific vehicle energy consumption

Another criterion that affects the GHG emission reduction potential of VIPV-BEVs is the specific vehicle energy consumption. A real-world driving dataset owned by Volvo Cars has been retrieved to construct the models. Table 3.2 presents the different signals used to perform the calculations.

Table 3.2. The car signals that were used in analyzing each energy pattern of a car.

Metric	Description
Event	An indication of the car's state (driving or charging). In case there is no event registered, the car is assumed to be parked.
Date and time	Starting date and time of the event
Discharged energy	Measures the total energy discharged from the high voltage (HV) battery, used for propulsion and climate/thermal systems.
Charging energy	Quantifies the energy influx to the HV battery, specifically categorizing it as charging energy.
State of Charge	Quantifies the remaining energy available in the HV battery expressed as a percentage of its full capacity (%).
Distance	Distance driven of vehicle (km)

From Volvo Cars' dataset, a subset of 352 vehicles, comprising XC40 and C40 models based in Gothenburg, was randomly selected. The subset was made to reduce computational time while ensuring that the sample is large enough for a meaningful analysis. For each vehicle, the dataset contains event-based metrics derived from the vehicle's sensor data, see Table 2.2. These metrics are calculated by processing the high-resolution time-series signals recorded by the vehicle's sensors during actual driving events. Each event in the dataset is associated with a specific start time, representing the moment when the driving commenced, and the vehicle's sensor data recording began. The metrics that were mentioned in Table 3.2 are used for the computing the absorbed solar energy, curtailed solar energy, and the VIPV-BEV electricity demand for charging as described in Figure 3.4. To match the hourly datasets from Renewables.ninja, the raw car sensor data encompassing charging energy, discharging energy, and distance were aggregated hourly. This synchronization ensures that the insights derived are based on comparable timeframes. Before integrating the vehicle energy datasets for the VIPV-BEV simulation model's development, each dataset was analyzed. Additionally, the patterns were examined across different seasons to assess any potential impact on the fleet's energy consumption and demand.

Considering that the ambient temperature can affect a car's energy consumption through factors such as increased air conditioning usage (i.e., heating or cooling), changes in aerodynamic drag, and altered battery performance, an ambient temperature correction factor provided by Volvo Cars was employed. This ambient temperature

correction factor is based on the same type of real-world fleet data used for driving and charging patterns, which associates temperature variations with the start time of driving events. It was applied to estimate the fleet's driving energy consumption in Los Angeles, Taipei, and Madrid relative to Gothenburg's driving pattern. Figure 3.6 below shows the ambient temperature correction factor utilized for this estimation, relating to ambient temperature deviations from Gothenburg to corresponding changes in energy consumption.

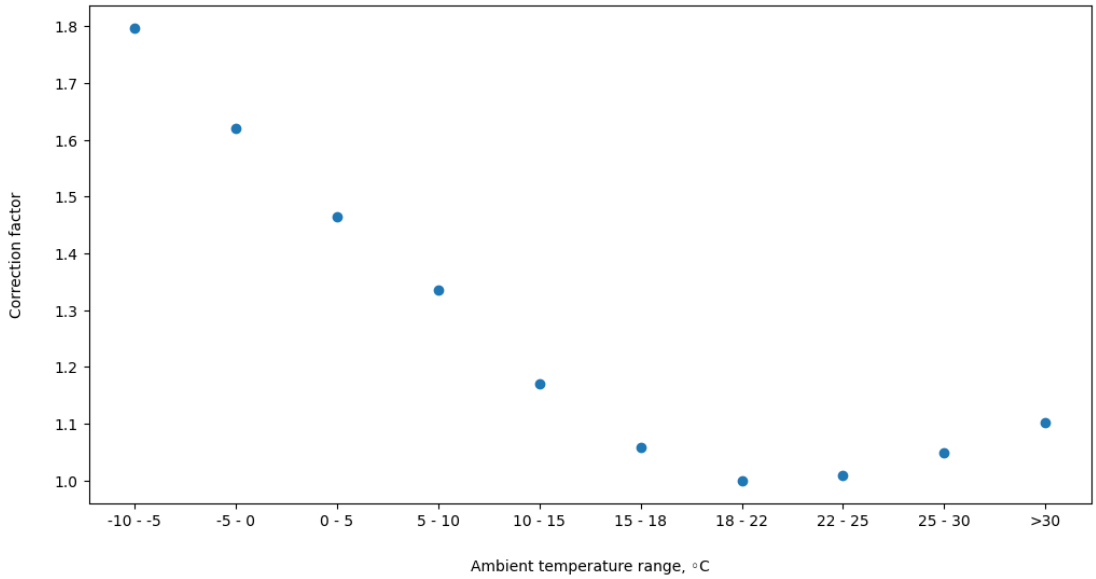

Figure 3.6. This figure shows the correlation used to extrapolate the energy consumption data from Gothenburg to the other cities.

A sample calculation for the manner of using the ambient temperature correction factor is available in the Appendix A which is governed by equation (2-4) below wherein *D* stands for energy consumption for driving while *A* is the Ambient temperature correction factor.

$$D_{city} = D_{Gothenburg} \cdot \frac{A_{temperature\ of\ the\ city}}{A_{temperature\ of\ Gothenburg}} \qquad (2\text{-}4)$$

3.3 GHG emission reduction potential analysis and comparison

The average carbon intensity is defined as the total GHG emissions released in the atmosphere divided by the electricity generated in a zone at a given time. The average carbon intensity may be computed at the country, regional, or global scale (Ang & Su, 2016). In contrast, the marginal carbon intensity at a specific point is defined as the reduction in GHG emissions within the electrical network resulting from a small decrease in electricity demand (Ruiz & Rudkevich, 2010). The carbon intensity of electricity in a given region is influenced by the composition of its power generation sources and their respective carbon intensity values as noted by Ang & Su (2016). Average carbon intensity was chosen in this study to help understand the general trend and impact of the entire electricity generation mix, making a broad overview of the

emissions associated with electricity generation over a period. Throughout the report, the term ‘carbon intensity’ or ‘GHG emission intensity’ is referring to average carbon intensity.

ElectricityMaps (*ElectricityMaps*, 2022) is an online database that collects real-time data from electricity generation and imports/exports from around 160 regions globally (Tranberg et al., 2019). The dataset representing a full year can be shown in hourly, daily, or monthly resolution. It provides the carbon intensity of electricity consumed in a specific region, which takes into account cradle-to-grave life-cycle emissions of electricity production. This metric is expressed in terms of grams of carbon dioxide equivalent per kilowatt-hour, gCO_2eq/kWh.

The carbon intensities were lifted from ElectrictyMaps which were computed based on the whole lifecycle of employed fuels and generation technologies. Emissions resulting from the extraction of resources required to build up installed capacity, emissions from direct operations, and end-of-life-related emissions are all accounted for. ElectricityMaps uses reliable sources to collect data, including transmission system operators, government agencies, and energy utilities. When real-time data is unavailable, ElectricityMaps employs estimation methods based on external and internal forecasts (*ElectricityMaps*, 2022).

Each city shows a distinct pattern of carbon emission intensity over the specified period. Figure 3.7 shows the daily interval of average carbon intensities for Gothenburg, Los Angeles, Taipei, and Madrid from January 01, 2021, to December 31, 2023. Gothenburg maintains a consistently low intensity, suggesting a relatively clean electricity grid likely due to a high share of renewable energy sources in its energy mix. In contrast, Taipei’s emission intensity is the highest, indicating a substantial dependence on carbon-based fuels. Los Angeles exhibits moderate emission levels with notable fluctuations, positioning its carbon intensity above Gothenburg's yet below Taipei's. Madrid also displays moderate emission intensities, punctuated by occasional spikes, yet its overall carbon footprint remains lower than that of Los Angeles. As for observation of the carbon emission intensity trend as the season varies, there is a clear recurring pattern in Los Angeles while in Gothenburg, Taipei, and Madrid data are less pronounced.

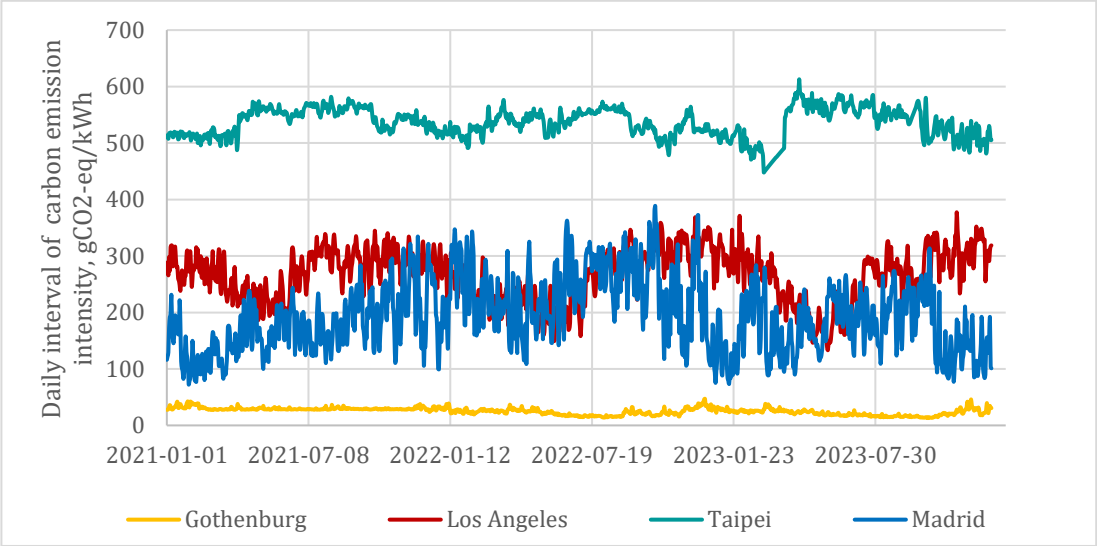

Figure 3.7. This figure displays the daily variation of carbon emission intensities for Gothenburg, Los Angeles, Taipei, and Madrid expressed in gCO2-eq per kWh spanning from January 01, 2023, to December 31, 2023.

Figure 3.7 highlights the differences in carbon intensity between cities and serves as the basis for analysis of GHG emissions. In this study, for each aggregated hour of electricity demand for charging (C) for the year 2023, there is a corresponding carbon intensity (I) at that hour for the year 2023 for the assumed location. The GHG emission for that hour are calculated by multiplying the electricity demand for charging (C) by the carbon intensity (I) which are shown in equation (2-5) and equation (2-6) below.

$$BEV_{GHG\ emission\ during\ operation,t} = C_{BEV,t} \cdot I_t \quad (2\text{-}5)$$

$$VIPV - BEV_{GHG\ emission\ during\ operation,t} = C_{VIPV-BEV,t} \cdot I_t \quad (2\text{-}6)$$

3.4 Sensitivity analysis

Building upon the assessment of the potential for solar energy integration in EV charging under current conditions, this study employs a sensitivity analysis to explore how advancements in technology might influence this potential by the year 2030. A sensitivity analysis offers a valuable alternative, allowing for an initial exploration of future scenarios by systematically varying key parameters within realistic future ranges. In-depth modeling of these advancements, while valuable for a comprehensive understanding, can be computationally intensive and time-consuming.

The sensitivity analysis incorporates the following parameters to explore potential future advancements in solar energy integration for EV charging, these assumed changes to the parameters were developed in collaboration with experts at Volvo Cars, based on discussions regarding projected technological advancements and practical implementation considerations.

Vehicle energy efficiency: Changes in vehicle energy consumption by decreasing both the driving energy consumption and charging energy demand by 10% are simulated to understand their effect on the overall energy consumption and the potential benefits of

solar charging. This is supported by the forecasted technical improvements such as improved tire rolling resistance, improved driveline and engine efficiency, improved aerodynamics, reduced weight and reduced cooling and heating loads of pure BEV.

Solar panel capacity: The impact of increased solar panel capacity from 0.5 kW to 1.0 kW on the solar energy generation potential is evaluated. While a doubling of PV cell efficiency by 2030 may not be fully anticipated, this range is used to illustrate the sensitivity of the system to potential advancements in solar technology, enabling higher wattage panels within the same area. Improvement in cell efficiency allows more solar energy generation without significantly increasing the required surface area on EVs.

System losses: The analysis assumes a 50% reduction in system losses for integrated PV cells in BEVs, from 25% to 12.5%, by 2030. This assumption is based on internal discussions and projected advancements in PV cell technology, optimized electrical connections, and improved manufacturing processes. Maturing integration designs will also minimize losses from curvature and shading.

Carbon intensity of electricity generation: The anticipated changes in carbon intensity, as projected by the IEA in the Sustainable Development Scenario, are examined across various regions worldwide. Trends from 2010 to 2040, as depicted in Figure 3.8 for different global regions, serve as a basis for the assumptions made in the sensitivity case. Focusing on the 2025 to 2030 timeframe, the IEA (2021)'s scenarios suggest an annual decrease of 9% in the United States, 7% in China, and 12% in Europe. Note that this analysis uses solely these percentages to serve as projections for changes in carbon intensity of the electricity generation in the future and does not incorporate considerations of the future electricity grid's actual configuration or other relevant parameters. The calculation of the decrease in carbon emission intensity is shown in the Appendix B which is governed by equation (2-7) below wherein *P* stands for the available carbon emission intensity data, *F* stands for the future carbon emission intensity, *n* as the number years in between *P* and *F* while *r* represents the rate of carbon emission intensity.

$$F = P(1 + r)^n \tag{2-7}$$

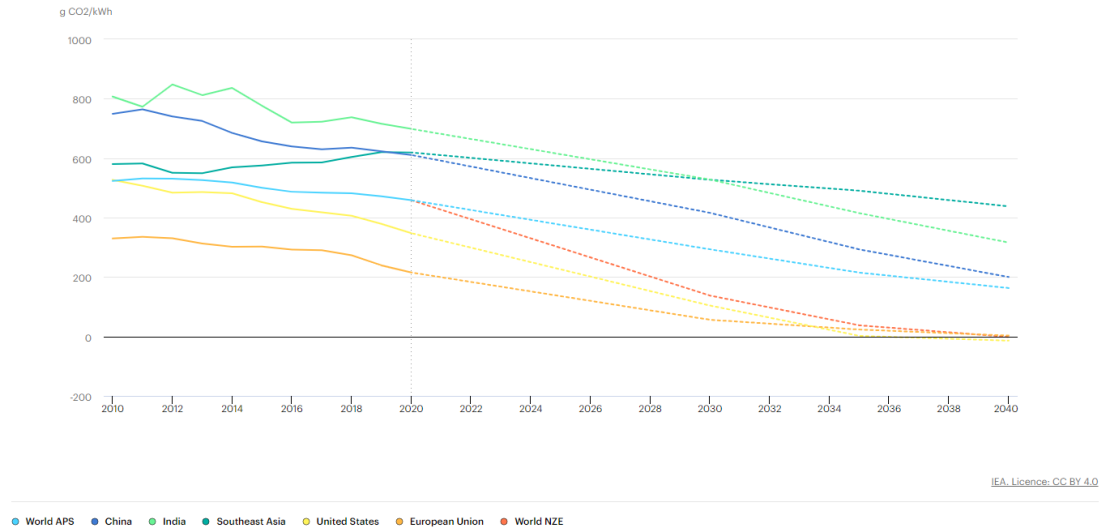

Figure 3.8. Projected changes in carbon intensity from 2010 to 2040 for different regions in the world (Source: IEA, 2021).

VIPV manufacturing: The analysis assumes that the GHG emissions for manufacturing a 500 Wp is lesser compared to the base case scenario. Aligned with the green manufacturing sensitivity case by Kanz et al. (2020), a 34% reduction was applied in the sensitivity analysis to represent potential improvements. Applying this projected improvement rate to the current GHG emissions for manufacturing was performed and used in the sensitivity analysis.

4 Results and analysis

This chapter presents the results and analysis obtained by integrating data on solar irradiance, vehicle energy consumption, and carbon emission intensity into the developed VIPV-BEV simulation model to understand the potential of VIPV-BEVs in terms of GHG emission reduction and energy conservation compared to grid energy usage. Additionally, this chapter explores the sensitivity of the results to key assumptions and parameters through a sensitivity analysis that is inspired by developments that may occur up until 2030.

4.1 The base case - energy use and greenhouse gas emissions for pure battery electric vehicles

The base case represents a fleet of 352 cars, featuring Volvo XC40 and C40 models as pure BEVs. The datasets for specific energy consumption, charging energy demand, state of charge (SOC), and distance travelled are sourced from a database that records signals reflecting the behavior of these cars, all situated in Gothenburg, Sweden.

4.1.1 Driving pattern of the fleet

To understand car usage behavior, the driving patterns of the fleet were analyzed. Figure 4.1 illustrates the average distance travelled by cars for each hour of the day which is expressed as average km/car. This was determined by taking the total distance travelled by all cars in the fleet during each hour throughout the year and dividing it by the total number of cars in the population. During the early morning hours (00:00 – 03:00), the average distance travelled is very low, indicating minimal car movement. At the start of the morning (04:00 – 06:00), there is a significant increase in the average distance travelled, starting at 04:00 and peaking around 05:00. This likely corresponds to morning commutes. From 07:00 to 12:00, the average distance travelled continues to increase, suggesting consistent car usage during these hours. The highest average distance travelled occurs in the afternoon (13:00 – 15:00), with a peak around 14:00, likely corresponding to afternoon commutes. There is a noticeable decline in the average distance travelled starting from 16:00, which continues to decrease through the evening hours until 21:00. During the late-night hours (22:00 – 23:00), the average distance travelled is low again, similar to the early morning hours, indicating minimal car movement.

It is worth mentioning that the peak travel times in this dataset occur earlier than is typically expected. A study by Liu et al. (2015) shows cumulative driving distances with later peak times compared to these findings. The earlier peaks in the data could be attributed to the specific characteristics of the sample.

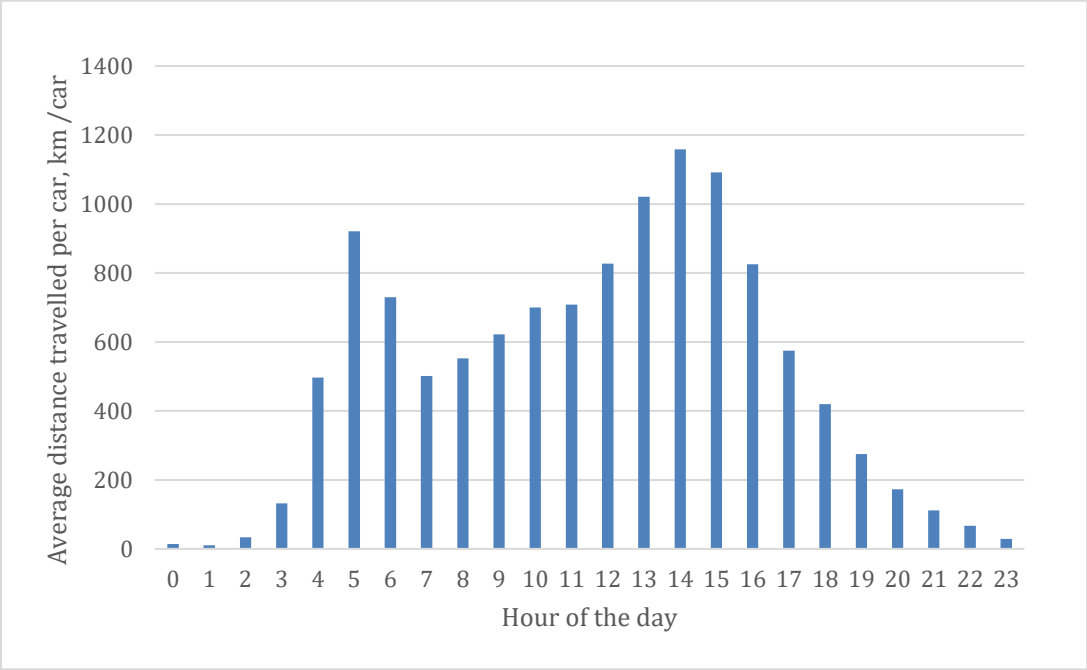

Figure 4.1 This figure illustrates the average distance travelled by cars for each hour of the day which is expressed as average km/car. This was calculated by taking the total distance travelled by all cars in the fleet during each hour throughout the course of the year 2023 and dividing it by the total number of cars in the population.

4.1.2 Energy use and charging patterns

To further understand car usage behavior, the fleet's energy use and charging patterns were analyzed. Figure 4.2 illustrates the average electricity consumption for driving for each hour of the day. This was done by obtaining the total electricity consumption in the fleet during each hour throughout the year and dividing it by the total number of cars in the population. During the early morning hours (00:00 – 3:00), the average electricity consumption is very low, indicating minimal vehicle activity and energy usage. This aligns with the low average distance travelled during these hours, as shown in the driving pattern analysis.

As the morning begins (04:00 – 06:00), average electricity consumption significantly increases, starting at 04:00 and peaking around 05:00. This increase corresponds to the morning commute period, when more vehicles are in use, leading to higher energy demands for transportation.

From 07:00 to 12:00, the average electricity consumption continues to rise, suggesting consistent and sustained vehicle activity and energy usage during these daytime hours. This period shows a steady increase in energy consumption, reflecting the ongoing use of vehicles for various activities.

The highest average electricity consumption occurs in the afternoon (13:00 – 15:00), with a peak around 14:00. This peak likely corresponds to the afternoon commute

period, where many vehicles are in use simultaneously, resulting in the highest energy demand of the day.

After the afternoon peak, the average electricity consumption begins to decline, gradually decreasing through the evening hours until around 21:00. This decline mirrors the reduction in vehicle activity as people return home and use their vehicles less frequently.

During the late-night hours (22:00 – 23:00), the average electricity consumption is low again, similar to the early morning hours, indicating reduced vehicle activity and energy usage.

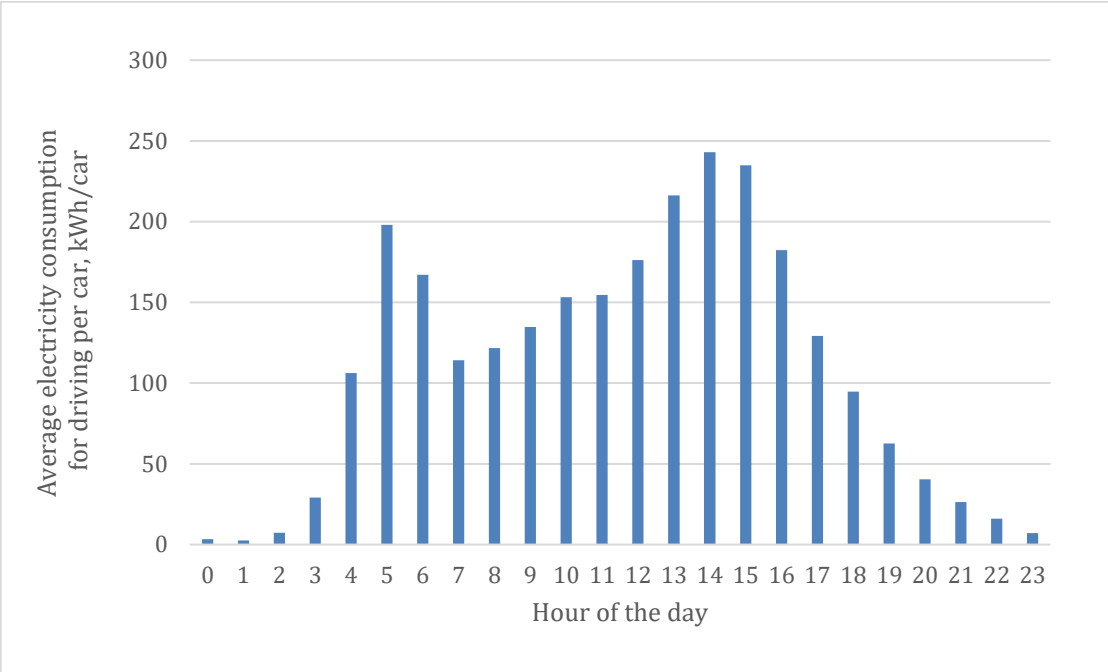

Figure 4.2. This figure shows the average electricity consumption for driving for each hour of the day. This was done by obtaining the total electricity consumption in the fleet during each hour throughout the year and dividing it by the total number of cars in the population.

The driving pattern of the fleet was further investigated by analyzing distinct seasonal variations, as depicted in Figure 3. This categorizes the electricity consumption for driving by season. December through February is designated winter, March to May as spring, June to August as summer, and September to November as fall. The seasonal variation graph reveals several interesting patterns.

Seasonal variations are evident, with winter showing generally lower consumption levels than other seasons, likely due to reduced driving activity in colder weather. Conversely, summer shows higher peaks, possibly due to the increased travel movement of vehicles. The graph shows moderate average electricity consumption during the spring and fall seasons. During the early morning hours (00:00 – 03:00), the average electricity consumption is very low across all seasons, indicating minimal vehicle activity.

At 04:00, there is a noticeable increase in electricity consumption, particularly in summer, spring, and fall, which suggests the beginning of early morning commutes. Winter also shows an increase but is less pronounced than other seasons.

At 05:00, the electricity consumption peaks significantly and starts to show some evident variation among the seasons. Summer, spring, and fall continue to exhibit higher consumption levels than winter. This indicates sustained vehicle activity as the morning commute continues (06:00 – 12:00). The lower consumption in winter can be attributed to reduced driving activity due to colder weather and possibly shorter daylight hours.

The highest average electricity consumption occurs in the afternoon (13:00 – 15:00), with a peak around 14:00, likely corresponding to the afternoon commute period. This peak is most pronounced in summer and fall, indicating higher energy demands during these seasons.

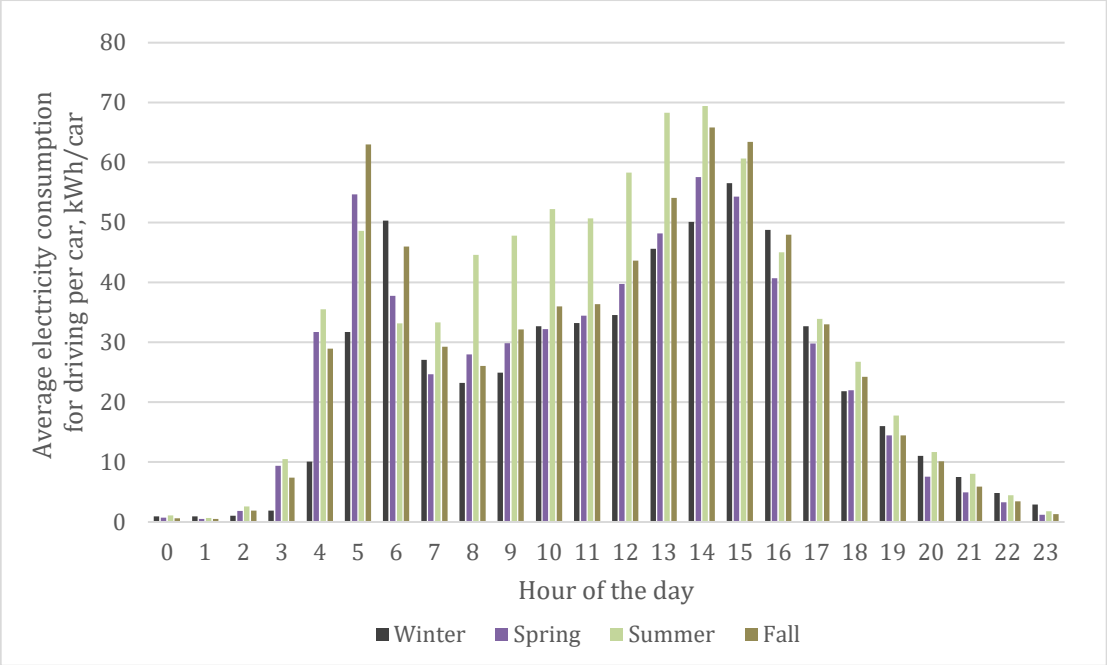

Figure 4.3. The graph illustrates the average hourly electricity consumption for driving throughout the day, categorized by season.

The charging pattern of the fleet was also analyzed, which is presented in the average electricity demand for charging electric vehicles throughout the day, measured in kilowatt-hours per car as illustrated in Figure 4.4. This was done by calculating the total electricity needed for charging of the fleet during each hour throughout the year and dividing it by the total number of cars in the population. The data reveals a pattern in the charging behavior of the fleet. During the early morning hours, between 00:00 to 03:00, there is a noticeable dip in the average electricity demand, suggesting minimal charging activities during these times. As the day progresses, the average electricity demand for charging gradually increases, starting from 04:00 and dips again until 8:00, a continued steady rise is observed from 09:00 until 23:00. This trend indicates a preference for nighttime charging over daytime charging. One possible contributing factor to this pattern is that people tend to charge their vehicles after arriving home from

work, with most of the charging occurring between 20:00 and 23:00. This allows them to ensure their vehicles are fully charged for the next day's commute.

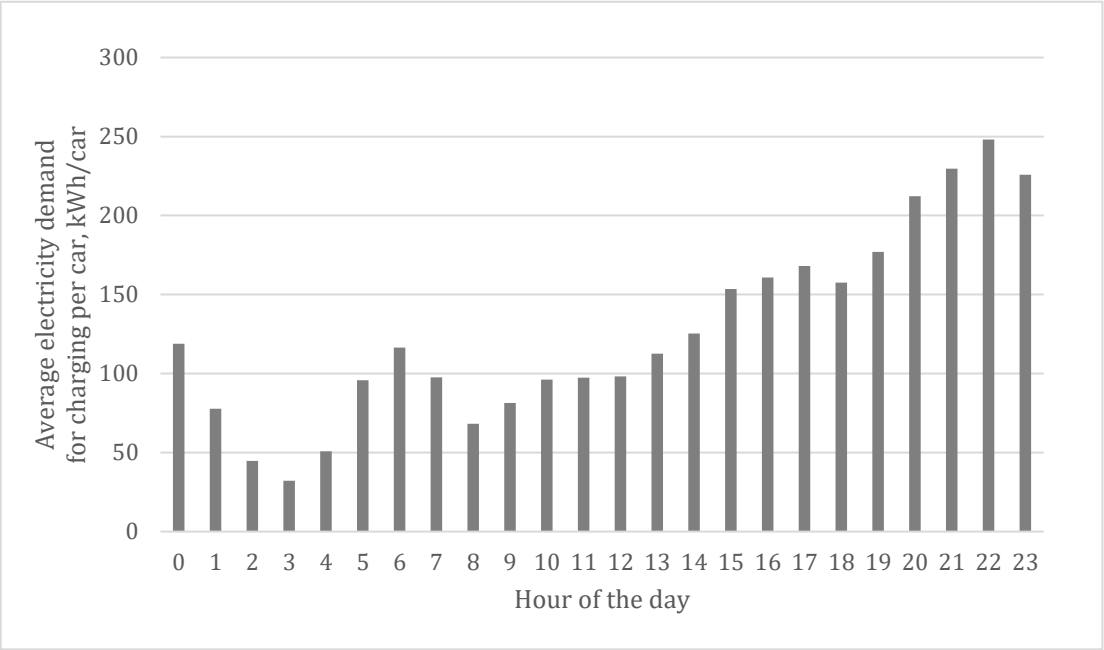

Figure 4.4. This figure shows the average electricity demand for charging for each hour of the day. This was done by calculating the total electricity needed for charging the fleet during each hour throughout the year and dividing it by the total number of cars in the population.

The charging pattern of the fleet was further examined, considering distinct seasonal variations, as presented in Figure 4.5. These fluctuations align with the overall system's charging behavior, as shown in Figure 4.4. Similar to the season variations for energy use, winter shows generally lower consumption levels than other seasons and summer shows higher peaks. Conversely, spring and fall show moderate average electricity demand for charging. The magnitude of these variations corresponds to the changes in average electricity consumption for driving.

In winter, the average electricity demand for charging starts relatively low during the early morning hours between 02:00 and 04:00, then remains moderate throughout the whole day. There is a noticeable increase in demand starting from the late afternoon around 16:00, peaking significantly between 21:00 and 23:00.

The summer graph shows a trend of low demand in the early morning hours between 01:00 and 04:00, and an increase with some fluctuations throughout the whole day. With an increase in average electricity demand for charging compared to other seasons, the data also suggest that car users tend to not only drive more during the daytime in summer but also charge more during the daytime. This observation suggests that car users often plug in their vehicles whenever they park, not just overnight. As for the average electricity demand for charging in summer compared to winter, the levels are higher. The peak demand occurs between 20:00 and 22:00.
In spring, there is low demand in the early morning hours between 02:00 and 03:00, the increase in demand starts earlier in the day, around 10:00, and remains relatively high

throughout the whole day. The peak demand occurs slightly earlier, between 20:00 and 22:00, compared to winter.

In fall, the peak demand occurs between 20:00 and 22:00 and shows an overall demand level which is closer to those observed in summer. Overall, these graphs highlight the seasonal variations in charging, with low trends of average electricity demand during the early morning (01-04:00) and peak during the evening (20:00 – 23:00).

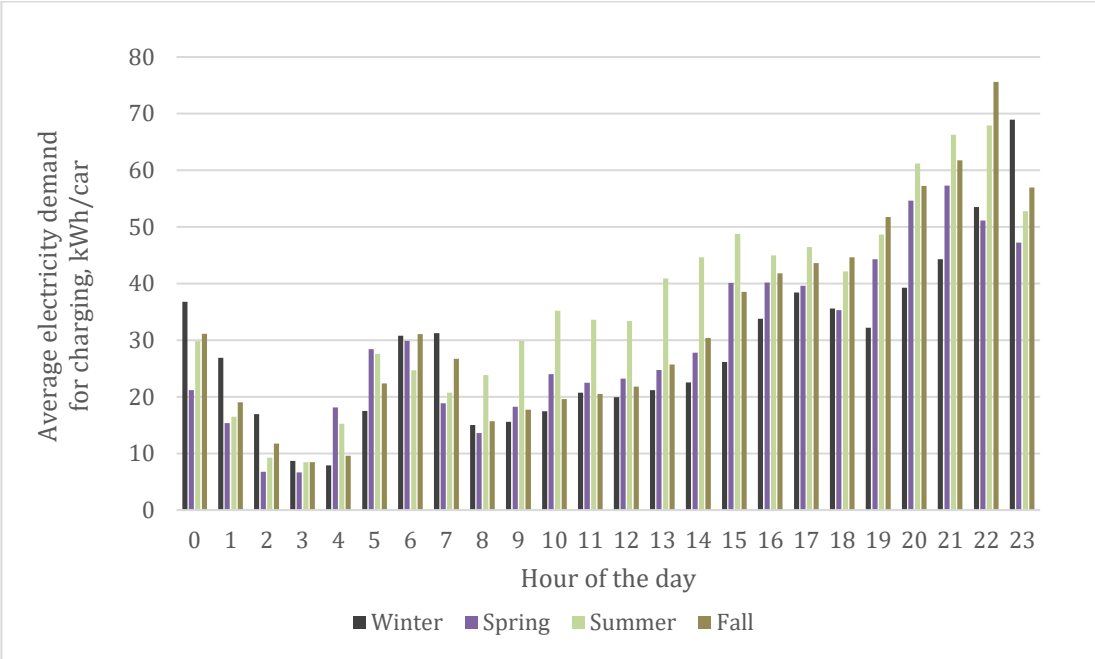

Figure 4.5. The graph illustrates the average electricity demand for charging throughout the day, categorized by season.

4.1.3 Impact of ambient temperature on vehicle energy consumption

Energy consumption during driving is significantly influenced by ambient temperature due to factors such as air density variations, tire rolling resistance, and demands for heating or cooling within the vehicle cabin. To explore the impact of ambient temperatures across different regions, energy consumption data from vehicles in Gothenburg were adjusted to simulate the conditions experienced in Los Angeles, Taipei, and Madrid. This adjustment allows for an assessment of how varying ambient temperatures affect energy consumption, while accounting for temperature differences among these locations.

The results are presented with a violin plot as shown in Figure 4.6 to illustrate the distribution of ambient temperatures across the four cities based on the hourly average temperature over the past five years. In Gothenburg, the plot indicates a median temperature of 8.2°C, as represented by a horizontal line inside the box, with a range from -2.5°C to 22.5°C. In contrast, Los Angeles displays a broader temperature range, with a median of 16.9°C. Taipei's plot appears the most compact, reflecting a consistent and less variable temperature range, with a median of 23.1°C, the highest among the cities, indicative of a warmer and more stable climate. Madrid's temperature distribution shows two peaks that suggest significant fluctuations between warm and

cool periods, with a mean temperature of 13.3°C and the widest range, highlighting a climate with substantial temperature variability.

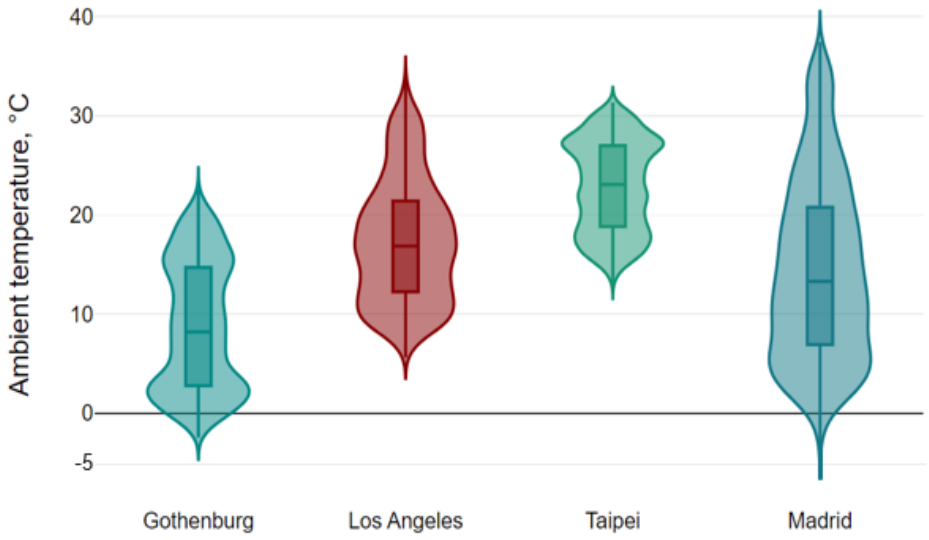

Figure 4.6. This figure shows the plot of the temperature distribution of the four regions. The data sets are sourced from Renewables.Ninja (2016).

The unique climatic characteristics of each city have a direct impact on energy consumption. Based on the method described in section 3.4, the findings revealed changes in energy consumption across different climates, as illustrated in Figure 4.7. In Los Angeles, Taipei, and Madrid, yearly energy consumption decreased by 9%, 14%, and 6% respectively, compared to Gothenburg.

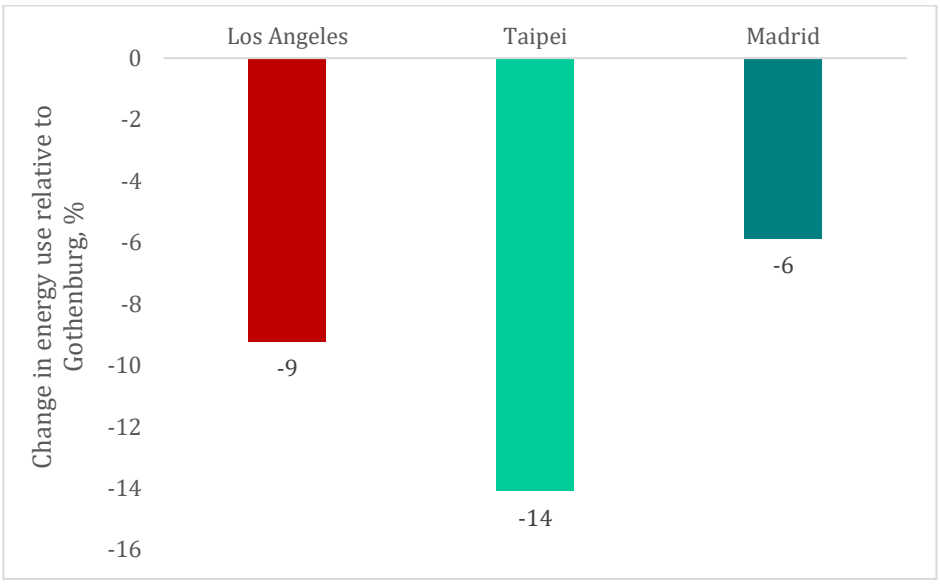

Figure 4.7. Yearly energy difference relative to Gothenburg across different locations.

4.2 The VIPV case – impact of VIPV-BEVs on energy demand and GHG emissions

A case incorporating VIPV has been developed to analyze the integration of solar charging capabilities into the operational patterns of pure BEVs. In the case presented in this section, the model analyzes a fleet of BEVs equipped with 0.5 kW VIPV systems. By maintaining charging times consistent with the empirical data, the model allows for an assessment of the impact of VIPV systems within a fleet, providing insights into potential energy demand reductions from the grid and GHG emission reductions.

4.2.1 Seasonal variation in solar charging and emissions

An analysis was conducted to examine the dynamics of the average daily absorbed solar energy measured in kilowatt-hours per day per car, average GHG emission, and GHG emission reduction during the usage phase measured in $kgCO_2$-eq per day per car over a one-year period for pure both BEV and VIPV-BEV. Figure 4.8, Figure 4.9, Figure 4.10, and Figure 4.11 represent Gothenburg, Los Angeles, Taipei, and Madrid respectively. The absorbed solar energy exhibits clear seasonal patterns, peaking during the summer months, due to longer daylight hours and higher sun intensity. This trend is consistent across all four cities, although the amplitude of seasonal variation differs. Gothenburg, Los Angeles, and Madrid show higher peaks and lower valleys compared to Taipei, which does not have a steep peak in solar energy absorption during the summer but maintains relatively higher absorption levels throughout other seasons.

The GHG emission reduction during the usage phase is influenced by the absorbed solar energy, suggesting that the higher the solar energy is harnessed by the VIPV-BEV fleet, the higher the chances for the GHG emission reduction during the usage phase though the magnitude of this intensity differs since carbon intensity of the grid at a given period also comes to consideration.

The bottom panel of the figures presents the daily emissions from pure BEVs and VIPV-BEV fleets. VIPV-BEVs emissions are lower in most days throughout the year than those of pure BEVs, demonstrating the effectiveness of solar integration in reducing the carbon footprint of EVs. Notably, Taipei exhibits higher variability and overall emission values compared to the other cities.

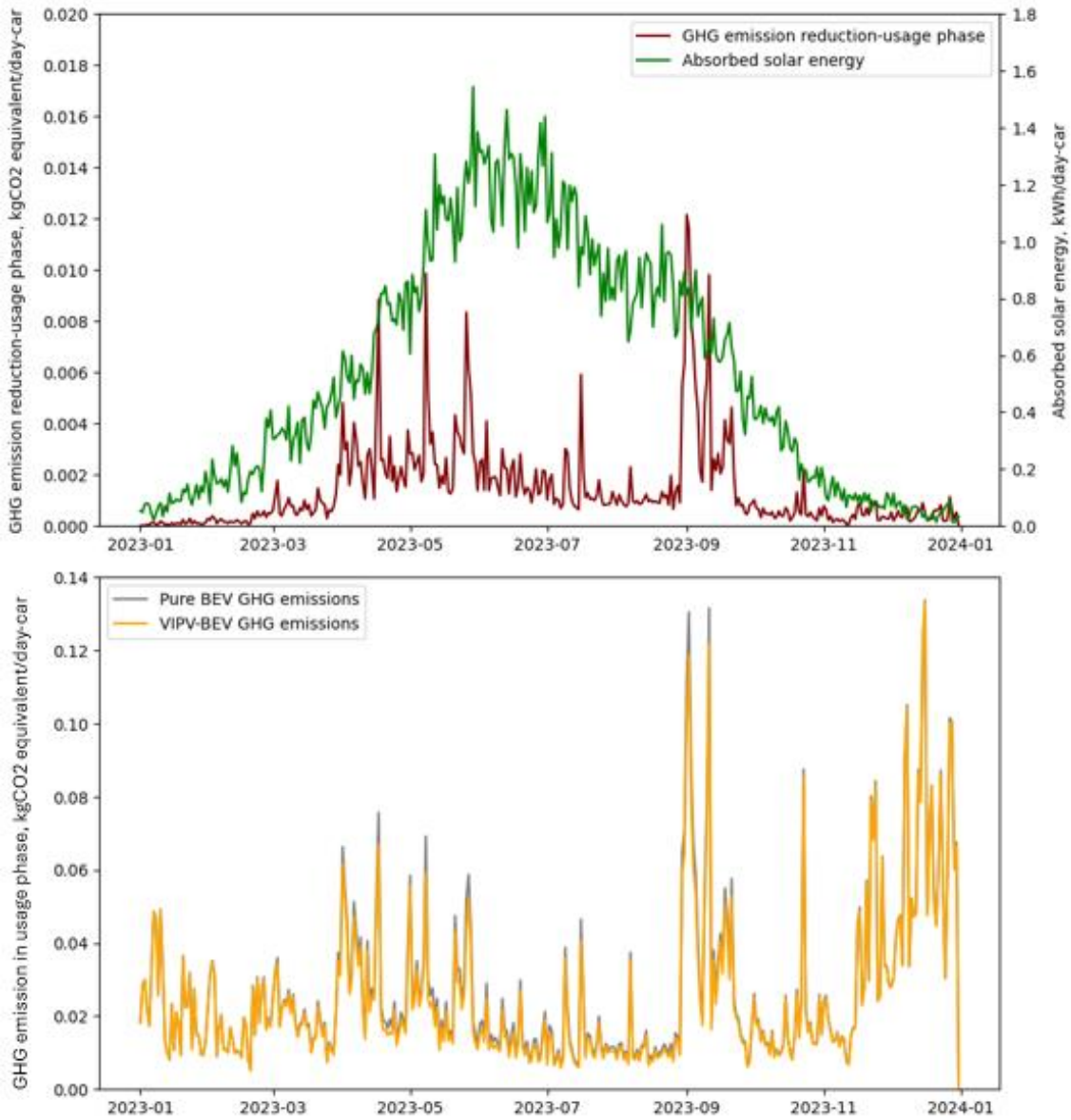

Figure 4.8. Top panel: GHG emission reduction – usage phase in Gothenburg throughout the year, illustrating variations in solar energy absorption. Bottom panel: compares emissions during usage phase between pure BEVs and VIPV-equipped vehicles.

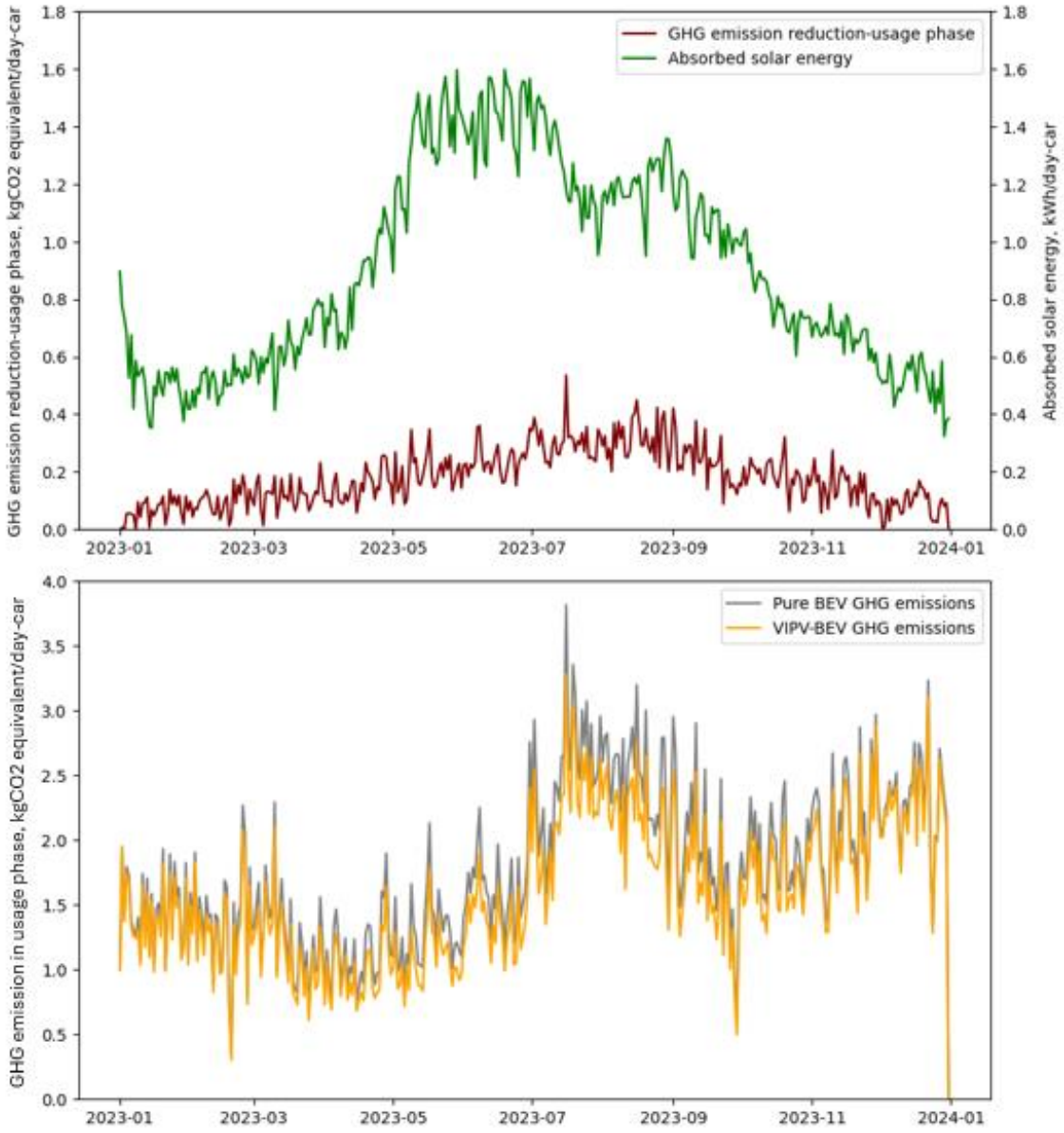

Figure 4.9. Top panel: GHG emission reduction – usage phase in Los Angeles throughout the year, illustrating variations in solar energy absorption. Bottom panel: compares emissions during usage phase between pure BEVs and VIPV-equipped vehicles.

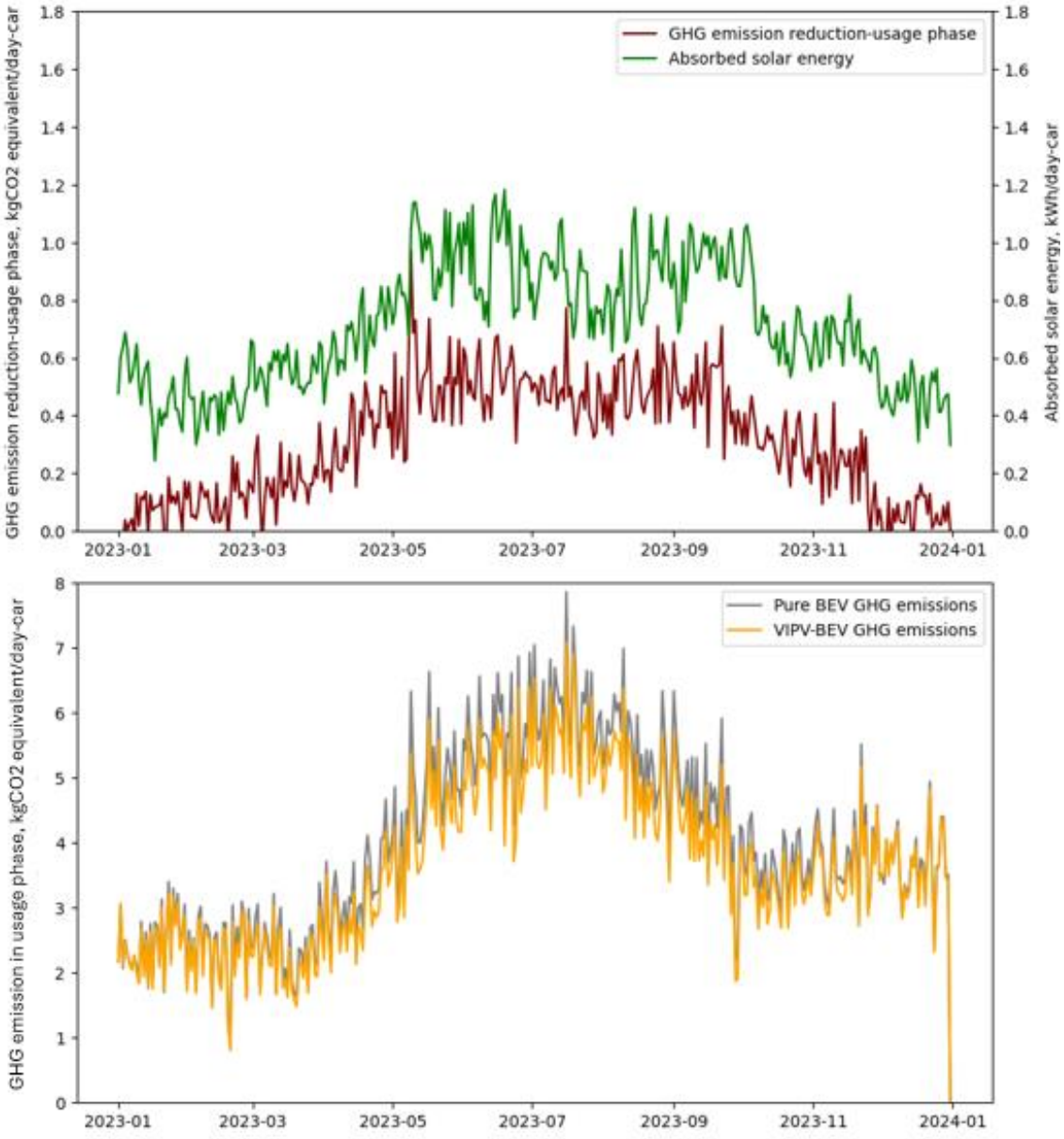

Figure 4.10. Top panel: GHG emission reduction – usage phase in Taipei throughout the year, illustrating variations in solar energy absorption. Bottom panel: compares emissions during usage phase between pure BEVs and VIPV-equipped vehicles.

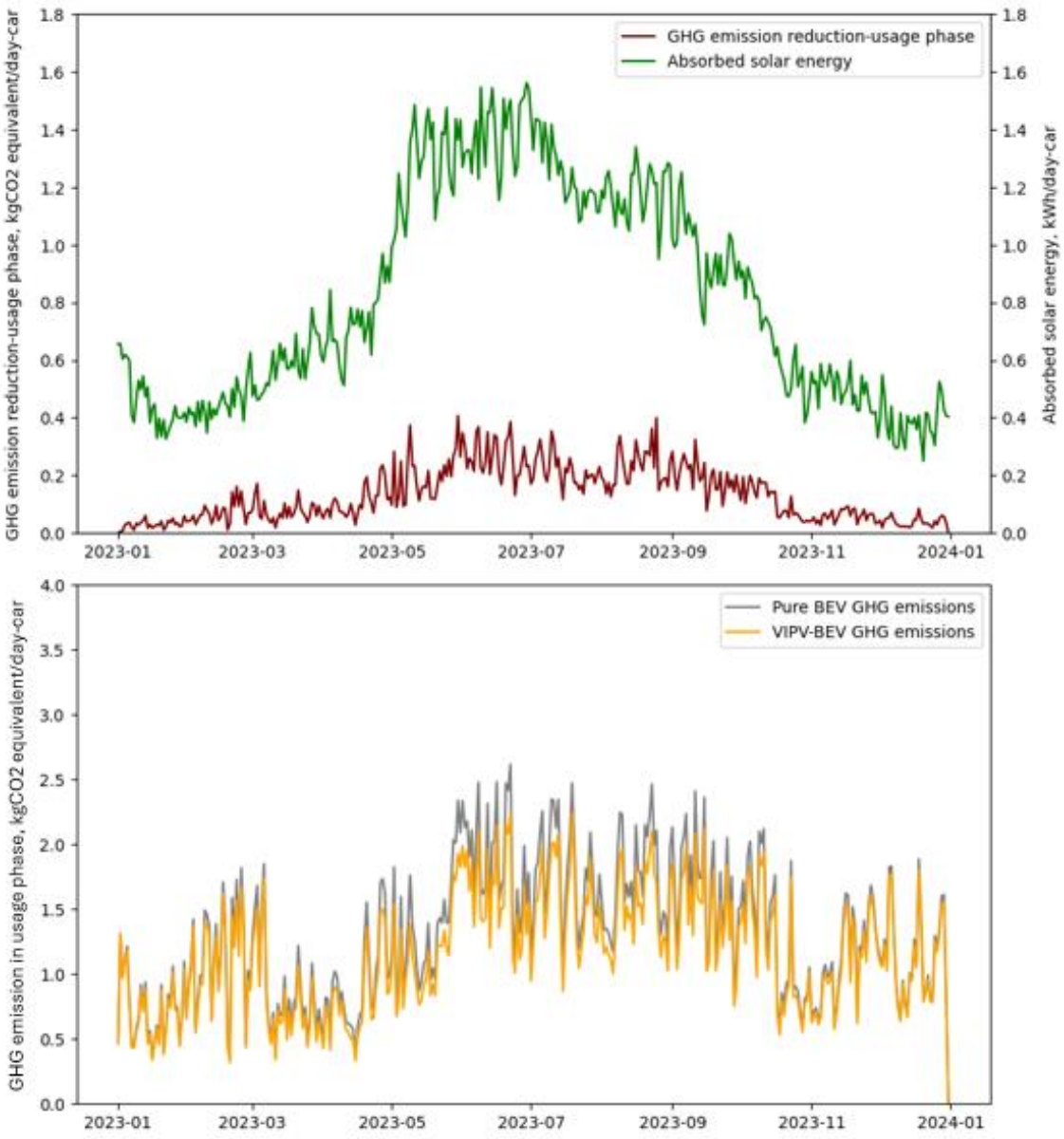

Figure 4.11. Top panel: GHG emission reduction – usage phase in Madrid throughout the year, illustrating variations in solar energy absorption. Bottom panel: compares emissions during usage phase between pure BEVs and VIPV-equipped vehicles.

4.2.2 Solar energy absorption and curtailment

An analysis comparing solar energy allocation between absorption and curtailment for Gothenburg, Los Angeles, Taipei, and Madrid reveal variations in PV system performance. Figure 4.12 illustrates this allocation for annual solar charging potential, annual curtailment, and annual absorbed solar energy per car through a stacked bar chart and the labels indicate the relative terms of absorbed solar energy or curtailment of its respective solar charging potential. Notably, as mentioned in section 3.1.4, 25% of the solar charging potential is dissipated due to system losses across all four locations, which is also evident when comparing the solar charging potential (red) with the sum of the absorbed solar energy (green) and curtailment (blue).

The analysis reveals that Gothenburg captures the most solar energy at 38% of its solar charging potential even if the magnitude is low at 201 kWh/year-car. It also has the lowest share of curtailment at 37% of its solar charging potential with an equivalent of 200 kWh/year-car. Los Angeles, which has the most solar irradiance, has a share of absorbed solar energy in solar charging potential at 35% with an equivalent absolute term of 333 kWh/year-car while its share of curtailment in solar charging potential is at 40% which is equivalent to 373 kWh/year-car.

Taipei and Madrid, which have higher solar irradiance than Gothenburg, have both shares of absorbed solar energy in solar charging potential at 36% while its share of curtailment in solar charging potential is 39%. Although their shares are similar, their absolute term for absorbed solar energy is 261 kWh/year-car and 302 kWh/year-car respectively. While for the absolute term of curtailment is 283 kWh/year-car and 320 kWh/year-car respectively. Moreover, these untapped levels of annual curtailment could be utilized in various ways, such as through Vehicle-to-Grid (V2G) technology.

Considering that the share of absorbed solar energy in the solar charging potential are relatively close, it implies that the portion of solar energy that is being utilized is close to constant across all the cities.

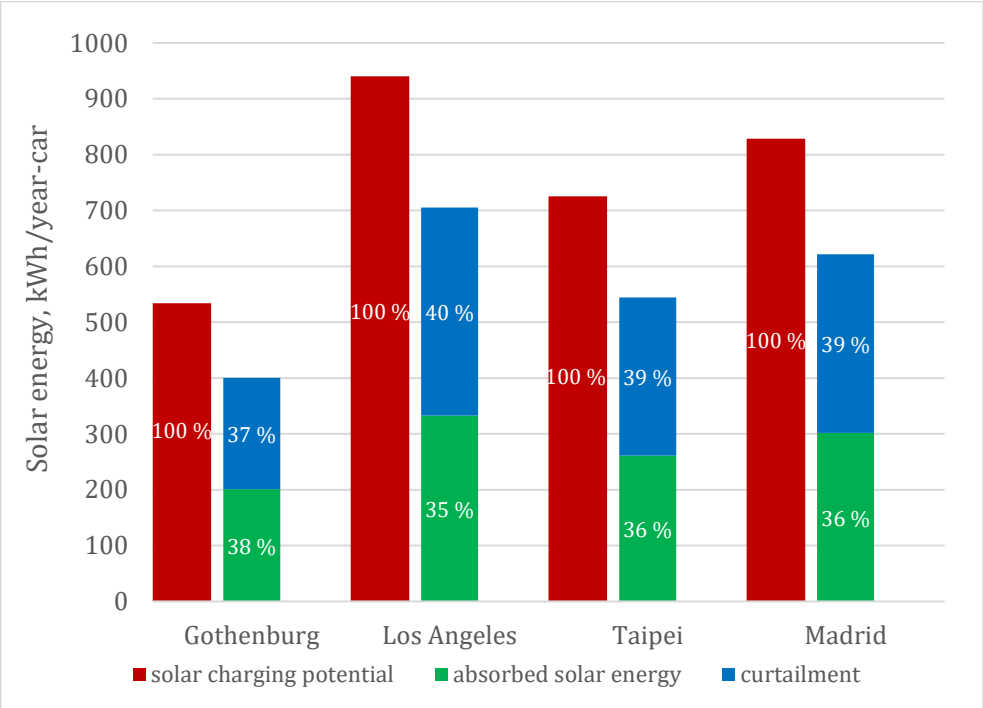

Figure 4.12. Comparison of annual solar energy allocation in Gothenburg, Los Angeles, Taipei, and Madrid

4.2.3 Solar share in energy demand for VIPV-BEVs

Figure 4.13 shows the comparison of the share of absorbed solar energy and curtailment in the total energy demand across the four regions. The figure shows a decrease in reliance on the grid for all regions upon the integration of VIPV, with reductions quantified at 7%, 12%, 10%, and 10% for Gothenburg, Los Angeles, Taipei, and

Madrid, respectively. Notably, the results show the highest solar energy gain and the greatest reduction in grid charging demand for Los Angeles.

All the VIPV-BEVs have a substantial portion of energy share coming from the grid, which is the dominant energy source of these vehicles. However, the solar energy potential is not fully harnessed, as shown by the level of curtailment, which is equivalent to 7%, 13%, 11%, and 11% of the total energy demand for the respective regions. The results show that Los Angeles has the highest level of curtailment, suggesting significant untapped solar energy potential. Curtailment occurs when the solar panels generate more energy than the battery can store or the vehicle can consume at that moment. When the battery is fully charged and the sun is still shining, the excess solar energy generated cannot be utilized and is therefore curtailed or wasted. This exists as a potential for this excess energy to be stored in the battery, provided it has sufficient capacity.

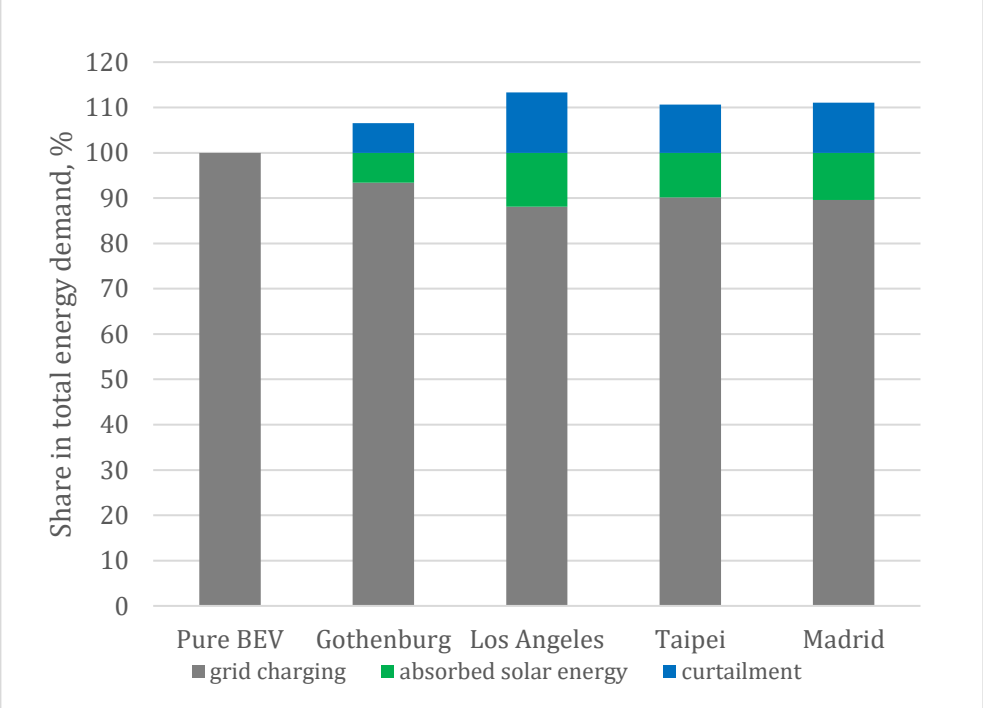

Figure 4.13. Comparison of annual solar energy allocation in Gothenburg, Los Angeles, Taipei, and Madrid.

4.2.4 Greenhouse gas emission comparison between pure BEV and VIPV-BEV during the usage phase

In the base case, the GHG emissions during the usage phase of pure BEVs and VIPV-BEVs are analyzed across four locations: Gothenburg, Los Angeles, Taipei, and Madrid as illustrated in Figure 4.14. The results show that in Gothenburg both pure BEVs and VIPV-BEVs have very low GHG emissions, with BEVs emitting 9.8 kg CO_2-eq per year per car and VIPV-BEVs slightly lower at 9.2 kg CO_2-eq per year per car. In Los Angeles, GHG emissions of pure BEVs are significantly higher at 664 kg CO_2-eq per year per car, while VIPV-BEVs show reduced emissions of 592 kg CO_2-eq per year per car. Taipei presents the highest GHG emissions, with pure BEVs emitting 1.5 tons CO_2-eq per year per car and VIPV-BEVs lower at 1.3 tons CO_2-eq per year per car. Madrid

shows lower emissions overall, with BEVs emitting 471 kg CO_2-eq and VIPV-BEVs slightly lower at 421 kg CO_2-eq per year per car. Overall, the base case scenario illustrates that integrating photovoltaics into electric vehicles consistently lowers use-phase GHG emissions compared to pure BEVs.

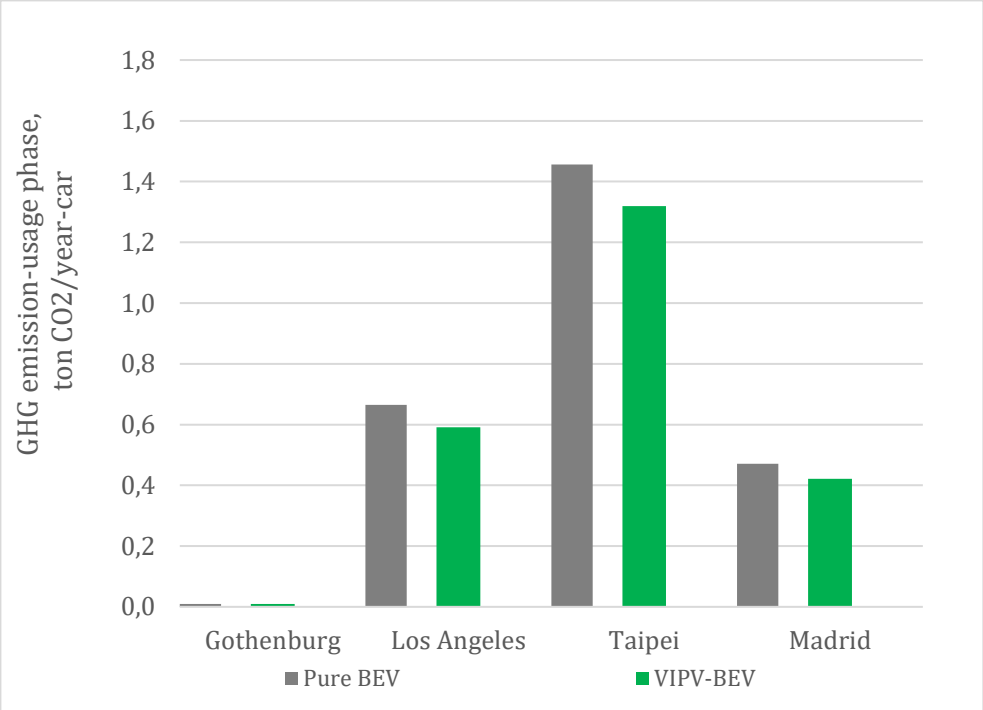

Figure 4.14. This figure shows the average GHG emission of pure BEV and VIPV-BEV during the usage phase only.

4.2.5 Greenhouse gas emission reduction potential of VIPV-BEV

To determine the GHG emission reduction potential of a VIPV-BEV compared to a pure BEV, an analysis was conducted that integrated the whole lifecycle emissions of both vehicle types as illustrated in Figure 4.15.
As mentioned in section 3.1.1, the GHG emission from vehicle and battery manufacturing and end-of-life of the pure BEV and VIPV-BEV are the same for both the pure BEV and VIPV-BEV, at 26.9 tons of CO_2-eq. This value was applied to both car types across all cities.

The usage phase emissions, described in section 4.2.4 were converted from annual GHG emission per car to total GHG emissions per car over the vehicle's 15-year lifespan as stated in section 3.1.1. An additional GHG emission component was added to the VIPV-BEV to account for the lifecycle emissions associated with the VIPV system which is at 615 kg CO_2-eq.

The analysis revealed that VIPV-BEVs in Los Angeles, Taipei, and Madrid reduced their GHG emission compared to pure BEVs, with emission reduction potentials of 1.3%, 2.9%, and 0.4%, respectively. However, the VIPV-BEV in Gothenburg emitted more GHG than the pure BEV, resulting in a 2.3% increase in emission. Despite the increased emission in Gothenburg, the VIPV-BEV in this city still had the lowest

overall GHG emission compared to the other cities analyzed. This shows the integration of VIPV technology into BEV has the potential to reduce GHG emissions in certain locations, with Taipei showing the most significant reduction potential among the cities studied.

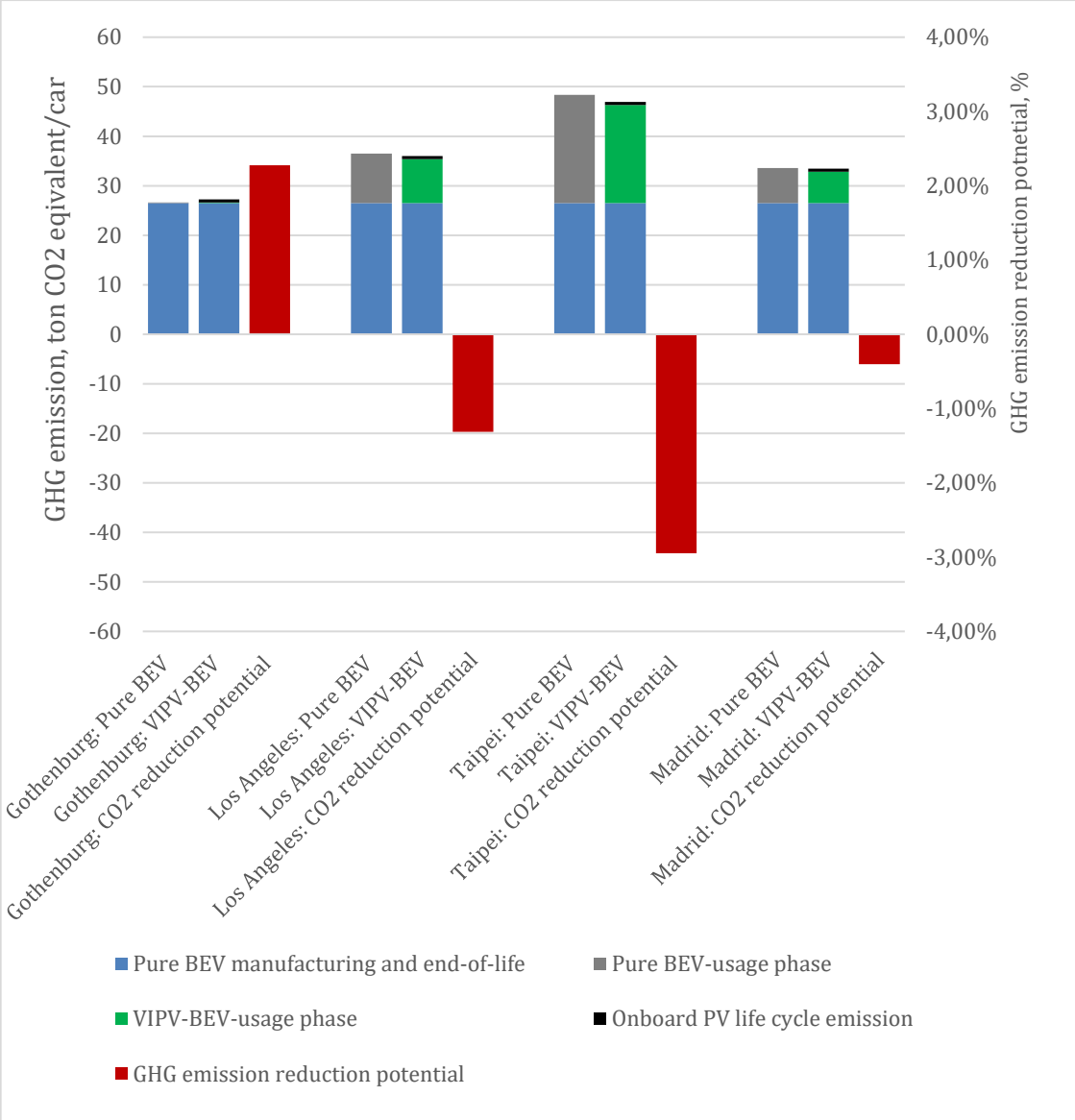

Figure 4.15. This figure shows the GHG emission of the whole life cycle of a car comparing a VIPV-BEV to pure BEV which are situated in Gothenburg, Los Angeles, Taipei, and Madrid. Its respective GHG emission reduction potential has also been presented.

4.2.6 Effect of annual car travel distance on VIPV-BEV greenhouse emissions

As mentioned in section 3.1.2, car users are categorized based on their annual distance travelled on the proportion of 25% each. With a fleet of 352 cars, an equal number of 88 cars are grouped to have a balanced representation and to compare groups of the same size, rather than dealing with varying sizes which are presented in Figure 4.16. As the cars have been grouped according to annual distance travelled, their respective solar energy absorption and GHG reduction during their usage phase were assessed as

shown in Figure 4.17, Figure 4.18, Figure 4.19, and Figure 4.20 for Gothenburg, Los Angeles, Taipei, and Madrid respectively.

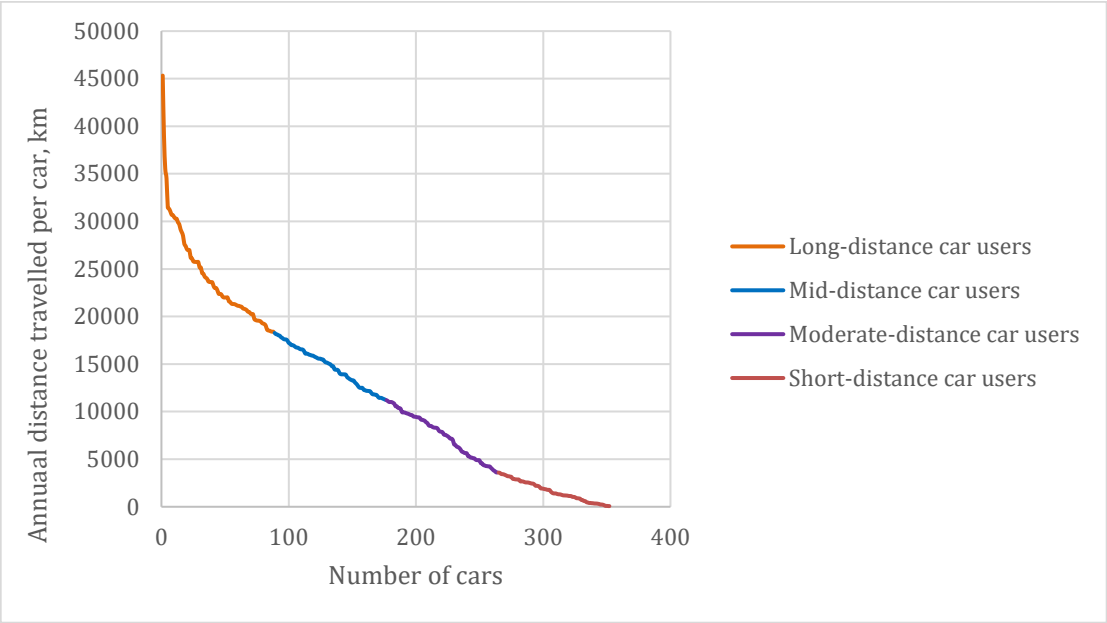

Figure 4.16. This figure presents the sorting of cars according to the annual distance travelled. Four groups with an equal number of 88 cars were formed wherein the long-distance car users wherein the long-distance car users travelled 18400 km to 45321 km annually (green), the mid-distance car users travelled 11238 km to 18267 km annually (blue), the moderate-distance car users travelled 4605 km to 11200 km annually (purple) and the short-distance car users travelled 70 km to 3591 km annually (peach).

Across all cities, the scatter plots reveal a general trend between the absorbed solar energy and the GHG emission reduction during the usage phase. As the absorbed solar energy increases, the GHG emission reduction during the usage phase also tends to rise, indicating that vehicles harnessing more solar energy are more effective at reducing GHG emissions during the usage phase.

The scatter plots between annual distance travelled and GHG reduction during the usage phase show an upward trend but are more spread out. Although it is more scattered there are still noticeable clusters worth mentioning that noticed across all the cities. It is evident that the short-distance car users (70 – 3591 km annually) benefited the least in terms of GHG emission reduction during its usage phase. Even though moderate-distance car users (3605 – 11200 km annually), mid-distance car users (11238 – 18267 km annually), and long-distance car users (18400 – 45321 km annually) are spread out, there is still evidence that long-distance car users tend to have high higher GHG emission reduction during the usage phase. This is evident by comparing the lowest extent of the GHG emission reduction among the different distance groups. Similarly, the mid-distance car users exhibit higher GHG emission reduction during the usage phase than the moderate-distance car users when comparing their least GHG emission reduction values.

Although there is an upward trend indicating that increasing the distance travelled increases the GHG emission reduction in the usage phase, this generalization has limits.

Some drivers who travel relatively short distances still see significant GHG reductions, while others driving similar distances have much lower emission savings.

Therefore, while increasing distance travelled is generally associated with higher potential GHG emission reduction, there can be considerable variation among drivers based on the amount of absorbed solar energy. The relationship is a broad trend, not an absolute rule.

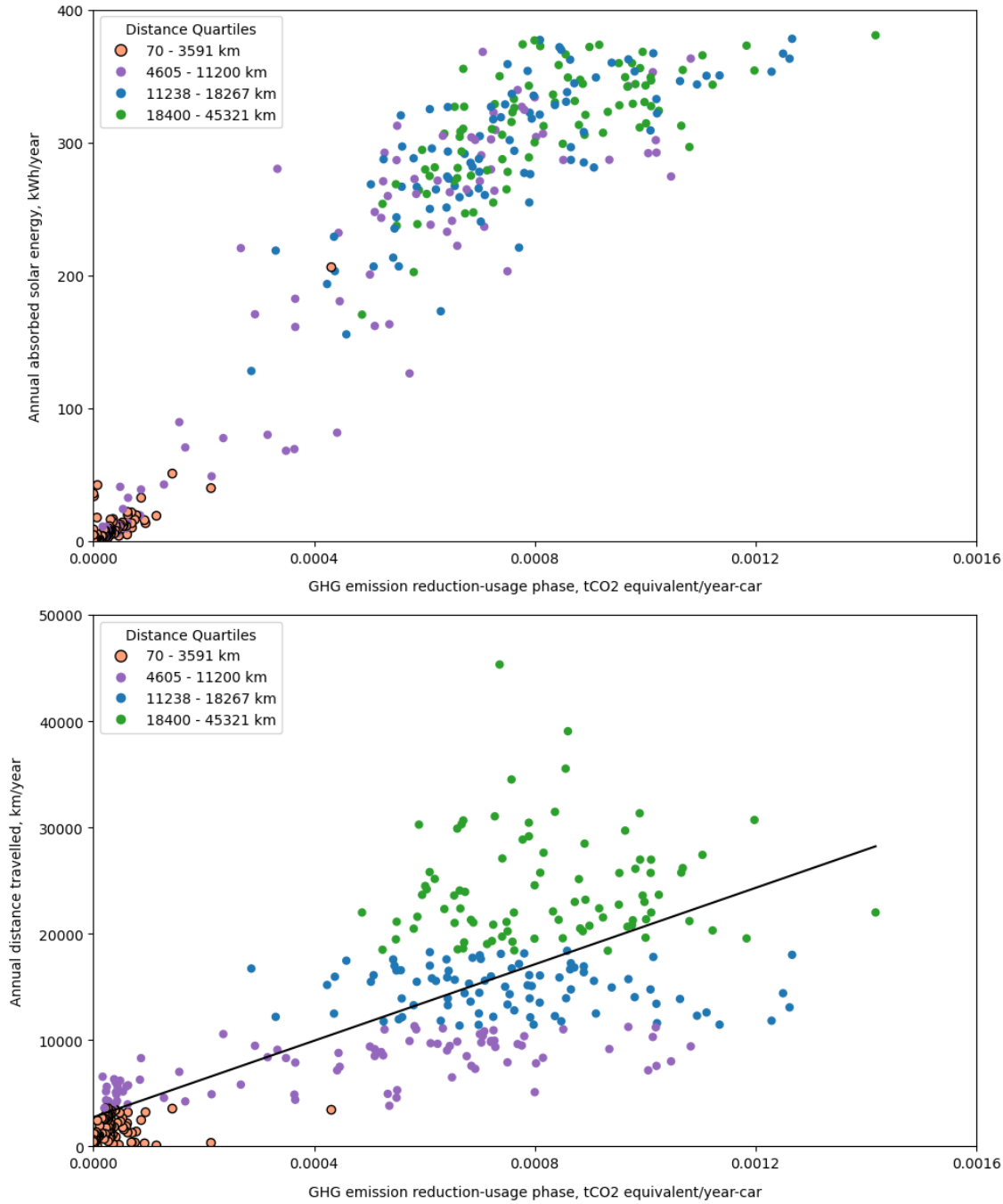

Figure 4.17. Relationship between vehicle solar energy absorption and potential GHG emission reduction in Gothenburg.

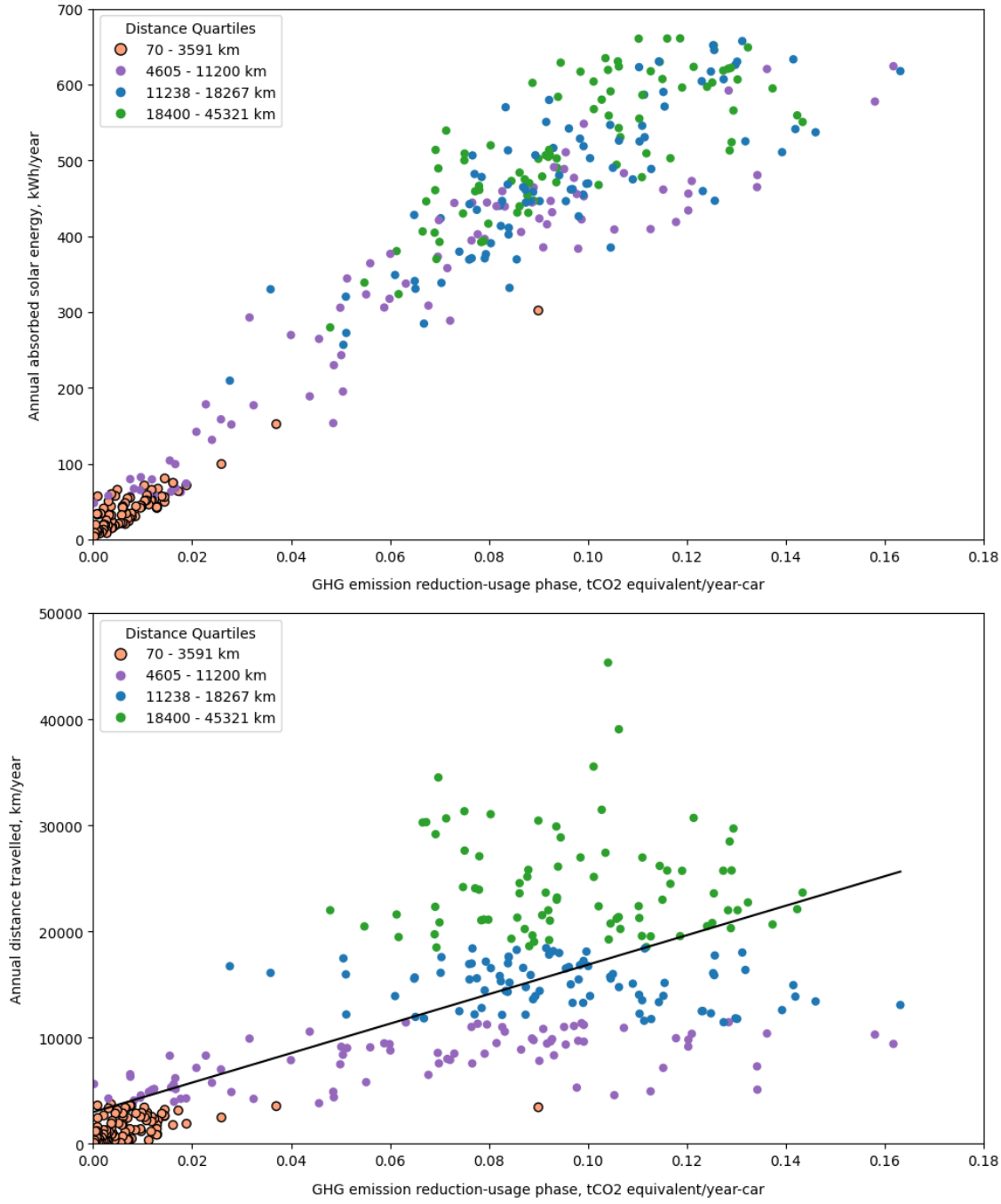

Figure 4.18. Relationship between vehicle solar energy absorption and potential GHG emission reduction in Los Angeles.

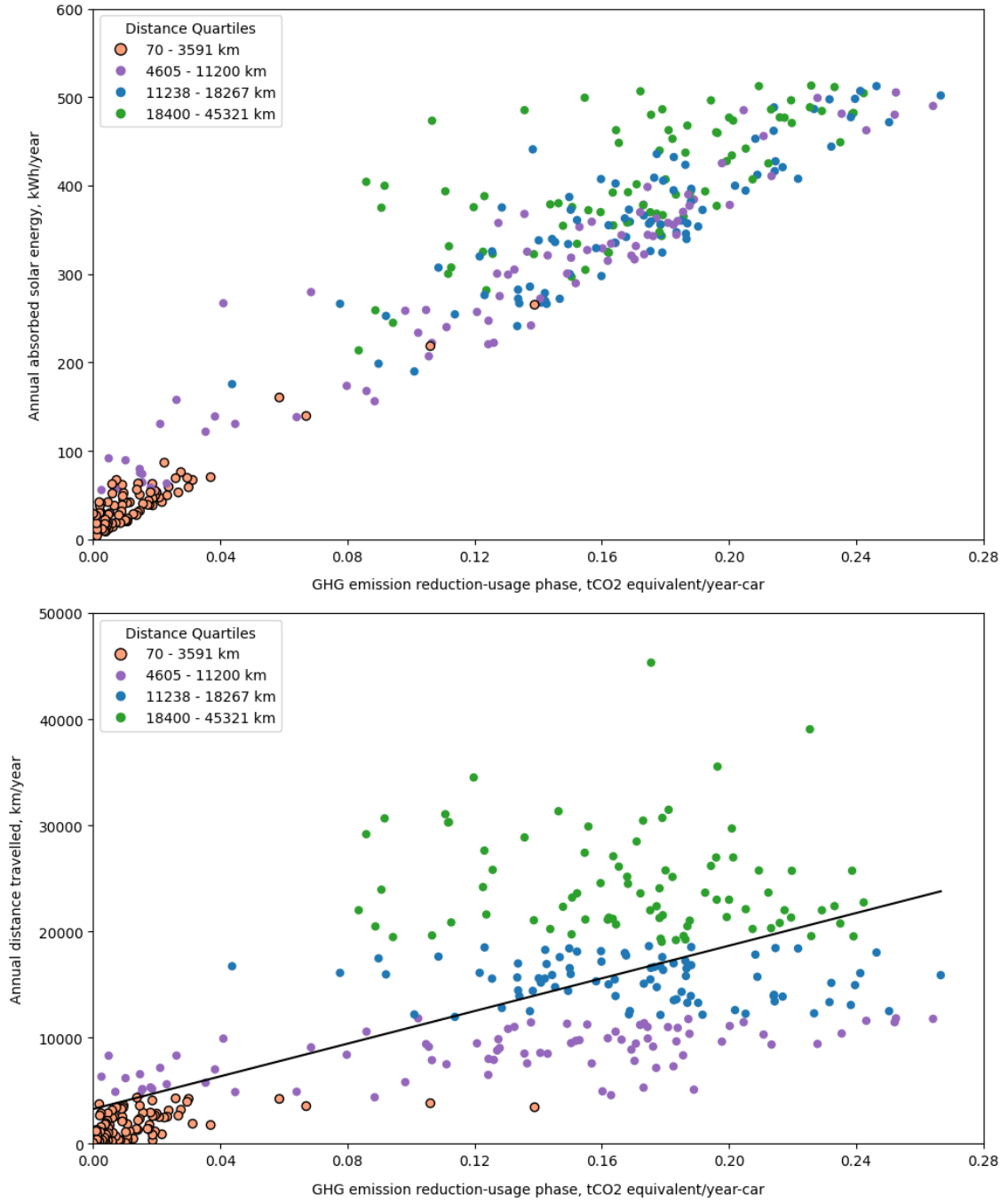

Figure 4.19. Relationship between vehicle solar energy absorption and potential GHG emission reduction in Taipei.

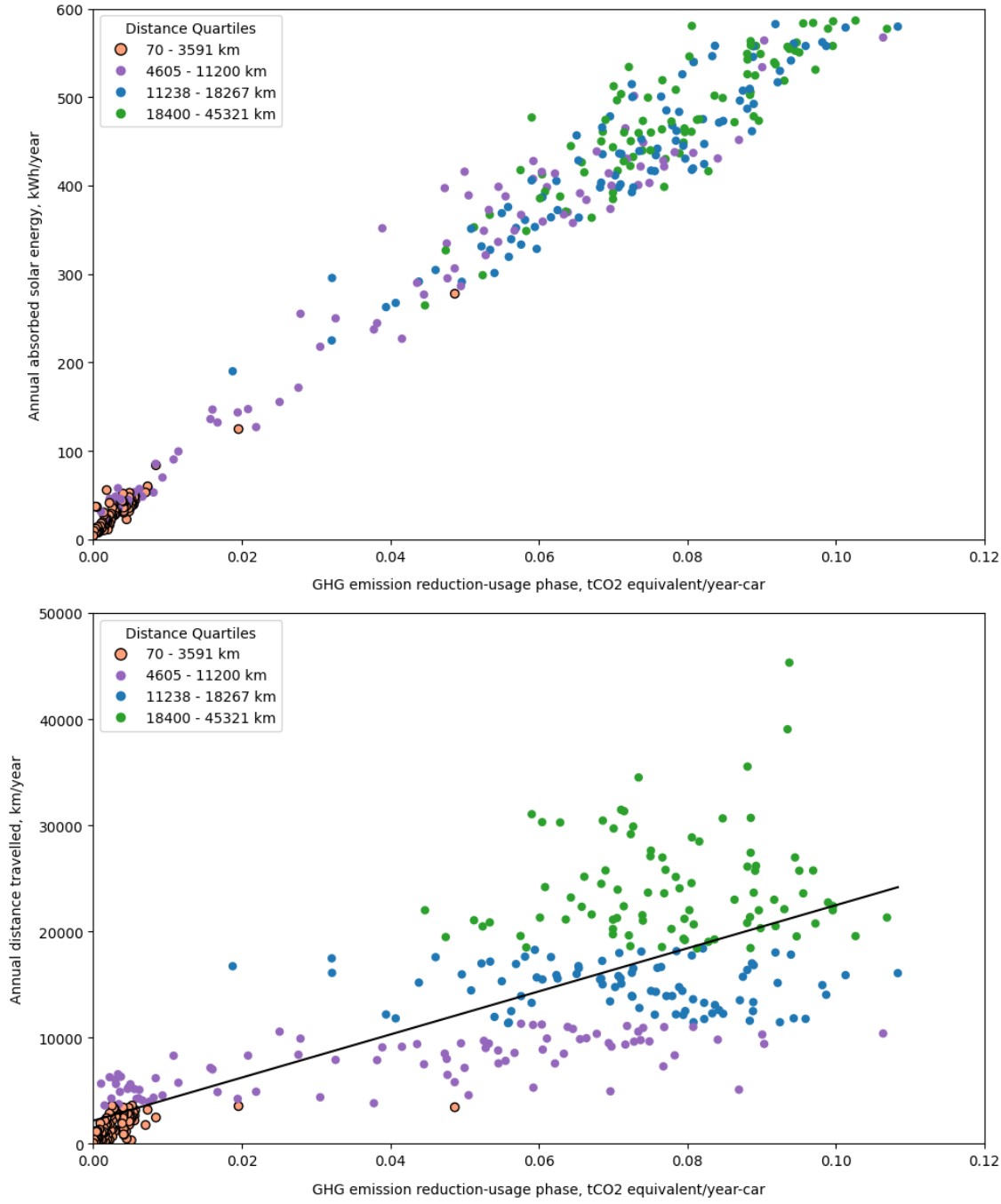

Figure 4.20. Relationship between vehicle solar energy absorption and potential GHG emission reduction in Madrid.

4.3 Sensitivity analysis

To assess the potential for integrating solar energy into EVs, under conditions that are likely in 2030, a sensitivity analysis was conducted. This analysis examines various parameters that could advance by 2030, as outlined in Table 4.1. These parameters include the capacity of solar PV systems, system losses, and vehicle energy efficiency, which were adjusted to reflect potential technological improvements mentioned in section 3.4.

Table 4.1: Sensitivity analyses

Parameter	Base Case	Sensitivity Case
Solar PV capacity	0.5 kW	1 kW
System losses	25%	12.5%
Vehicle energy efficiency	-	Improved by 10%
Carbon emission intensity	-	Gothenburg: decreased by 12% Los Angeles: decreased by 9% Taipei: decreased by 7% Madrid: decreased by 12%

For the sensitivity analysis, the average temperature over the past five years (2019 to 2023) was considered, as detailed in the methodology section. Additionally, carbon intensity projections were based on estimates from a scenario analysis provided by the International Energy Agency (IEA), as previously discussed in section 3.4. The sensitivity analysis aims to provide insights into how these advancements could impact the GHG reduction potential of the integration of solar energy into EVs.

4.3.1 Solar energy absorption and curtailment

The sensitivity analysis for 2030 indicates notable improvements in the solar charging potential for VIPV-BEVs across all cities, as depicted in Figure 4.21. VIPV-BEVs in Los Angeles have the highest solar energy charging potential, increasing from approximately 940 kWh/year-car in the base case to about 2195 kWh/year-car in the sensitivity analysis. This increase in potential is accompanied by a higher share of curtailment, rising to approximately 46% compared to 40% in the base case. In Gothenburg, solar charging potential increases from approximately 534 kWh/year-car in the base case to about 1246 kWh/year-car in the sensitivity analysis, with its curtailment share increasing from 37% to around 43%. This reflects improved solar PV capacity but also highlights the limitations in the VIPV-BEV system, such as battery capacity and charging patterns, which result in higher curtailment of the absorbed solar energy. Madrid's solar charging potential rises from approximately 829 kWh/year-car to about 1931 kWh/year-car. Curtailment also increases from 39% to approximately 44%, indicating that despite advancements, some energy remains underutilized. In Taipei, solar charging potential grows from approximately 725 kWh/year-car to about 1693 kWh/year-car. The curtailment increases from 39% to approximately 44%, suggesting persistent challenges in optimizing solar energy utilization despite the improvements.

Comparing the base case to the sensitivity analysis case, it is evident that advancements in technology by 2030 lead to significant increases in solar charging potential across all

cities. However, the increase in curtailment across these cities highlights the ongoing challenge of effectively utilizing the enhanced solar charging potential. Optimizing solar energy utilization strategies for future EV charging infrastructure is crucial to address these challenges. One energy utilization strategy is vehicle-to-X (V2X) technology, which enables electric vehicles to act as distributed energy resources through bidirectional energy flow between the vehicle's battery and the grid or other energy systems. By using the V2X capabilities, excess solar energy generated during peak production hours can be stored in EV batteries and later discharged to support grid stability, power buildings, or charge other EVs during periods of high demand. This approach enhances renewable energy utilization, provides additional revenue streams for EV owners, and supports the integration of intermittent renewable energy sources into the broader energy system.

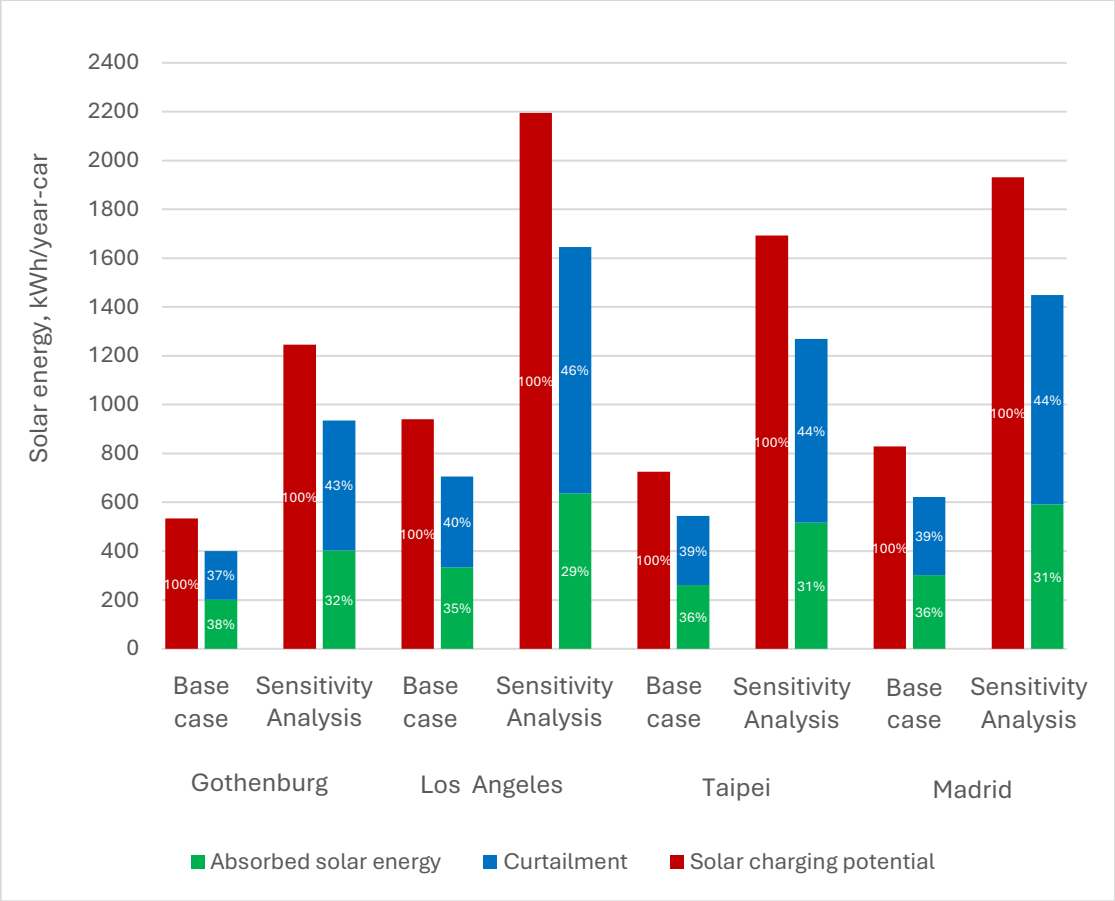

Figure 4.21. Comparison of annual solar energy allocation in Gothenburg, Los Angeles, Madrid, and Taipei between the base case and the sensitivity analysis.

4.3.2 Solar share in energy demand for VIPV-BEVs

In the sensitivity analysis for 2030, shifts in the share of solar energy in the energy demand are observed across the regions due to technological advancements and efficiency improvements, as shown in Figure 4.22. Notably, the data from Los Angeles reveals a considerable reduction in grid charging by approximately 15% and a substantial increase in absorbed solar energy by approximately 13%. Similarly, Gothenburg and Taipei also demonstrate significant increases in absorbed solar energy

by approximately 31% and 15%, respectively, compared to the base case. However, these regions also show higher curtailment rates, with increases of approximately 73% and 50%, respectively. Madrid exhibits a similar trend, with a notable increase in absorbed solar energy by approximately 21% and reduced reliance on grid charging by approximately 11%. Nonetheless, curtailment remains a challenge in maximizing solar energy utilization across all regions, with increases ranging from approximately 34% to 33% compared to the base case.

The comparison between the base case and the sensitivity analysis case highlights significant shifts in energy distribution and challenges across the regions. Los Angeles, Gothenburg, Taipei, and Madrid show varying degrees of change in grid reliance, absorbed solar energy, and curtailment rates, indicating the potential impacts of technological advancements on VIPV-BEV charging dynamics. While the sensitivity analysis provides insights into the transformative effects of VIPV-BEV integration, challenges such as curtailment underscore the importance of continued innovation and optimization in integrating solar photovoltaics into vehicles.

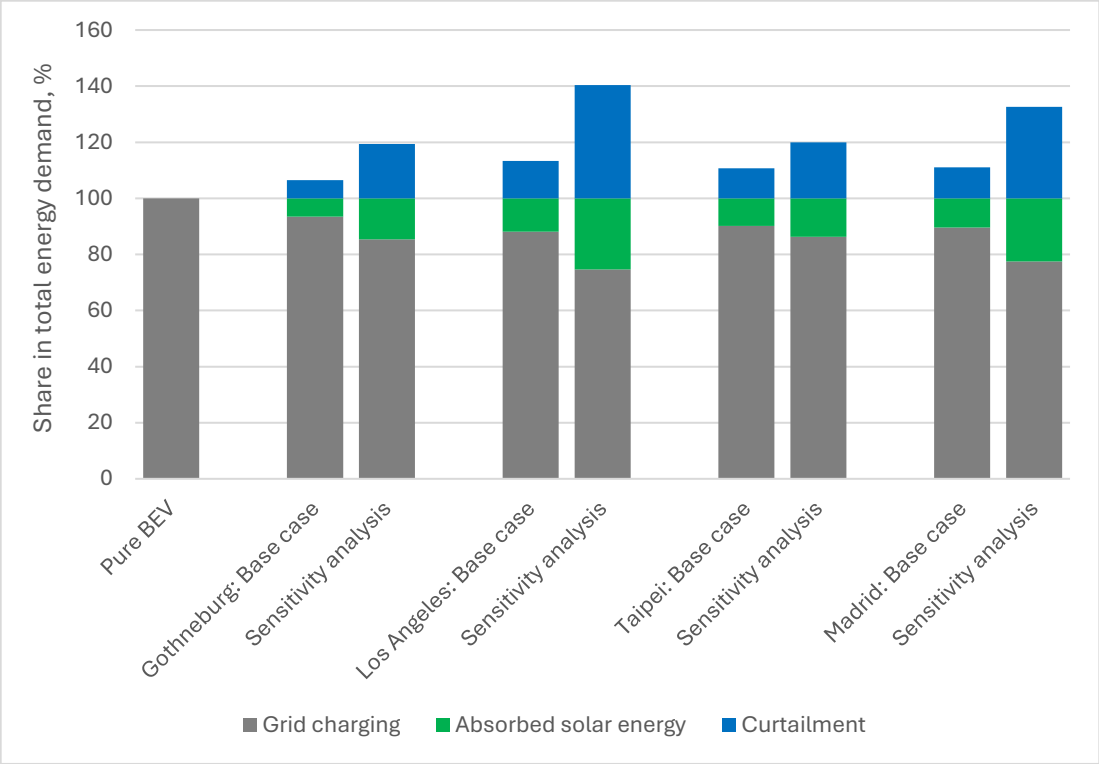

Figure 4.22. This figure shows the comparison of the solar share in energy demand between the results of the base case and sensitivity analysis across the cities.

4.3.3 Greenhouse gas emission comparison between pure BEV and VIPV-BEV during the usage phase

In the sensitivity analysis, similar trends are observed as it is depicted in Figure 4.23, though the emission values are lower due to different assumptions. In Gothenburg, emissions remain minimal, decreasing for both vehicle types. Pure BEVs emit 3.6 kg CO_2-eq per year per car, a reduction from 9.8 kg in the base case, while VIPV-BEVs emit 3.1 kg, down from 9.2 kg in the base case. In Los Angeles, pure BEV emissions

drop to 302.6 kg CO_2-eq per year per car, lower than the 664.4 kg in the base case. VIPV-BEVs further reduce emissions to 230.4 kg, down from 591.6 kg in the base case. Taipei continues to exhibit the highest emissions, with pure BEVs at 830.5 kg CO_2-eq per year per car, a decrease from 1455.7 kg in the base case. VIPV-BEVs emit 659.1 kg, down from 1319.7 kg in the base case. In Madrid, pure BEVs emit 173.5 kg CO_2-eq per year per car, a decrease from 471.3 kg in the base case, while VIPV-BEVs reduce this further to 133.2 kg, down from 421.3 kg in the base case. The sensitivity analysis confirms that VIPV-BEVs consistently produce lower GHG emissions during the usage phase than pure BEVs across all locations.

The absolute emission values differ, with the base case showing higher emissions due to different underlying assumptions. However, the overall trend remains unchanged: VIPV-BEVs exhibit lower emissions during the usage phase compared to pure BEVs. This suggests that integrating photovoltaics into electric vehicles is an effective strategy for reducing their environmental impact, particularly in terms of GHG emissions, regardless of the underlying assumptions.

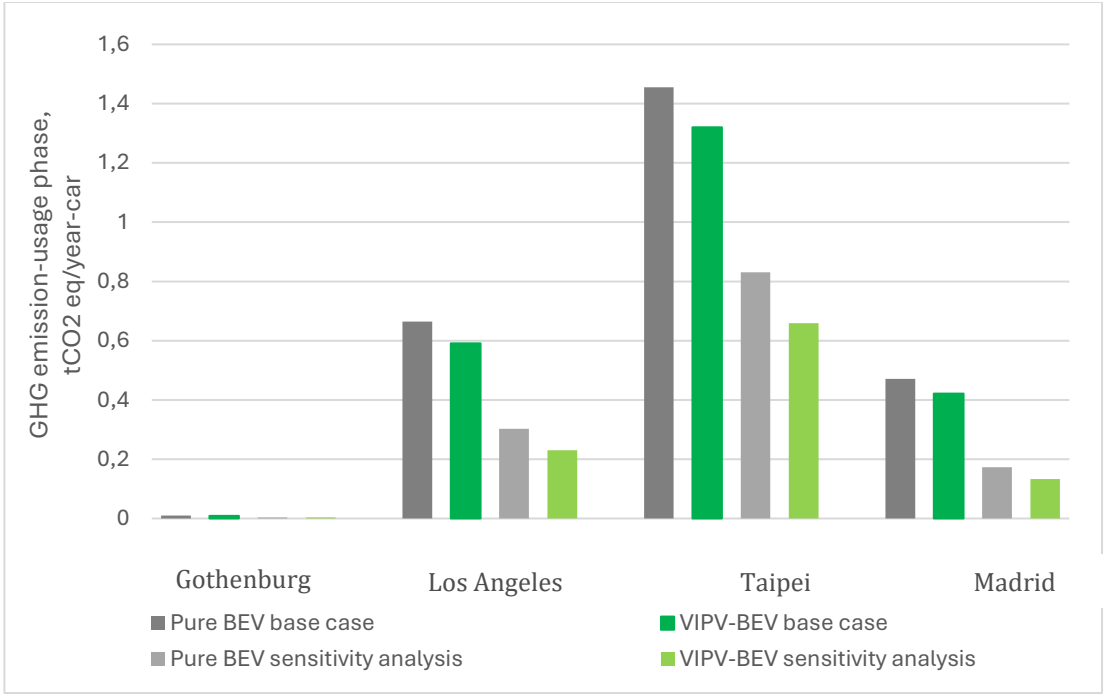

Figure 4.23. This figure shows the comparison between the average GHG emission of the fleet during the usage phase presenting the results of the base case and sensitivity analysis.

4.3.4 Greenhouse gas emission reduction potential of VIPV-BEV

A determination of the GHG emission reduction potential of a VIPV-BEV compared to a pure BEV through sensitivity analysis was also conducted with integrating the whole lifecycle emissions of both vehicle types which is illustrated in Figure 4.24.
Similar in section 4.2.5, the GHG emission from vehicle and battery manufacturing and end-of-life of the pure BEV and VIPV-BEV are the same for both the pure BEV and VIPV-BEV, at 26.9 tons of CO_2-eq. This value was applied to both car types across all cities.

The usage phase emissions of the sensitivity analysis results described in section 4.3.3 were converted from annual GHG emission per car to total GHG emissions per car over the vehicle's 15-year lifespan. An additional GHG emission component was added to the VIPV-BEV to account for the lifecycle emissions associated with the VIPV system which is at 458 kg CO_2-eq. This was calculated using the assumption stated in section 3.4.

The analysis revealed that VIPV-BEVs in Los Angeles, Taipei, and Madrid reduced their GHG emission compared to pure BEVs, with emission reduction potentials of 2.0%, 5.4%, and 0.5%, respectively. However, the VIPV-BEV in Gothenburg emitted more GHG than the pure BEV, resulting in a 1.7% increase in emission. Despite the increased emission in Gothenburg, the VIPV-BEV in this city still had the lowest overall GHG emission compared to the other cities analyzed. This shows the integration of VIPV technology into BEV has the potential to reduce GHG emissions in certain locations, with Taipei showing the most significant reduction potential among the cities studied.

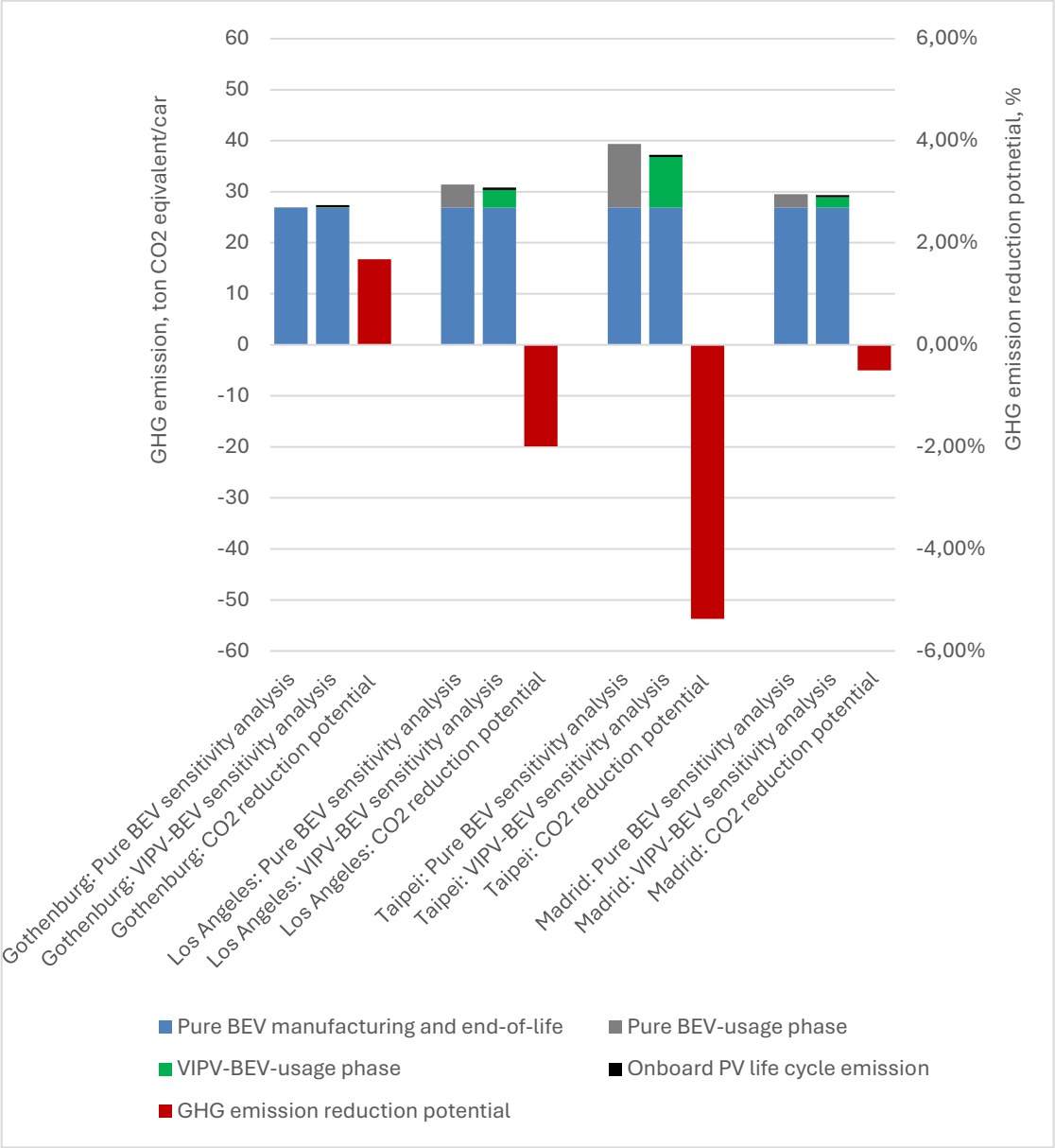

Figure 4.24. This figure shows the GHG emission of the whole life cycle of a car comparing a VIPV-BEV to pure BEV which are situated in Gothenburg, Los Angeles, Taipei, and Madrid. Its respective GHG emission reduction potential has also been presented.

5 Concluding discussion

In this chapter, the research questions are discussed based on the findings in chapter 4, followed by conclusions. Lastly, potential improvements and suggestions for future research are presented.

5.1 The potential for VIPV to reduce grid electricity usage and lifecycle carbon dioxide emissions

Research question 1: How does the geographical location influence the potential for reducing electricity usage from the grid and lifecycle carbon dioxide emissions by using VIPV systems in BEVs?

The geographical location influences the potential for reducing electricity usage from the grid and lifecycle carbon dioxide emissions by using VIPV systems in BEVs. Locations with higher solar irradiance, such as Los Angeles, demonstrate greater solar charging potential compared to locations with lower irradiance like Gothenburg. This directly affects the amount of electricity that can be generated by VIPV systems. The absorption of solar energy by VIPV systems varies seasonally, with summer months generally providing higher solar energy absorption and greater potential for decreasing electricity demand for charging EVs across all studied locations.

Ambient temperature impacts vehicle energy consumption. For instance, Los Angeles, Taipei, and Madrid showed a decrease in electricity demand for driving and electricity consumption for charging compared to Gothenburg due to climate differences.

Introducing VIPV systems with a capacity of 0.5 kW GHG emissions. Based on the analysis of electricity consumption for driving and electricity demand for charging data from 2023, along with 5-year historical data of solar irradiance from 2019 to 2023, the VIPV-BEV simulation showed a decrease in charging energy demand on the grid of approximately 7%, 12%, 10%, and 10% for Gothenburg, Los Angeles, Taipei, and Madrid respectively.

The carbon emission intensity of the local electricity grid also plays a role in the GHG emissions reduction potential. Even with the full electrification of passenger cars, there are still inherent GHG emissions associated with the usage of BEVs and the manufacturing and integration of PV systems into vehicles. The emissions related to the usage phase are influenced by the carbon emission intensity of the local grid, which varies across each examined city and fluctuates over the course of the year and day. The data obtained on carbon emission intensities show that Taipei has been consistently the highest and Gothenburg has been the lowest. This underscores the varying energy strategies across the four cities, reflecting their diverse approaches to energy production and carbon emission management.

Furthermore, an analysis of seasonal dynamics revealed additional insights into how geographical location influences the potential for reducing grid electricity usage and lifecycle carbon dioxide emissions with VIPV systems in BEVs. The study examined average daily absorbed solar energy, GHG emissions, and GHG emission reductions in the usage phase over a one-year period for both pure BEVs and VIPV-BEVs across the four cities. The absorbed solar energy shows clear seasonal patterns in all locations, with peaks during summer months due to longer daylight hours and higher solar irradiance. However, the magnitude of these seasonal variations differs between cities. Gothenburg, Los Angeles, and Madrid exhibit more pronounced variation in solar energy absorption compared to Taipei, which maintains relatively consistent absorption levels throughout the year. This seasonal variation in solar energy absorption is associated with the GHG reduction of VIPV-BEVs in the usage phase. As more solar energy is harnessed during peak periods, the potential for GHG reduction increases.

Moreover, the study found that VIPV-BEVs generally produced lower GHG emissions than pure BEVs across all locations during the usage phase. However, the magnitude of these reductions varied significantly based on location. Combined with the increased manufacturing emissions from producing the VIPV systems, Taipei showed the highest potential for GHG emission reduction at 2.9%, followed by Los Angeles with 1.3% and Madrid with 0.4%. Interestingly, Gothenburg saw a slight increase in emissions of 2.3% attributed by the GHG emission from the manufacturing of the VIPV system. These findings highlight the importance of considering geographical factors when assessing the potential benefits of VIPV systems in BEVs for reducing grid electricity usage and lifecycle carbon dioxide emissions.

5.2 Impact of driving patterns in greenhouse gas emissions

Research question 2: Which types of users would benefit the most from VIPV-BEVs in terms of driving pattern and geographical location?

Based on the results presented in section 4.2.6, the types of users who would benefit the most from VIPV-BEVs in terms of driving patterns are long-distance drivers. The analysis divided car users into four groups based on annual distance travelled: short-distance (70-3,591 km), moderate-distance (3,605-11,200 km), mid-distance (11,238-18,267 km), and long-distance (18,400-45,321 km). The results show an upward trend in GHG emission reduction during the usage phase as the annual distance travelled increases. Long-distance car users demonstrated the highest tendency for GHG emission reduction, followed by mid-distance users. Short-distance users benefited the least. However, the relationship between distance travelled and emission reduction is not absolute. Some drivers with relatively short annual distances still achieved significant GHG reductions, while others with similar distances had much lower savings. The variation in benefits is also influenced by the amount of absorbed solar energy. Overall, while increasing distance travelled is generally associated with higher potential GHG emission reduction from VIPV-BEVs, there can be considerable variation among individual drivers.

5.3 Technological advancements and their impact on greenhouse gas emissions of VIPV-BEV

Research question 3: How could future advancements in solar PV capacity, system losses, energy consumption, charging demand, and carbon emission intensity affect the GHG emissions reduction potential of VIPV-BEVs?

The sensitivity analysis, inspired by a 2030 case scenario, revealed that the future advancements in solar PV capacity, vehicle energy efficiency, system losses and carbon emission intensity resulted in a decrease in GHG emission in the usage phase. Doubling the solar PV capacity from 0.5 kW to 1.0 kW and decreasing the system losses from 25% to 12.5% led to substantial increases in solar charging potential across all studied cities, allowing VIPV-BEV to capture more of the available solar energy. A 10% decrease in the electricity consumption for driving and electricity demand for charging decreased the overall demand for energy in the grid and therefore decreased the GHG emission of the car during the usage phase. The calculated decrease in carbon emission intensity ranging from 7% to 12% depending on the location further reduced the GHG emission reduction in the usage phase.

The combined effect of these advancements led to an increase in solar share in the energy demand of VIPV-BEV. The cars situated in Gothenburg, Los Angeles, Taipei, and Madrid showed a 15%, 25%, 14%, and 22% decrease in grid charging, respectively, compared with the base case, which had a 7%, 12%, 10%, and 10% decrease in grid charging.

These advancements also resulted to GHG emission reduction potential of 2.0%, 5.4%, and 0.5% for Los Angeles, Taipei, and Madrid respectively, compared with the base case results of 1.3%, 2.9% and 0.4%. While the situation in Gothenburg emitted more GHG than pure BEV, resulting in 1.7% increase in emission compared to 2.3% increase in emission that was revealed in the base case scenario.
To sum up, these future advancements could decrease the grid charging of cars situated in these studied cities though the extent of GHG emission reduction potential varies by location emphasizing the importance of considering regional factors in VIPV-BEV implementation strategies.

5.4 Potential improvements and recommendations for future research

In the conclusion of this thesis, several key findings and potential improvements have been identified to enhance the integration of VIPV systems and their impact on reducing grid electricity usage and GHG emissions.

- The analysis revealed levels of curtailment of solar energy, especially in locations with high solar irradiance. To maximize the utilization of solar energy

and minimize curtailment, a Vehicle-to-Grid (V2G) integration can be explored. In the VIPV-BEV simulation, with 0.5 kW of installed PV, annual curtailments of 200 kWh/car, 373 kWh/car, 283 kWh/car, and 320 kWh/car were observed for vehicles situated in Gothenburg, Los Angeles, Taipei, and Madrid, respectively. This curtailment represents untapped potential in the vehicle's battery system, indicating an opportunity to store excess solar energy in the grid, and interesting area to explore to improve the solar energy absorption of the VIPV systems.

- Another area not covered in the current analysis is the potential for reducing battery sizes in VIPV-equipped EVs. Given that VIPV systems can provide supplementary solar energy, future research should evaluate whether this can enable smaller battery capacities while maintaining or even enhancing vehicle range and efficiency. Reducing battery size could lead to decreased manufacturing costs, lower vehicle weight, and reduced lifecycle GHG emissions. This would make VIPV systems more economically viable and environmentally beneficial, presenting a compelling direction for further investigation.

- Improvements in assumptions regarding grid charging behavior for VIPV-BEVs should be considered in future studies. Current models assume similar grid charging patterns for both VIPV-equipped and pure BEVs, which may not reflect the actual behavior of VIPV users. In reality, users of VIPV-BEVs are likely to adapt their charging habits due to the supplementary solar energy their vehicles generate. They may charge less frequently, relying more on solar energy, and may also avoid charging the battery to full SOC to reduce curtailment and maximize solar energy absorption. Future research should investigate these behavioral differences and incorporate more realistic charging profiles into simulations. For example, studies could explore partial charging strategies or off-peak charging habits that could further reduce grid dependence and enhance the system's efficiency. By improving these assumptions, the models would yield more accurate estimations of energy savings and GHG reduction potential, offering deeper insights into the real-world advantages of VIPV systems.

- Further studies on the influence of car user behavior other than distance travelled on the performance of VIPV systems can provide better estimates of the GHG reduction potential of VIPV-BEV.

In conclusion, the integration of VIPV systems into EVs presents a viable option for reducing grid dependency and life cycle GHG emissions. Future research could focus on optimizing solar energy utilization, reducing GHG emissions during manufacturing, and comparing VIPV systems with other renewable energy integration strategies for EVs. As technology advances, the benefits of VIPV systems may become more substantial, but at present, they represent one of several

approaches to reducing GHG emissions in the transportation sector, each with its own set of advantages and limitations.

6 Appendix

A. Estimates of energy consumption for driving

Sample calculation for estimating the energy consumption for driving for Los Angeles, Taipei and Madrid relative to Gothenburg.

Table 6.1 Summary of results for estimating the fleet's driving energy consumption in Los Angeles, Taipei and Madrid using the ambient temperature correction factor.

City	Temperature	Electricity consumption for driving
Gothenburg	1.2 ℃	3.6 kWh
Los Angeles	12 ℃	2.8 kWh (a)
Taipei	16 ℃	2.6 kWh (b)
Madrid	-1.1 ℃	4.0 kWh (c)

$$D = Energy\ consumption\ for\ driving$$
$$A = Ambient\ temperature\ correction\ factor$$
$$D_{city} = D_{Gothenburg} \cdot \frac{A_{corresponds\ to\ temperature\ of\ the\ city}}{A_{corresponds\ to\ temperature\ of\ Gothenburg}}$$

(a)

$$D_{Los\ Angeles} = D_{Gothenburg} \cdot \frac{A_{corresponds\ to\ temperature\ of\ Los\ Angeles}}{A_{corresponds\ to\ temperature\ of\ Gothenburg}}$$

$$D_{Los\ Angeles} = 3.6\ kWh \cdot \frac{1.17}{1.46}$$
$$D_{Los\ Angeles} = 2.8\ kWh$$

(b)

$$D_{Taipei} = D_{Gothenburg} \cdot \frac{A_{corresponds\ to\ temperature\ of\ Taipei}}{A_{corresponds\ to\ temperature\ of\ Gothenburg}}$$

$$D_{Los\ Taipei} = 3.6\ kWh \cdot \frac{1.06}{1.46}$$
$$D_{Los\ Angeles} = 2.6\ kWh$$

(c)

$$D = D_{Gothenburg} \cdot \frac{A_{corresponds\ to\ temperature\ of\ Madrid}}{A_{corresponds\ to\ temperature\ of\ Madrid}}$$

$$D_{Los\ Taipei} = 3.6\ kWh \cdot \frac{1.62}{1.46}$$
$$D_{Los\ Angeles} = 4.0\ kWh$$

B. Carbon emission intensity in 2030 estimates

Sample calculation for estimating the carbon emission intensity for Gothenburg, Los Angeles, Taipei and Madrid.

Table 6.2 Calculation for the decrease in the carbon emission intensity

	Carbon emission intensity by 2025	Carbon emission intensity by 2030	Calculated rate of carbon emission intensity
European Union	137 gCO_2 eq/kWh	72 gCO_2 eq/kWh	12%
USA	263 gCO_2 eq/kWh	163 gCO_2 eq/kWh	9%
China	478 gCO_2 eq/kWh	340 gCO_2 eq/kWh	7%

F = Carbon emission intensity by 2030 r = rate of carbon emission intensity
P = Carbon emission intensity by 2025 n = number of years between 2025 and 2030

$$F = P(1 + r)^n$$

European Union

$$72 = 137(1 + r)^5$$
$$r = -12\%$$

United States

$$163 = 263(1 + r)^5$$
$$r = -9\%$$

China

$$478 = 340(1 + r)^5$$
$$r = -7\%$$

The value calculated for the European Union was used in the sensitivity analysis for Gothenburg and Madrid. For the USA, the value was used for Los Angeles, and for Taipei, the value calculated for China was used.

Table 6.3 Sample calculation for the carbon emission intensity used for sensitivity analysis

City	Calculated decrease of carbon emission intensity	Carbon emission intensity by 2023	Calculated Carbon emission intensity used for sensitivity analysis
Gothenburg	12%	2.3 gCO_2 eq/kWh	0.9 gCO_2 eq/kWh
Los Angeles	9%	285 gCO_2 eq/kWh	147 gCO_2 eq/kWh
Taipei	7%	532 gCO_2 eq/kWh	320 gCO_2 eq/kWh
Madrid	12%	114 gCO_2 eq/kWh	47 gCO_2 eq/kWh

F = Carbon emission by 2030 r = rate of carbon emission intensity
P = Carbon emission by 2023 n = number of years between 2023 and 2030

$$F = P(1 + r)^n$$

Gothenburg

$$F = 2.3(1 + (-0.12))^7$$
$$F = 0.9\ gCO2\ eq\ /kWh$$

Los Angeles

$$F = 285(1 + (-0.09))^7$$
$$F = 147\ gCO2\ eq\ /kWh$$

Taipei

$$F = 532(1 + (-0.07))^7$$
$$F = 320\ gCO2\ eq\ /kWh$$

Madrid

$$F = 114(1 + (-0.12))^7$$
$$F = 47\ gCO2\ eq\ /kWh$$

7 References

Al Garni, H. Z., Awasthi, A., & Ramli, M. A. M. (2018). Optimal design and analysis of grid-connected photovoltaic under different tracking systems using HOMER. *Energy Conversion and Management*, *155*, 42–57. https://doi.org/10.1016/j.enconman.2017.10.090

Ang, B. W., & Su, B. (2016). Carbon emission intensity in electricity production: A global analysis. *Energy Policy*, *94*, 56–63. https://doi.org/10.1016/j.enpol.2016.03.038

Araki, K., Carr, A. J., Chabuel, F., Commault, B., Derks, R., Ding, K., Duigou, T., Ekins-Daukes, N. J., Gaume, J., Hirota, T., Kanz, O., Komoto, K., Newman, B. K., Peibst, R., Reinders, A., Roman Medina, E., Sechilariu, M., Serra, L., Sierra, A., … Zurfluh, D. (2021). *IEA-PVPS T17 State-of-the-Art and Expected Benefits of PV-Powered Vehicles 2021* (No. IEA-PVPS T17-01:2021). International Energy Agency Photovoltaic Power Systems Programme Task 17. https://iea-pvps.org/wp-content/uploads/2021/07/IEA_PVPS_T17_State-of-theart-and-expected-benefits-of-VIPV_report.pdf

Araki, K., Ota, Y., Nagaoka, A., & Nishioka, K. (2023). 3D Solar Irradiance Model for Non-Uniform Shading Environments Using Shading (Aperture) Matrix Enhanced by Local Coordinate System. *Energies*, *16*(11), 4414. https://doi.org/10.3390/en16114414

Arvesen, A., Völler, S., Hung, C. R., Krey, V., Korpås, M., & Strømman, A. H. (2021). Emissions of electric vehicle charging in future scenarios: The effects of time of charging. *Journal of Industrial Ecology*, *25*(5), 1250–1263. https://doi.org/10.1111/jiec.13144

Arvidsson, R., Tillman, A., Sandén, B. A., Janssen, M., Nordelöf, A., Kushnir, D., & Molander, S. (2018). Environmental Assessment of Emerging Technologies: Recommendations for Prospective LCA. *Journal of Industrial Ecology*, *22*(6), 1286–1294. https://doi.org/10.1111/jiec.12690

Centeno Brito, M., Santos, T., Moura, F., Pera, D., & Rocha, J. (2021). Urban solar potential for vehicle integrated photovoltaics. *Transportation Research Part D: Transport and Environment*, *94*, 102810. https://doi.org/10.1016/j.trd.2021.102810

Chandrasekharam, D., & Ranjith Pathegama, G. (2020). CO2 emissions from renewables: Solar pv, hydrothermal and EGS sources. *Geomechanics and Geophysics for Geo-Energy and Geo-Resources*, *6*(1), 13. https://doi.org/10.1007/s40948-019-00135-y

Commault, B., Duigou, T., Maneval, V., Gaume, J., Chabuel, F., & Voroshazi, E. (2021). Overview and Perspectives for Vehicle-Integrated Photovoltaics. *Applied Sciences*, *11*(24), 11598. https://doi.org/10.3390/app112411598

Desai, A., Mukhopadhyay, I., & Ray, A. (2021). Effect of Azimuth and Tilt Angle on Ideally Designed Rooftop Solar PV Plant for Energy Generation. *2021 IEEE 48th Photovoltaic Specialists Conference (PVSC)*, 0522–0527. https://doi.org/10.1109/PVSC43889.2021.9519091

ElectricityMaps. (2022). [Dataset]. https://www.electricitymaps.com/

Evrard, E., Davis, J., Hagdahl, K.-H., Palm, R., Lindholm, J., Lindholm, J., & Dahllöf, L. (2021). *Carbon footprint report—Volvo C40 Recharge* (p. 51). Volvo Cars. https://www.volvocars.com/images/v/-/media/market-assets/intl/applications/dotcom/pdf/c40/volvo-c40-recharge-lca-report.pdf

Frischknecht, R., Itten, R., Sinha, P., De Wild-Scholten, M., Zhang, J., Heath, G., & Olson, C. (2015). *Life Cycle Inventories and Life Cycle Assessments of*

Photovoltaic Systems (No. NREL/TP--6A20-73853, IEA-PVPS-TASK-12, IEA-PVPS-12-04:2015; p. NREL/TP--6A20-73853, IEA-PVPS-TASK-12, IEA-PVPS-12-04:2015). https://doi.org/10.2172/1561526

Golubev, T., & Lunt, R. R. (2021). Evaluating the Electricity Production of Electric Vehicle-Integrated Photovoltaics via a Coupled Modeling Approach. *2021 IEEE 48th Photovoltaic Specialists Conference (PVSC)*, 0155–0159. https://doi.org/10.1109/PVSC43889.2021.9518941

Green, M. A., Dunlop, E. D., Hohl-Ebinger, J., Yoshita, M., Kopidakis, N., & Hao, X. (2021). Solar cell efficiency tables (Version 58). *Progress in Photovoltaics: Research and Applications*, *29*(7), 657–667. https://doi.org/10.1002/pip.3444

Heinrich, M., Kutter, C., Basler, F., Mittag, M., Alanis, L. E., Eberlein, D., Schmid, A., Reise, C., Kroyer, T., Neuhaus, D. H., & Wirth, H. (2020). Potential and Challenges of Vehicle Integrated Photovoltaics for Passenger Cars [Application/pdf]. *37th European Photovoltaic Solar Energy Conference and Exhibition; 1695-1700*, 6 pages, 6119 kb. https://doi.org/10.4229/EUPVSEC20202020-6DO.11.1

Hiselius, L. W., & Rosqvist, L. S. (2018). Segmentation of the current levels of passenger mileage by car in the light of sustainability targets – The Swedish case. *Journal of Cleaner Production*, *182*, 331–337. https://doi.org/10.1016/j.jclepro.2018.02.072

Hoth, P., Heide, L., Grahle, A., & Göhlich, D. (2024a). Vehicle-Integrated Photovoltaics—A Case Study for Berlin. *World Electric Vehicle Journal*, *15*(3), 113. https://doi.org/10.3390/wevj15030113

Hoth, P., Heide, L., Grahle, A., & Göhlich, D. (2024b). Vehicle-Integrated Photovoltaics—A Case Study for Berlin. *World Electric Vehicle Journal*, *15*(3), 113. https://doi.org/10.3390/wevj15030113

Hoth, P., Heide, L., Grahle, A., & Göhlich, D. (2024c). Vehicle-Integrated Photovoltaics—A Case Study for Berlin. *World Electric Vehicle Journal*, *15*(3), 113. https://doi.org/10.3390/wevj15030113

Huld, T., Gottschalg, R., Beyer, H. G., & Topič, M. (2010). Mapping the performance of PV modules, effects of module type and data averaging. *Solar Energy*, *84*(2), 324–338. https://doi.org/10.1016/j.solener.2009.12.002

Idris, M., & Koestoer, R. H. (2023). Environmental life cycle assessment of conventional and electric vehicles: Lessons learned from selected countries. *Journal of Innovation Materials, Energy, and Sustainable Engineering*, *1*(1). https://doi.org/10.61511/jimese.v1i1.2023.27

IEA. (2021, November 4). *Carbon intensity of electricity generation in selected regions in the Announced Pledges and Net Zero scenarios, 2000-2040 – Charts – Data & Statistics*. IEA. https://www.iea.org/data-and-statistics/charts/carbon-intensity-of-electricity-generation-in-selected-regions-in-the-announced-pledges-and-net-zero-scenarios-2000-2040

IEA. (2023). *Net Zero Roadmap: A Global Pathway to Keep the 1.5 °C Goal in Reach—2023 Update*.

Intergovernmental Panel On Climate Change (Ipcc) (Ed.). (2023). Transport. In *Climate Change 2022—Mitigation of Climate Change* (1st ed., pp. 1049–1160). Cambridge University Press. https://doi.org/10.1017/9781009157926.012

Kanz, O., Reinders, A., May, J., & Ding, K. (2020). Environmental Impacts of Integrated Photovoltaic Modules in Light Utility Electric Vehicles. *Energies*, *13*(19), 5120. https://doi.org/10.3390/en13195120

Leftheriotis, G., & Yianoulis, P. (2012). Glazings and Coatings. In *Comprehensive Renewable Energy* (pp. 313–355). Elsevier. https://doi.org/10.1016/B978-0-08-087872-0.00310-3

Liu, Z., Wu, Q., Christensen, L., Rautiainen, A., & Xue, Y. (2015). Driving pattern analysis of Nordic region based on National Travel Surveys for electric vehicle integration. *Journal of Modern Power Systems and Clean Energy*, *3*(2), 180–189. https://doi.org/10.1007/s40565-015-0127-x

Lodi, C., Seitsonen, A., Paffumi, E., De Gennaro, M., Huld, T., & Malfettani, S. (2018). Reducing CO 2 emissions of conventional fuel cars by vehicle photovoltaic roofs. *Transportation Research Part D: Transport and Environment*, *59*, 313–324. https://doi.org/10.1016/j.trd.2018.01.020

Mahmoudi, E., Dos Santos Barros, T. A., Alvarez, H., Garcia, R., Marques, F. C., & Villalva, M. G. (2023). The Effect of Tilt and Azimuth Angle Variations on Monthly and Annual Incident Solar Radiations for Locations in Brazil. *2023 IEEE 50th Photovoltaic Specialists Conference (PVSC)*, 1–7. https://doi.org/10.1109/PVSC48320.2023.10359567

Mulvaney, D., & Bazilian, M. (2023). Price volatility, human rights, and decarbonization challenges in global solar supply chains. *Energy Research & Social Science*, *102*, 103167. https://doi.org/10.1016/j.erss.2023.103167

Needell, Z., Wei, W., & Trancik, J. E. (2023). Strategies for beneficial electric vehicle charging to reduce peak electricity demand and store solar energy. *Cell Reports Physical Science*, *4*(3), 101287. https://doi.org/10.1016/j.xcrp.2023.101287

Pavlovic, A., Sintoni, D., Fragassa, C., & Minak, G. (2020). Multi-Objective Design Optimization of the Reinforced Composite Roof in a Solar Vehicle. *Applied Sciences*, *10*(8), 2665. https://doi.org/10.3390/app10082665

Peibst, R., Fischer, H., Brunner, M., Schießl, A., Wöhe, S., Wecker, R., Haase, F., Schulte-Huxel, H., Blankemeyer, S., Köntges, M., Hollemann, C., Brendel, R., Wetzel, G., Krügener, J., Nonnenmacher, H., Mehlich, H., Salavei, A., Ding, K., Lambertz, A., … Korte, L. (2022). Demonstration of Feeding Vehicle-Integrated Photovoltaic-Converted Energy into the High-Voltage On-Board Network of Practical Light Commercial Vehicles for Range Extension. *Solar RRL*, *6*(5), 2100516. https://doi.org/10.1002/solr.202100516

Pfenninger, S., & Staffell, I. (2016). Long-term patterns of European PV output using 30 years of validated hourly reanalysis and satellite data. *Energy*, *114*, 1251–1265. https://doi.org/10.1016/j.energy.2016.08.060

Posselt, R., Mueller, R. W., Stöckli, R., & Trentmann, J. (2012). Remote sensing of solar surface radiation for climate monitoring—The CM-SAF retrieval in international comparison. *Remote Sensing of Environment*, *118*, 186–198. https://doi.org/10.1016/j.rse.2011.11.016

Que, Z., Wang, S., & Li, W. (2015). Potential of Energy Saving and Emission Reduction of Battery Electric Vehicles with Two Type of Drivetrains in China. *Energy Procedia*, *75*, 2892–2897. https://doi.org/10.1016/j.egypro.2015.07.584

Reddy, V. J., Hariram, N. P., Maity, R., Ghazali, M. F., & Kumarasamy, S. (2024). Sustainable Vehicles for Decarbonizing the Transport Sector: A Comparison of Biofuel, Electric, Fuel Cell and Solar-Powered Vehicles. *World Electric Vehicle Journal*, *15*(3), 93. https://doi.org/10.3390/wevj15030093

Renewables.ninja. (2016). [Dataset]. https://www.renewables.ninja

Rienecker, M. M., Suarez, M. J., Gelaro, R., Todling, R., Bacmeister, J., Liu, E., Bosilovich, M. G., Schubert, S. D., Takacs, L., Kim, G.-K., Bloom, S., Chen, J., Collins, D., Conaty, A., Da Silva, A., Gu, W., Joiner, J., Koster, R. D.,

Lucchesi, R., … Woollen, J. (2011). MERRA: NASA's Modern-Era Retrospective Analysis for Research and Applications. *Journal of Climate*, *24*(14), 3624–3648. https://doi.org/10.1175/JCLI-D-11-00015.1

Rödger, J.-M., Beier, J., Schönemann, M., Schulze, C., Thiede, S., Bey, N., Herrmann, C., & Hauschild, M. Z. (2021). Combining Life Cycle Assessment and Manufacturing System Simulation: Evaluating Dynamic Impacts from Renewable Energy Supply on Product-Specific Environmental Footprints. *International Journal of Precision Engineering and Manufacturing-Green Technology*, *8*(3), 1007–1026. https://doi.org/10.1007/s40684-020-00229-z

Ruiz, P. A., & Rudkevich, A. (2010). Analysis of Marginal Carbon Intensities in Constrained Power Networks. *2010 43rd Hawaii International Conference on System Sciences*, 1–9. https://doi.org/10.1109/HICSS.2010.59

Samadi, H., Ala, G., Lo Brano, V., Romano, P., & Viola, F. (2023). Investigation of Effective Factors on Vehicles Integrated Photovoltaic (VIPV) Performance: A Review. *World Electric Vehicle Journal*, *14*(6), 154. https://doi.org/10.3390/wevj14060154

Tahir, Z. U. R., Ali, M. J., Asim, M., Ahmad, S. U., Hayat, N., Hussain, A., & Azhar, M. (2018). Evaluation of Solar Radiation from MERRA, MERRA-2, ERA-Interim and CFSR Reanalysis Datasets Against Surface Observations for Multan, Pakistan. *Proceedings of EuroSun 2018*, 1–7. https://doi.org/10.18086/eurosun2018.09.04

Thiel, C., Gracia Amillo, A., Tansini, A., Tsakalidis, A., Fontaras, G., Dunlop, E., Taylor, N., Jäger-Waldau, A., Araki, K., Nishioka, K., Ota, Y., & Yamaguchi, M. (2022). Impact of climatic conditions on prospects for integrated photovoltaics in electric vehicles. *Renewable and Sustainable Energy Reviews*, *158*, 112109. https://doi.org/10.1016/j.rser.2022.112109

Tiano, F. A., Rizzo, G., Marino, M., & Monetti, A. (2020). Evaluation of the potential of solar photovoltaic panels installed on vehicle body including temperature effect on efficiency. *eTransportation*, *5*, 100067. https://doi.org/10.1016/j.etran.2020.100067

Tranberg, B., Corradi, O., Lajoie, B., Gibon, T., Staffell, I., & Andresen, G. B. (2019). Real-time carbon accounting method for the European electricity markets. *Energy Strategy Reviews*, *26*, 100367. https://doi.org/10.1016/j.esr.2019.100367

Vehicle-Integrated Photovoltaics—Fraunhofer ISE. (2024). Fraunhofer Institute for Solar Energy Systems ISE. https://www.ise.fraunhofer.de/en/key-topics/integrated-photovoltaics/vehicle-integrated-photovoltaics-vipv.html

Vuilleumier, L., Meyer, A., Stöckli, R., Wilbert, S., & Zarzalejo, L. F. (2020). Accuracy of satellite-derived solar direct irradiance in Southern Spain and Switzerland. *International Journal of Remote Sensing*, *41*(22), 8808–8838. https://doi.org/10.1080/01431161.2020.1783712

Wetzel, G., Salomon, L., Krügener, J., Bredemeier, D., & Peibst, R. (2022). High time resolution measurement of solar irradiance onto driving car body for vehicle integrated photovoltaics. *Progress in Photovoltaics: Research and Applications*, *30*(5), 543–551. https://doi.org/10.1002/pip.3526

Wijewardane, S., & Kazmerski, L. L. (2023). Inventions, innovations, and new technologies: Flexible and lightweight thin-film solar PV based on CIGS, CdTe, and a-Si:H. *Solar Compass*, *7*, 100053. https://doi.org/10.1016/j.solcom.2023.100053

Yamaguchi, M., Nakamura, K., Ozaki, R., Kojima, N., Ohshita, Y., Masuda, T., Okumura, K., Satou, A., Nakado, T., Yamada, K., Tanimoto, T., Zushi, Y., Takamoto, T., Araki, K., Ota, Y., & Nishioka, K. (2023). Analysis for the

Potential of High-Efficiency and Low-Cost Vehicle-Integrated Photovoltaics. *Solar RRL, 7*(8), 2200556. https://doi.org/10.1002/solr.202200556

DEPARTMENT OF SPACE, EARTH AND ENVIRONMENT
CHALMERS UNIVERSITY OF TECHNOLOGY
Gothenburg, Sweden 2024
www.chalmers.se

CHALMERS
UNIVERSITY OF TECHNOLOGY